INFORMATION TO USERS

This manuscript has been reproduced from the microfilm master. UMI films the text directly from the original or copy submitted. Thus, some thesis and dissertation copies are in typewriter face, while others may be from any type of computer printer.

The quality of this reproduction is dependent upon the quality of the copy submitted. Broken or indistinct print, colored or poor quality illustrations and photographs, print bleedthrough, substandard margins, and improper alignment can adversely affect reproduction.

In the unlikely event that the author did not send UMI a complete manuscript and there are missing pages, these will be noted. Also, if unauthorized copyright material had to be removed, a note will indicate the deletion.

Oversize materials (e.g., maps, drawings, charts) are reproduced by sectioning the original, beginning at the upper left-hand corner and continuing from left to right in equal sections with small overlaps.

Photographs included in the original manuscript have been reproduced xerographically in this copy. Higher quality 6" x 9" black and white photographic prints are available for any photographs or illustrations appearing in this copy for an additional charge. Contact UMI directly to order.

ProQuest Information and Learning
300 North Zeeb Road, Ann Arbor, MI 48106-1346 USA
800-521-0600

AN ANATOMICALLY RELEVANT MODEL OF CENTRAL PROCESSING IN THE 3D SLOW-PHASE VESTIBULO-OCULAR REFLEX

Gillian Walter

August, 1999

A thesis submitted to the

Faculty of Graduate Studies and Research

in partial fulfillment of the requirements for the degree of

Masters of Engineering

Department of Biomedical Engineering

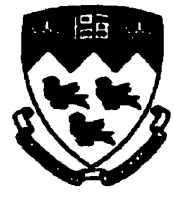

McGill University, Montréal

Abstract

A bilateral model of central processing in the 3D slow-phase vestibulo-ocular reflex (VOR) has been developed. Two possible implementations of the model have been examined, one placing required nonlinearities in a feedforward pathway and the other using an additional feedback path instead. The behaviour of the two forms was investigated for parameter variation and under artificial lesion conditions. A literature review was conducted to propose an anatomical substrate for the model and possible sites for required cross-talk between the horizontal and vertical/torsional pathways. Neural network models of the VOR and oculomotor integrator were reviewed and discussed. A neural network simulation was presented to illustrate how simple thresholding and saturation of neuron responses may aid in generating the proposed nonlinearities without separate specialized computing stages.

Résumé

Un modèle bilatéral des processus centraux dans le réflexe vestibulo-oculaire (VOR) en 3D a été developé. Deux formes du modèle ont été examinées, une avec toutes les nonlinéaritées requises placées avant, et une les plaçent dans un circuit fermé. Le comportement des deux formes a été étudié avec des paramètres variés et en cas de lésion artificielle. Une revue de la litérature a été exécutée dans le but de déterminer une structure anatomique pour le modèle. Une autre revue résume des modèles du VOR qui emploit des réseaux neuronaux. Un simple réseau neuronal a été présenté pour démontrer que la présence de simples seuils d'activation et de saturation pourrait suffire pour créer les effets nonlinéaires désirés.

Acknowledgments

I would like to thank Dr. H.L. Galiana for her guidance and constructive criticism in supervising this project. I would like to thank Dr. Ross Wagner and Sunil Kukreja for their help in dealing with a variety of computer problems and LaTeX. The funding for this research was provided by an MRC grant and an NSERC PGS A scholarship.

Contents

List of Figures

Chapter 1

Background

1.1 Introduction

The vestibulo-ocular reflex (VOR) is a mechanism used to keep the line of sight stable in space as the head moves. It consists of a slow phase during which the gaze is kept stable, and a fast phase that resets the eye position as it approaches the limits of its physical range. This thesis presents a 3D model of central processing for the slow phase component of the VOR. The following sections will give a brief overview of eye movement, relevant anatomy and physiology, and existing models of the oculomotor integrator and VOR.

1.2 Relevant Anatomy and Physiology

1.2.1 The Eye

A diagram of the eye and its muscles is shown in Figure 1.1. Light passes through the pupil to a sensitive region on the back of the eye, the retina. In some animals, there is a central region on the retina, the fovea, with increased sensitivity for more specialized visual functions such as target tracking. Horizontal movements of the eye are controlled largely by the lateral and medial rectus muscles; vertical and torsional movements by the inferior and superior rectus and inferior and superior oblique muscles. The direction of pull of the superior oblique muscle is altered as it passes through a loop of cartilage, the trochlea. A detailed description of eye orbital anatomy and mechanics can be found in ([91], [78]).

Figure 1.1: The eye and its muscles, reprinted from [11] with the permission of the Royal Society. A,C- lateral and medial rectus muscles; B,D- superior and inferior rectus muscles; E,G- superior and inferior oblique muscles; a- trochlea.

1.2.2 The Vestibular Sense Organs

The otolith organs and semicircular canals provide the body's mechanism for detecting linear and angular head accelerations. The canals are oriented in the head such that one lies roughly horizontal when the head is upright, and the others lie almost perpendicular to the horizontal, mutually perpendicular at about 45 degrees with respect to the medial plane of symmetry of the body. A diagram of the canals and otolith organs, and their location on each side of the head, is shown in Figure 1.2. For a more detailed description of semicircular canal orientation in man, the reader is referred to [12].

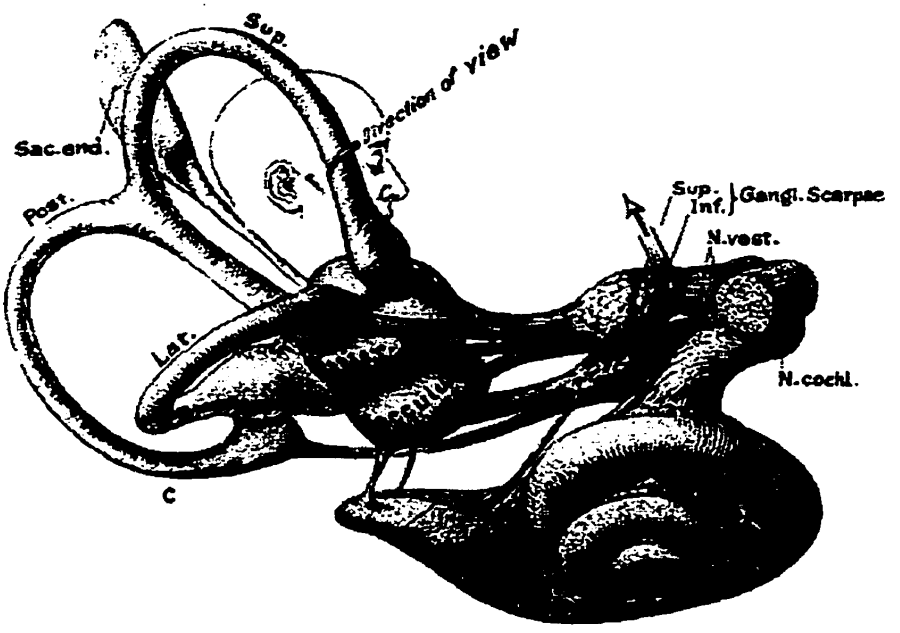

Figure 1.2: The semicircular canals and otolith organs, reprinted from [56] by permission of John Wiley and Sons, Inc.

The canals and otolith organs are filled with a fluid that is displaced as the head accelerates. They are lined with receptor cells that have hair-like projections extending through this fluid into a gelatinous substance. The firing rates of these cells are

sensitive to the hair bending in a particular direction. In the canals, the hairs are aggregated in a watertight flap, the cupula. The canal hair cells are all oriented for sensitivity in the same direction, so the canals are one-dimensional motion detectors. When the head rotates in the canal plane, the fluid tends to stay where it is, bending the cupula and stimulating the embedded hair cells. The degree of bending and resulting stimulation will depend on the component of angular acceleration in the canal plane.

The otolith organs are the utricle and the saccule, which detect linear acceleration magnitude and direction in the horizontal and vertical planes respectively. The otolith organs differ from the semicircular canals in that the hair cells attach to a weighted substance that is free-floating in the fluid to allow bending in any direction within a plane. Each organ is sensitive to two-dimensional motion, as the receptor cells are oriented in a variety of directions.

The canal responses are more important than those of the otoliths for the angular VOR dealt with in this thesis. While the responses are elicited by angular acceleration of the head, the dynamics of the canals are such that the receptor cell firing rates are more representative of angular velocity during natural movements. Thus, the canal output is generally taken to be proportional to the angular velocity rather than the angular acceleration of the head [19].

1.3 Eye Movements

1.3.1 Major Categories of Eye Movement

Eye movements may be divided into several categories, reflexive and voluntary [19]. The following paragraphs summarize the main types of eye movements.

Vestibular eye movements are reflexive and occur in response to head acceleration. Responses that occur as a result of linear acceleration due to postural changes are referred to as static; those that occur as a result of time-varying linear or angular acceleration are called dynamic. In the dark, the object of these movements is to keep the gaze stationary in space as the head moves. Dynamic vestibular movements are comprised of two alternating phases; a slow phase in which eye angular velocity is equal and opposite to head angular velocity, and a fast phase which resets the eye position as it approaches the limits of its physical range.

Optokinetic and smooth pursuit eye movements serve to minimize the slip of an image across the retina. Optokinetic movements occur when a large part of the image moves uniformly across the retina during head-turning or locomotion. Smooth pursuit movements are used when the eye is tracking a moving target, responding to the slip of the target image over the retina. This image does not necessarily cover a large part of the retina. Smooth pursuit movements can override the optokinetic tendency to keep the retinal image as a whole stable.

Saccades are fast, voluntary eye movements used to foveate a different part of the visual field. Saccades are also associated with reflexive movements; the fast phase of the VOR is an example.

In frontal-eyed animals (animals with both eyes facing forward), the visual fields of the eyes overlap considerably. Vergence movements occur when a target object is too near to be foveated properly on both eyes for parallel eye positions. They allow the eyes to move separately, so even close targets can be focused on the retina.

1.3.2 The Angular VOR (aVOR)

The object of the aVOR is to generate an eye angular velocity roughly equal and opposite to the current head angular velocity. The passive and active tissues surrounding the eye provide a torque of the form $T(t) = K\Phi(t)\hat{n}(t) + r\vec{\omega}(t)$, where $\Phi(t)$ is the angular displacement of the eye about axis $\hat{n}$, $\vec{\omega}(t)$ is the current angular velocity, and K and r are scalar constants [86]. The contribution required to overcome the eye's inertia is very small compared to these forces, so the required motor command is generally taken to be $I(t) = -\bar{M}_a^{-1}(t)(K\Phi(t)\hat{n}(t) + r\vec{\omega}(t))/S$, where S is a constant relating innervation to muscle force and $\bar{M}_a(t)$ is a matrix describing the current muscle pull axes, usually assumed to be constant. The position component is often referred to as the *step* component, and the velocity component as the *pulse* component. As expected, extraocular motoneuron firing rates have been found to vary with both eye position and velocity [105].

The backbone of the VOR circuitry is a three-neuron arc involving primary afferent vestibular neurons, secondary vestibular neurons, and motoneurons. The primary neurons lead from the semicircular canals to the vestibular nucleus (VN), and are characterized by a resting discharge rate and positive sensitivity to ipsilaterally-directed

head velocity. Secondary vestibular neurons lead from the vestibular nucleus to the oculomotor, abducens, or trochlear nuclei. These VN cells have a resting discharge rate modulated by eye position and eye or head velocity, depending on the protocol and the cell classification approach used. The motoneurons have a resting discharge rate modulated by eye position and velocity within a particular plane. They lie in the oculomotor nuclei and their axons terminate on the extraocular muscles.

There are numerous other structures involved in the VOR, having connections with the vestibular and oculomotor nuclei. These structures are involved in creating the eye position sensitivity observed in the secondary vestibular neurons and motoneurons, and in converting the signals from the canal coordinate system to that of the extraocular muscles. The neural process converting sensory velocity signals into estimates of eye position is called the *neural integrator* (NI). The implementation of this neural integrator is still a matter of debate, as is the relationship between the horizontal and the vertical/torsional pathways.

1.4 1D VOR and Integrator Models

In the following subsections, descriptions of one-dimensional models have been included because they formed the basis for three-dimensional models. Furthermore, some aspects of the one-dimensional model proposed by Galiana and Outerbridge [48] have not been used in other three-dimensional models and are incorporated into the model developed for this thesis. The transfer functions in the sections that follow describe actions on only the modulated component of each neuron's firing rate; each

neuron also exhibits a constant background firing rate that sums with the modulated component, but this is ignored here.

1.4.1 Robinson Model of the VOR

D.A.Robinson proposed a four-stage model of the one-dimensional VOR ([90], [92]) shown in Figure 1.3. The basic elements of this model have been used in all subsequent models, with some extensions and modifications.

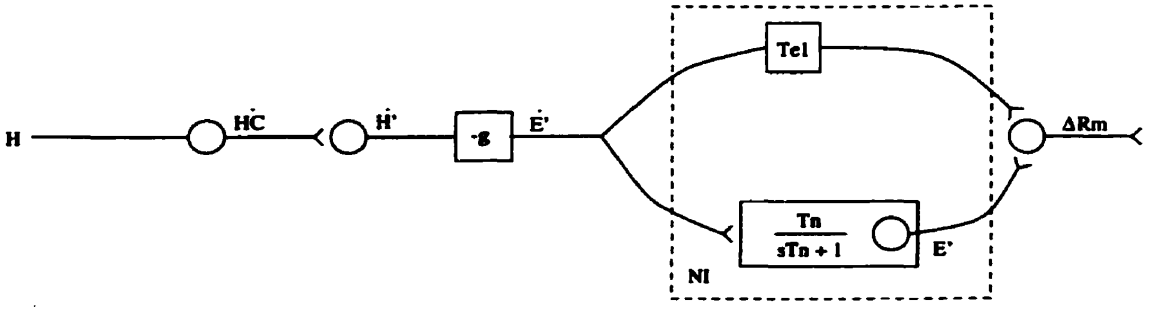

Figure 1.3: Robinson model of 1D VOR, redrawn from [92].

The first stage describes the transfer function of the semicircular canals, relating the primary vestibular afferent firing rate changes ($\dot{H}_c$) to head angular acceleration (s^2H):

$$\frac{\dot{H}_c}{H} = s\frac{sT_c}{(sT_c+1)}\frac{sT_a}{(sT_a+1)}(sT_z+1)\ , \tag{1.1}$$

where T_c is the dominant cupula time constant and the term with T_a represents the peripheral adaptation of the canals. The T_z term describes the high frequency dynamics.

The second and third stages occur at the level of the secondary vestibular neurons. They serve to replace the cupula time constant with the larger VOR time constant,

and to generate appropriate velocity and position sensitivities via direct and indirect pathways. The corresponding transfer functions are given below for $T_n \gg 1$, where T_n is the time constant of the NI.

$$\frac{\dot{H}'}{\dot{H}_c} = \frac{T_{vor}}{T_c}\frac{(sT_c+1)}{(sT_{vor}+1)} \tag{1.2}$$

$$\frac{\Delta R_m}{\dot{E}'} = -g\frac{(sT_{e1}+1)}{s} \tag{1.3}$$

The motoneurons weight the outputs of the secondary vestibular neurons to form the extraocular muscle commands, represented here by ΔR_m. The fourth stage of the model describes the eye plant dynamics:

$$\frac{E}{\Delta R_m} = \frac{e^{-s\tau}}{(sT_{e1}+1)(sT_{ez}+1)} \, . \tag{1.4}$$

This gives an overall equation:

$$\frac{E}{H} = -g\frac{sT_{vor}}{(sT_{vor}+1)}\frac{sT_a}{(sT_a+1)}\left[\frac{(sT_z+1)e^{-s\tau}}{(sT_{ez}+1)}\right] \, . \tag{1.5}$$

The terms in the square brackets are high-frequency terms that roughly cancel each other at low frequencies. The eye plant is often approximated without its high-frequency terms, becoming simply

$$\frac{E}{\Delta R_m} = \frac{1}{(sT_{e1}+1)} \, . \tag{1.6}$$

Discarding the remaining high-frequency terms gives an overall transfer function:

$$\frac{E}{H} = -g\frac{sT_{vor}}{(sT_{vor}+1)}\frac{sT_a}{(sT_a+1)} \, . \tag{1.7}$$

Adjustments to this model have included a one-dimensional bilateral version using an alternative implementation of the third-stage transfer function [48], and the extension of the integrator stage to three dimensions [114].

1.4.2 Galiana/Outerbridge Model

Galiana and Outerbridge proposed a modified model of the one-dimensional VOR [48]. The significant features of this model are a bilateral structure, and filtering feedback loops in place of the conventional feedforward integrator. A simplified diagram of the model structure is given in Figure 1.4.

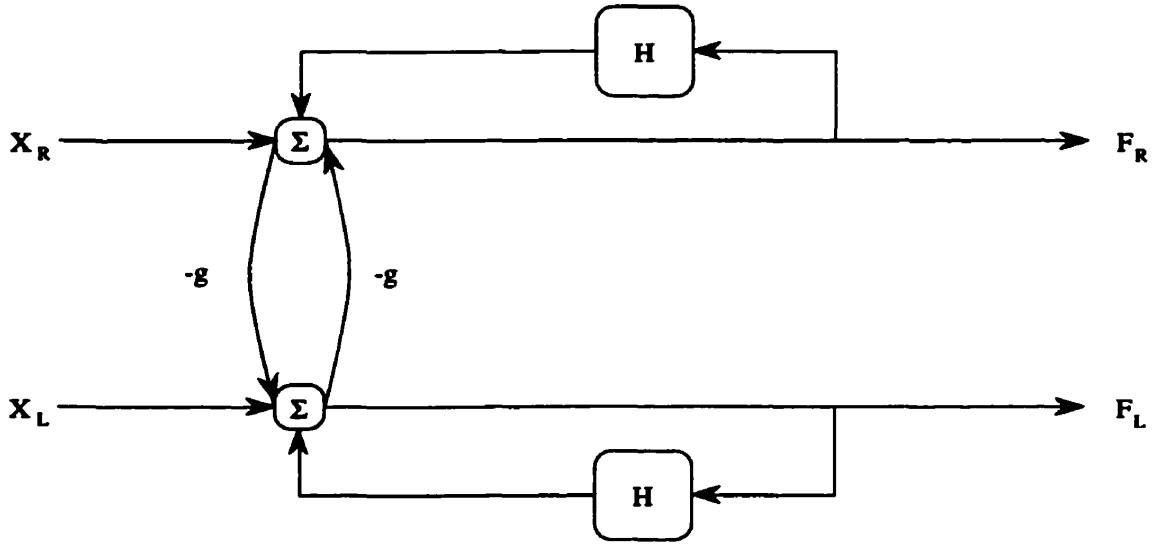

Figure 1.4: Galiana/Outerbridge bilateral model of 1D slow-phase VOR.

These two modifications give a model more consistent with certain neurophysiological findings. The feedback approach is supported by the observed eye position dependencies of VN neuron firing rates, and by experimental results that demonstrate the effect of VN lesion on gaze holding. The bilateral structure gives the reflex a larger expected range of linearity than that predicted by previous models [106], also in keeping with experimental observation. The equations for firing rate on the right and left sides reduce to:

$$F_R = \frac{(1-H)X_R - gX_L}{(1-H+g)(1-H-g)} \tag{1.8}$$

$$F_L = \frac{(1-H)X_L - gX_R}{(1-H+g)(1-H-g)} \tag{1.9}$$

where $H = \frac{K}{(0.15s+1)}$. This gives different time constants for difference mode ($X_L = -X_R$) and common mode ($X_L = X_R$) inputs. To illustrate this, let $X_D = \frac{X_R - X_L}{2}$ and $X_C = \frac{X_R + X_L}{2}$. Then $X_R = X_C + X_D$ and $X_L = X_C - X_D$. Replacing X_R and X_L in the above equations yields:

$$F_R = \frac{X_C}{1-H+g} + \frac{X_D}{1-H-g} \tag{1.10}$$

$$F_L = \frac{X_C}{1-H+g} - \frac{X_D}{1-H-g} \tag{1.11}$$

or,

$$F_R = \frac{(0.15s+1)X_C}{0.15(1+g)s + (1+g-K)} + \frac{(0.15s+1)X_D}{0.15(1-g)s + (1-g-K)} \tag{1.12}$$

$$F_L = \frac{(0.15s+1)X_C}{0.15(1+g)s + (1+g-K)} - \frac{(0.15s+1)X_D}{0.15(1-g)s + (1-g-K)}. \tag{1.13}$$

Thus, $T_D = \frac{0.15(1-g)}{(1-g-K)}$ and $T_C = \frac{0.15(1+g)}{(1+g-K)}$. Here, T_D implements the equivalent NI function described by T_n in the previous section. Rearranging the expression for T_D gives the desired relation between K and g: $K = (1 - \frac{0.15}{T_D})(1-g)$.

1.5 3D Integrator and VOR Models

There are two main issues that lead to differences between one-dimensional and three-dimensional VOR models: the non-commutativity of rotations, and the geometry of the canals and extraocular muscles. This section describes these problems and how

they have been investigated.

1.5.1 3D vs 1-D: Commutativity Issue

The first question one might ask is 'Why not simply have three separate integrators, one each for horizontal, vertical, and torsional directions?'. The problem is that rotations are noncommutative. Consider the following scenario, depicted in Figure 1.5.

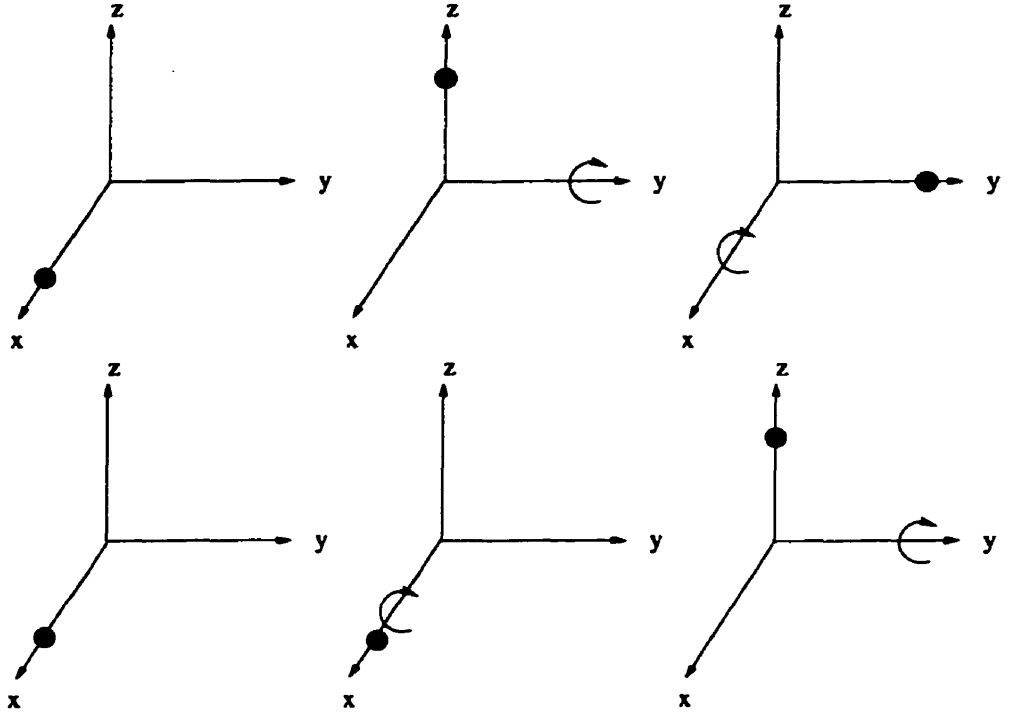

Figure 1.5: Rotational non-commutativity.

Define a coordinate system with perpendicular x, y, and z axes, and assume an object (say, the pupil) to lie some distance R along the x axis. Now consider 2 rotations, one 90 degrees about the y axis and the other 90 degrees about the x axis. If the y axis rotation is performed first, the pupil lands at a point R along the y axis. If the x axis rotation is performed first, the pupil lands at a point R along the

z axis. Thus the rotations cannot be considered without also considering the current position of the pupil. This problem does not arise in the one-dimensional case because when rotation is limited to one plane, the angular position does simply reduce to the integral of angular velocity.

1.5.2 Tweed/Vilis Model

Tweed and Vilis [114] proposed a quaternion model for the oculomotor integrator which accounts for the non-commutative properties of three dimensional rotations. A brief introduction to quaternion math is provided in Appendix A. Using the properties of quaternions, Tweed and Vilis showed that the time derivative of a quaternion (q) describing position for rotation at angular velocity $\vec{\omega}$ is given by $\dot{q} = \frac{\vec{\omega} q}{2}$. Setting $q = 2\cos\frac{a}{2} + 2\vec{n}\sin\frac{a}{2} = q_0 + \vec{q}$, where $\vec{a} = a\hat{n} = q^{-1}\vec{a_0}q$ describes the current eye orientation, they modeled the motoneuron firing rate as $\vec{m} = \bar{K}\vec{q} + \bar{r}\vec{\omega}$, where $\bar{K}$ and $\bar{r}$ were fixed matrices. Ideally, $\vec{m} = \bar{K}\vec{a} + \bar{r}\vec{\omega}$, but $\vec{q}$ differs from $\vec{a}$ by less than four percent for angles up to 55 degrees, so the approximation was valid for the range of eye movements considered in their simulations. This gives a net model as shown in Figure 1.6.

This model predicts that eye position signals and head velocity signals converge multiplicatively on vestibular nucleus neurons, and that tonic neurons carrying different components of the eye position signal are interdependent. This model was tested behaviourally in conjunction with the VOR and Saccadic systems, though cell firing rates were not examined ([114], [112], [110], [107]).

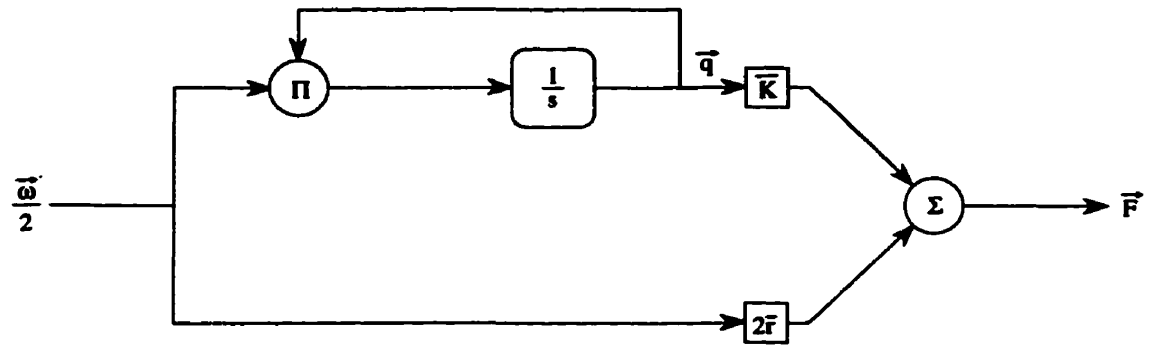

Figure 1.6: Tweed/Vilis model of the 3D oculomotor integrator. The required motoneural firing rate $\vec{F}$ combines current head angular velocity with computed eye orientation $\vec{q}$.

1.5.3 Schnabolk/Raphan Model

Schnabolk and Raphan [102] modeled the three-dimensional velocity to position transformation for saccades using three parallel, non-interconnecting pathways, as shown in Figure 1.7. The matrices $\bar{G}p$,$\bar{C}p$,$\bar{D}$,$\bar{H}p$, and $\bar{M}$ were diagonal, with static scalar elements.

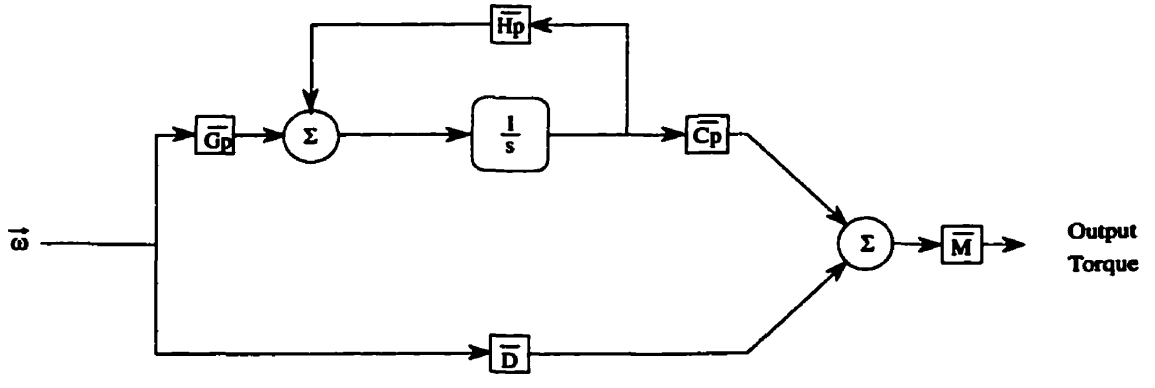

Figure 1.7: Schnabolk/Raphan model of the 3D saccadic integrator.

Their justification for ignoring the non-commutative nature of rotations was that the CNS generates muscle torques rather than an eye orientation vector, and a given set of muscle torques corresponds to a particular equilibrium eye orientation regardless of past torque and position values. Direct integration of each of the three angular

velocity components will give a set of torques that is independent of the order in which the rotations occured, yielding a unique equilibrium orientation. The eye plant dynamics ensure that the eye quickly settles to a position independent of the order of rotations, and the non-commutativity of the rotations will only be reflected in the *paths* taken to reach the equilibrium orientation. The differences in results between this model and the Tweed/Vilis model are negligible for angles less than 15 degrees. Schnabolk and Raphan argue that non-linear eye plant dynamics play a much larger role than rotational non-commutativity in determining eye position, and that the integrators need not and do not account for it. While this model may work for saccades [86], there are problems in extending this model to the VOR [107] (see section 1.5.5).

1.5.4 Geometrical Issues

The integrator models discussed so far have not dealt with the issue of the geometrical misalignment between the canal and muscle intrinsic reference frames. However, several investigators have looked at the transformation of the velocity component. Two main approaches have been taken: matrix analysis ([93], [117], [94]), and tensor analysis ([83], [82], [85], [84], [80]).

The matrix approach breaks down the VOR into 3 parts: sensory detection of angular velocity by primary canal afferents, central processing, and motor implementation of the processed signal. In this case, the semicircular canals and extraocular muscles are each lumped together into 3 coplanar pairs. The VOR is assumed to

be exactly compensatory, giving an equation $\dot{\vec{E}} = \bar{M}\bar{B}\bar{C}\dot{\vec{H}} = -\dot{\vec{H}}$, where the matrices $\bar{C}$, $\bar{B}$, and $\bar{M}$ represent the canal, brainstem, and eye muscle transformations respectively. Anatomical data was used to determine the average maximal activation directions of the 2 canals/muscles in each coplanar pair, and the $\bar{M}$ and $\bar{C}$ matrices were generated accordingly. For a perfectly compensatory VOR, $\bar{B}$ was therefore taken to be $(\bar{M}^{-1})(-\bar{I})(\bar{C}^{-1})$, where $\bar{I}$ is the identity matrix. Note that $\bar{C}^{-1}$ and $\bar{M}^{-1}$ serve to compensate for the non-orthogonality of the canals and muscles in addition to their relative misalignment.

While the matrix approach can be used to represent net movement of the eye as a result of a given input, it is limited in that it ignores the issue of how the brain translates a three-dimensional intended movement vector into an appropriate 6-dimensional set of muscle commands.

Pellionisz ([83], [82], [85], [84]) developed a tensor network based model of the VOR that allows the system to be decomposed in a relevant fashion and deals directly with the above problem. As with the matrix approach, the analysis dealt only with the issue of generating an appropriate velocity component, not with the position command. Pellionisz still paired coplanar canals (the differences between canal pair planes are less radical than those between muscles), but noted that the method does not necessitate this pairing. This model was also investigated in the context of position-dependent muscle pull directions [80].

For the tensor and matrix models, it is important to understand the difference between covariant and contravariant representations of a vector in a reference frame.

An explanation of this difference is included in Appendix A.

The Pellionisz model breaks down the VOR into the following stages:

• Covariant perception of angular head velocity by the semicircular canals (represented by a 3x3 matrix).

• Conversion of the covariant perceived signal into a contravariant internal representation of the sensed signal (3x3 matrix).

• Covariant representation of the contravariant sensory signal (taken to be the desired motor command) in terms of the 6 muscle axes (6x3 matrix).

• Conversion of the covariant representation of the motor command into a contravariant representation that will give the correct eye movement (6x6 matrix).

The authors noted that, as the VOR is a 3-neuron arc, some of the transformations must be contracted. Whether the first two or last two steps were the ones combined would not result in differences at the output level. The authors also mentioned the issue of temporal transformation required because of various delays in the system, but this will not be addressed here. The crucial difference between this approach and the matrix method lies in the fourth step. There are six muscles controlling 3 degrees of freedom, leading to an infinite number of possible solutions. The matrix approach bypasses the issue by assuming that paired extra-ocular muscles are coplanar and reciprocally innervated. The tensor approach dealt with this problem using the Moore-Penrose generalized inverse to form the 6x6 conversion matrix. This allows a unique solution by imposing the additional restriction that the eigenvectors of the matrix converting from covariant to contravariant representation be the same as those of its inverse. They cited several justifications for this choice [85], including

experimental evidence and the fact that this generates a minimal-energy set of muscle commands.

The tensor analysis was applied to the cat [85], and the results indicated that in the case of the VOR, the muscles do act largely in agonist-antagonist pairs, and that the horizontal and vertical eye movers act mostly separately.

Although the Tweed/Vilis and Schnabolk/Raphan 3D integrator models did not consider the issue of geometry, Smith and Crawford [107] incorporated non-orthogonal coordinate transformations into the quaternion model using Robinson's matrix approach. This initially lead to unstable results, but they found two solutions to the problem:

- Separate brainstem coordinate transformation into two (sensory and motor) transformations to undo non-orthogonalities.
- Compute correct tensor components in arbitrary coordinates.

They hypothesized that the VOR uses a dual coordinate transformation to optimize intermediate brainstem coordinates.

1.5.5 The Extraocular Muscles and Commutativity

A number of investigations have been conducted to examine a possible role for extraocular muscles in dealing with the commutativity issue for saccades ([86], [89]). While the torque supplied by the restoring tissues is generally agreed to be as described earlier, the actions of the muscles are a matter of some debate. One of the major issues is whether or not the muscle pull axes remain constant. Traditionally it

has been assumed that the muscle pulling planes remain more or less constant with eye orientation, and the required innervation is a constant combination of current orientation and angular velocity. Recent studies indicate that this assumption may not be correct [30]. Demer et al. have found evidence of fibromuscular pulleys that could alter the direction of muscle pull by a fraction of the current eye orientation. Thus, $\bar{M}_a(t) = \bar{R}(\beta, \hat{n})\bar{M}_{a0}$, where $\bar{M}_{a0}$ describes the muscle pull axes in primary orientation, and $\bar{R}$ is the matrix representing the rotation of the muscle pull axes by β about the current orientation axis $\hat{n}$. Then the necessary innervation signals are

$$\vec{I}(t) = \bar{M}_{a0}{}^{-1}\bar{R}(\beta, \hat{n})^{-1}(\bar{K}\Phi(t)\hat{n}(t) + \bar{r}\vec{\omega}(t)) \ . \tag{1.14}$$

Using the matrix properties that $\bar{R}(\beta, \hat{n})\hat{n} = \hat{n}$ and $\bar{R}(\beta, \hat{n})^T = \bar{R}(\beta, \hat{n})^{-1} = \bar{R}(-\beta, \hat{n})$,

$$\vec{I}(t) = \bar{M}_{a0}{}^{-1}(\bar{K}\Phi(t)\hat{n}(t) + \bar{R}(\beta, \hat{n})^{-1}\bar{r}\vec{\omega}(t)) \ . \tag{1.15}$$

That is, the muscles have position-dependent effects on the pulse component, but not the step. Quaia and Optican [86] demonstrated that given proper pulley placement, the required pulse component $\bar{R}^{-1}\bar{r}\vec{\omega}(t)$ is very close to the derivative of the step. This means that a commutative controller (ie. one that integrates the three pulley components individually) will not give much drift, although this final position may not be the desired one if the pulse is not chosen appropriately. Proof that these pulleys are properly oriented remains to be established.

While the pulley model may mean that a commutative integrator can be used for saccades, it could not be used without adjustment in the case of the VOR as the semicircular canals detect angular head velocity rather than the derivative of eye orientation. In the case of the VOR, some means of converting from angular velocity

to the derivative of eye orientation prior to integration would be required. From a VOR standpoint, the only issue is whether the desired muscle command is

$$K\Phi(t)\hat{n}(t) + r\vec{\omega}(t) \tag{1.16}$$

or

$$K\Phi(t)\hat{n}(t) + r\frac{d(\Phi(t)\hat{n}(t))}{dt} . \tag{1.17}$$

$\Phi(t)\hat{n}(t)$ must be computed using a mechanism that converts $\vec{\omega}(t)$ to $\frac{d(\Phi(t)\hat{n}(t))}{dt}$ before integration, as final desired eye orientation cannot be known apriori. For this thesis, the desired output was taken to be $\vec{m} = K\vec{E} + r\dot{\vec{E}}$, where $\vec{E}$ is the current eye orientation, some representation of $\Phi(t)\hat{n}(t)$.

Recently, Smith and Crawford [107] investigated the performance of the Tweed-Vilis and Schnabolk-Raphan models in the context of the VOR. The eye was simulated with both standard constant muscle pull axes and with the pulley model of the axes (in the pulley case, the quaternion model was adjusted slightly to give $\vec{m} = K\vec{E} + r\dot{\vec{E}}$ rather than $\vec{m} = K\vec{E} + r\vec{\omega}$). They found that a multiplicative interaction was required in both the direct and the indirect paths for the pulley plant, and in the indirect path for the standard plant. They confirmed that the commutative integrator would not be sufficient for the VOR in either case.

1.6 Thesis Outline

The objectives of this thesis were two-fold. The first goal was to create a 3D model of slow-phase central processing of the VOR, using a feedback neural filter instead

of separate velocity and integrating pathways. The second goal was to propose an approximate anatomical substrate for this model, based on available literature concerning neuron anatomy, firing rates and lesion studies. The layout of the remainder of this thesis is as follows.

Chapter Two develops a monocular 3D feedback filter model of slow-phase VOR. Two possible implementations of the model are considered.

Chapter Three considers the bilateral extension of the monocular forms.

Chapter Four reviews literature concerning the horizontal and vertical integrators, and provides a compilation of information regarding the cross-talk between them. Neural network implementations of VOR and integrator models and their implications are also reviewed and discussed here. A simple neural network to investigate one aspect of the proposed 3D model is presented.

Chapter Five contains the discussion and conclusions, including recommendations for future work.

Chapter 2

A Monocular Model

This chapter describes a new model for 3D slow-phase processing in the central VOR. The objective was to extend the Galiana and Outerbridge [48] feedback filtering loop implementation of the integrator to three dimensions, and to determine what sort of interconnections between horizontal and vertical/torsional systems might be expected. It is important to note that there are two reasons why such interconnections may be required. First, the semicircular canal planes don't correspond exactly to the planes of pull of the extraocular muscles. Second, 3D cross-connections are required to account for the non-commutativity of rotations. This thesis deals primarily with the investigation of the second point.

For simplicity, a monocular version of the model was first considered, as relevant for purely conjugate eye movement. The bilateral extension of the model will be discussed in a later chapter, to explore the disconjugate eye movements that could result from malfunctioning sensors or unilaterally lesioned brain structures.

2.1 Assumptions and Simplifications

The following assumptions and simplifications were made in constructing an initial model:

- The coordinate system chosen was an orthogonal head-fixed system with the x axis extending forward through the line of sight when the eye is in primary orientation, the y axis pointing towards the left temple, and the z axis extending upwards perpendicular to the x and y axis. Canal sensitivities and primary orientation muscle pull directions were assumed to align with the main axes of this frame.

- It was assumed that the signal entering the system was a desired eye angular velocity. Differences between head angular velocity and desired eye angular velocity due to the eye rotating about its center rather than the head center were ignored.

- It was assumed that the desired outputs of the system correspond to a horizontal command for movement about the z axis, a vertical command for movement about the y axis, and a torsional command for movement about the x axis. The output of the model was taken to be $\vec{F} = \bar{K}\vec{E} + \bar{r}\dot{\vec{E}}$, where $\vec{E}$ is a vector composed of the three components representing eye orientation, and $\bar{K}$ and $\bar{r}$ are diagonal matrices.

- Coplanar muscles were paired.

- The effects of time delays in neuronal implementation were not considered.

- It was assumed that the eye would not exceed 90 degrees of rotation from primary position in any direction (in fact, less is observed).

- Only the modulated component of neuron firing rates was considered.

2.2 Representation of Orientation

The first issue that one must tackle in forming a 3D model is how to represent orientation. For rotation about a single axis, the net rotation about that axis is a simple and logical representation. However, in three dimensions there are many different ways to interpret orientation- as sequences of 3 consecutive rotations about space-fixed or object-fixed axes, as a single rotation about a general axis, or in terms of more abstract quantities such as quaternions. An outline of some of the more common systems for describing 3D orientation is given in Appendix A.

If one wishes to consider the ideal VOR and does not wish to try to map individual functions to different anatomical sites, the representation used is irrelevant. If an anatomical mapping is desired though, the representation chosen could become very important. For instance, the Nucleus Prepositus Hypoglossi (NPH) is thought to encode mainly the 'horizontal' component of eye position and velocity, but expressing position with these different representations yields many alternatives for a 'horizontal' position component. Even if one eliminates the representations that break down orientation into consecutive rotations as unphysiological and assumes that the reference frame is that of the canals or muscles, it is still possible to come up with alternative representations.

For the purposes of this thesis, only two representations will be considered. The first representation defines three variables, two corresponding to the current gaze direction in space and one corresponding roughly to torsion about this gaze line in space. The second representation defines three variables corresponding to the net

angular displacement multiplied by the components of the current orientation axis. These both reduce to standard definitions of 1D horizontal, vertical and torsional displacement for rotations from primary orientation about the primary axes.

With the simplifying assumption that the canals and muscles align with the reference frame given above, both representations assume a canal/muscle based coordinate system. The difference between the two is conceptual- whether the line of gaze in the head is represented apart from the torsion about this line, or whether all three degrees of freedom are represented identically. The argument for the first representation would be that the VOR is probably learned and adapted with the aid of retinal slip. Rotation about the gaze line corresponds to rotation of the image about a point on the retina, whereas a change in direction of the gaze line corresponds to slip of the image off the retina. One could imagine then that rotation of the gaze line and rotation about the gaze line might be regarded separately, particularly if the integrator were shared with other systems that could benefit from this type of representation. The argument for the second representation is that the VOR doesn't need to make this distinction- its purpose is to avoid retinal slip of any kind, rotating the eye opposite to the head without regard for the slip direction. The simplest representation would then be a direct mapping of canal responses to muscle commands, with the minimal adjustments required to account for rotational non-commutativity and canal/muscle misalignment.

These alternative interpretations are examined only to illustrate that results are affected by how orientation is represented for non-ideal VOR. Even if canal and muscle plane geometry were accounted for, more would have to be known about how

the VOR is learned and adapts before choosing an appropriate representation. A three-variable representation may prove to be insufficient, particularly for the first representation. It is important to note that the first representation would require position-dependent mapping of its output to the muscles, as it doesn't give the components of rotation about the three axes directly. Neurons involved in the VOR display a range of thresholds and sensitivities ([105], [76], [61], [103]). These may just account for eye plant nonlinearities, or they may have some other role. There may be other unexamined nonlinearities that could perform this conversion.

For both representations, the method used to convert from 1D to 3D was the same: a position-dependent matrix converting angular velocity to the derivative of eye orientation was placed before three parallel 1D pathways of the form used in the Galiana/Outerbridge horizontal VOR model. An alternative set of pathways was also considered: it provides the same instantaneous transfer function by placing the position dependency in a feedback loop.

2.2.1 First Representation

The first representation was developed as follows. Let $\bar{R}$ be a rotation matrix describing the current orientation of the eye relative to primary gaze position. Then

$$\begin{pmatrix} x_G \\ y_G \\ z_G \end{pmatrix} = \bar{R} \begin{pmatrix} 1 \\ 0 \\ 0 \end{pmatrix} \quad \text{and} \quad \begin{pmatrix} x_\psi \\ y_\psi \\ z_\psi \end{pmatrix} = \bar{R} \begin{pmatrix} 0 \\ -1 \\ 0 \end{pmatrix} \tag{2.1}$$

describe the location of the pupil and a point corresponding to the oblique attachment (under the assumption that the pupil lies at (1,0,0) and the obliques attach at (0,-1,0)

for the right eye in primary orientation).

The following three variables were then defined:

$$\phi = \arcsin(y_G/\rho) \tag{2.2}$$

$$\theta = \arcsin(z_G/\rho) \tag{2.3}$$

$$\psi = \arcsin(z_\psi/\rho) \tag{2.4}$$

where ρ is the radius of the eye. For rotations about the primary axis from primary orientation ϕ reduces to the standard 1D horizontal variable, θ to the vertical, and ψ to torsion. ϕ will not change for rotations about the y axis from any orientation; θ and ψ will not change for rotations about the z axis. The gaze line is determined completely by ϕ and θ; ψ sets the torsion about this line. In the remainder of the model development, the measurement units will be defined such that ρ has a value of one. The desired outputs were taken to be:

$$F_\phi = K_\phi\phi + r_\phi\dot{\phi} \tag{2.5}$$

$$F_\theta = K_\theta\theta + r_\theta\dot{\theta} \tag{2.6}$$

$$F_\psi = K_\psi\psi + r_\psi\dot{\psi} \tag{2.7}$$

with K and r dependent on the gain and time constant of the eye plant. For the purposes of this thesis, K=1 and r=0.15. Now consider the relationship between the

attachment point positions and the general rotation matrix $\bar{R}$. Letting

$$\bar{R} = \begin{pmatrix} r_{11} & r_{12} & r_{13} \\ r_{21} & r_{22} & r_{23} \\ r_{31} & r_{32} & r_{33} \end{pmatrix} \tag{2.8}$$

The locations of the attachment points become

$$\begin{pmatrix} x_G \\ y_G \\ z_G \end{pmatrix} = \begin{pmatrix} r_{11} \\ r_{21} \\ r_{31} \end{pmatrix} \quad \text{and} \quad \begin{pmatrix} x_\psi \\ y_\psi \\ z_\psi \end{pmatrix} = \begin{pmatrix} -r_{12} \\ -r_{22} \\ -r_{32} \end{pmatrix} \tag{2.9}$$

To examine how these change as the eye rotates, let $R_{\omega\Delta t}$ be a matrix corresponding to a rotation $\omega\Delta t$ about general axis $(\omega_x, \omega_y, \omega_z)/\mid \vec{\omega} \mid$. Then the instantaneous rate of change of the attachment points with time will be described by:

$$\begin{pmatrix} \dot{x_G} \\ \dot{y_G} \\ \dot{z_G} \end{pmatrix} = \lim_{\Delta t \to 0} \frac{\left\{ \bar{R}_{\omega\Delta t}\bar{R} \begin{pmatrix} 1 \\ 0 \\ 0 \end{pmatrix} - \bar{R} \begin{pmatrix} 1 \\ 0 \\ 0 \end{pmatrix} \right\}}{\Delta t} \tag{2.10}$$

and

$$\begin{pmatrix} \dot{x_\psi} \\ \dot{y_\psi} \\ \dot{z_\psi} \end{pmatrix} = \lim_{\Delta t \to 0} \frac{\left\{ \bar{R}_{\omega\Delta t}\bar{R} \begin{pmatrix} 0 \\ -1 \\ 0 \end{pmatrix} - \bar{R} \begin{pmatrix} 0 \\ -1 \\ 0 \end{pmatrix} \right\}}{\Delta t} \tag{2.11}$$

for current orientation $\bar{R}$ and current angular velocity $\vec{\omega}$. Combining the above equations, rewriting $\bar{R}_{\omega\Delta t}$ with the expression given by Spong and Vidyasagar for a general

rotation matrix in terms of its angle and rotation axis [108] (see Appendix A), expanding the matrices into their individual components, and taking the limit as Δt approaches zero,

$$\frac{d}{dt}\begin{pmatrix}\psi\\ \theta\\ \phi\end{pmatrix} = \begin{pmatrix}\frac{-r_{22}}{\cos\psi} & \frac{r_{12}}{\cos\psi} & 0\\ \frac{r_{21}}{\cos\theta} & \frac{-r_{11}}{\cos\theta} & 0\\ \frac{-r_{31}}{\cos\phi} & 0 & \frac{r_{11}}{\cos\phi}\end{pmatrix}\begin{pmatrix}\omega_x\\ \omega_y\\ \omega_z\end{pmatrix} = \bar{T}\begin{pmatrix}\omega_x\\ \omega_y\\ \omega_z\end{pmatrix} \tag{2.12}$$

Here, the relations $\frac{dy_G}{dt} = \cos\phi\frac{d\phi}{dt}$, $\frac{dz_G}{dt} = \cos\theta\frac{d\theta}{dt}$, and $\frac{dz_\psi}{dt} = \cos\psi\frac{d\psi}{dt}$ have been substituted in for $\frac{dy_G}{dt}$, $\frac{dz_G}{dt}$, and $\frac{dz_\psi}{dt}$. To implement the model, it is necessary to express the orientation matrix $\bar{R}$ in terms of ϕ, θ, and ψ. From the definitions given earlier, $r_{21} = \sin\phi$, $r_{31} = \sin\theta$, and $r_{32} = -\sin\psi$. Using the fact that rotation matrices do not change the length of a position vector, six equations relating the remaining components to r_{21}, r_{31}, and r_{32} can be found and solved (considering initial conditions and small rotations to determine ambiguous signs) to give:

$$r_{11} = \sqrt{1-(\sin\phi)^2-(\sin\theta)^2} \tag{2.13}$$

$$r_{12} = \frac{-r_{11}r_{31}r_{32} - r_{21}\sqrt{1-r_{31}^2-r_{32}^2}}{(\cos\theta)^2} \tag{2.14}$$

$$r_{22} = \frac{-r_{21}r_{31}r_{32} + r_{11}\sqrt{1-r_{31}^2-r_{32}^2}}{(\cos\theta)^2} \tag{2.15}$$

as well as expressions for r_{13}, r_{23} and r_{33}, though these are not included here since they don't enter into model calculations. Using a unilateral version of the feedback filter model, the model is as shown in Figure 2.1. $\bar{H}$ is $\frac{1}{0.15s+1}\bar{K}$, where $\bar{K}$ is a diagonal matrix. Note that the input is scaled by $\frac{0.15}{K} = \frac{0.15}{(1-\frac{0.15}{T_D})}$ to get a position gain of 1 for desired time constant T_D (for large T_D this approaches 0.15). If the three pathways

have different time constants, the scaling is represented by a diagonal matrix $\bar{I}_0$ after the T matrix. This yields $\vec{F} = \bar{H}\vec{F} + \bar{I}_0\bar{T}\vec{X}$, which gives $\vec{F}$ a velocity component $\frac{0.15\bar{T}_{i,1..3}}{K_{ii}}\vec{X}$ and an integrated component with a time constant $\frac{0.15}{(1-K_{ii})}$, where K_{ii} is the feedback filter coefficient for the pathway under consideration.

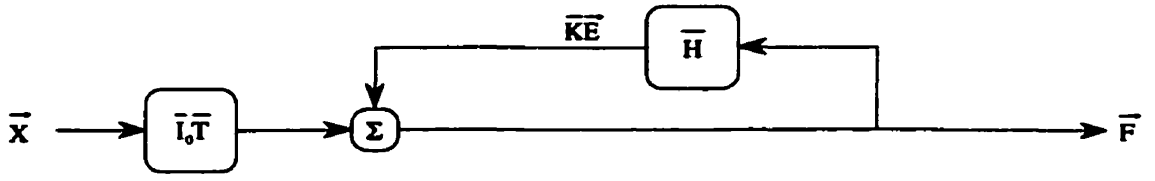

Figure 2.1: 3D monocular model, first form. $\bar{T}$ is the position-dependent matrix of equation 2.12 .

To check that the model was tracking the correct orientation, the integrator time constant was set at a high value (500s) and the model was simulated with small increments for a sequence of rotations about various axis. The results were compared to those determined using the rotation matrices of Spong and Vidyasagar, and found to agree as shown in Figure 2.2.

2.2.2 Second Representation

In this representation of position, $\phi = \Phi k_x$, $\theta = \Phi k_y$, and $\psi = \Phi k_x$, where the current orientation is a rotation Φ about axis $\hat{k} = k_x\hat{x} + k_y\hat{y} + k_z\hat{z}$. Using the expressions of Spong and Vidyasagar (see Appendix A), ϕ, θ, and ψ can be re-expressed in terms of the components of the general rotation matrix $\bar{R}$:

$$\begin{pmatrix} \phi \\ \theta \\ \psi \end{pmatrix} = \frac{\Phi}{2\sin\Phi} \begin{pmatrix} r_{21} - r_{12} \\ r_{13} - r_{31} \\ r_{32} - r_{23} \end{pmatrix} \tag{2.16}$$

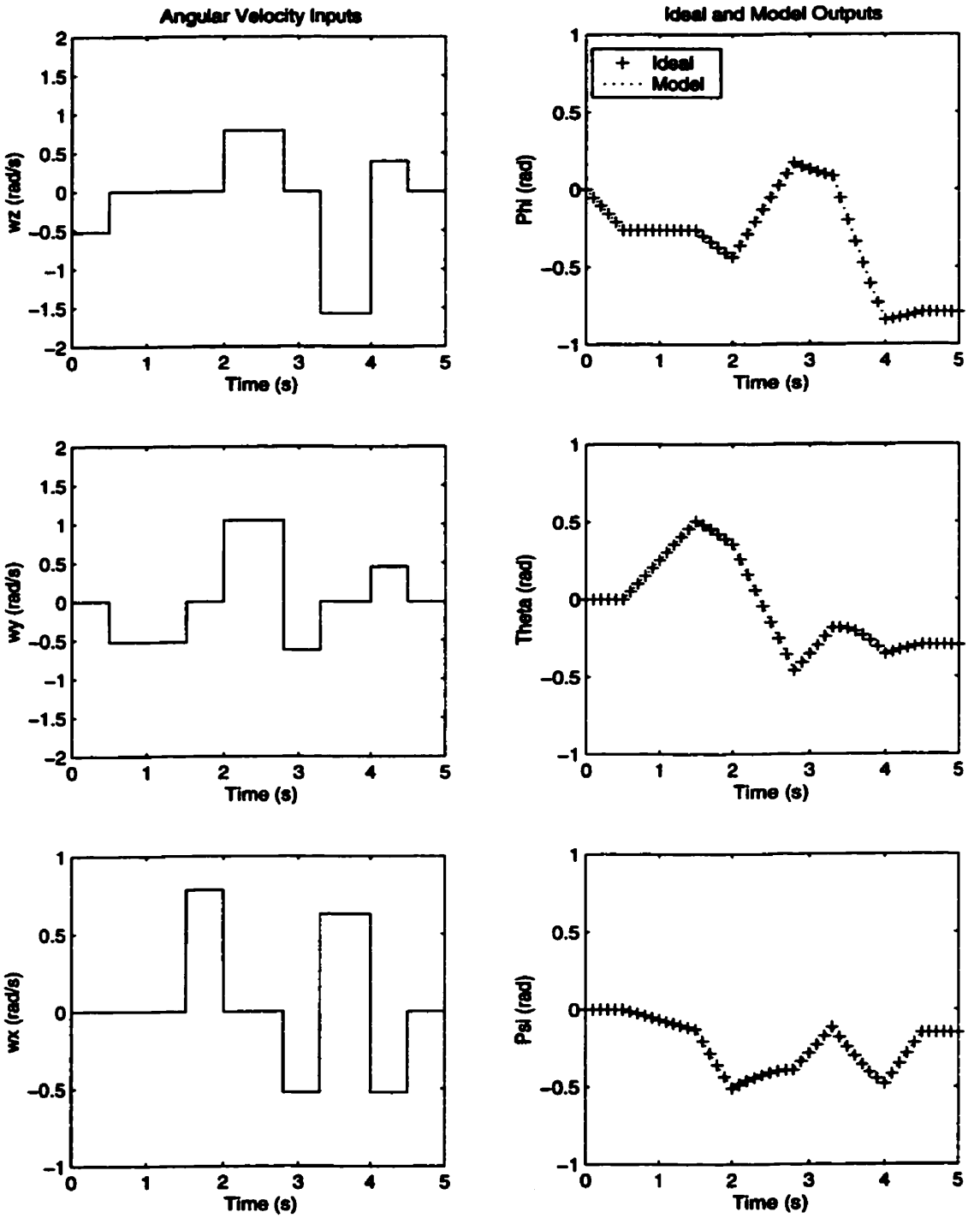

Figure 2.2: Testing model output for a sequence of rotations about various axes.

where

$$\Phi = \sqrt{\phi^2 + \theta^2 + \psi^2} = \arccos\left(\frac{r_{11} + r_{22} + r_{33} - 1}{2}\right). \tag{2.17}$$

Taking the derivative of $\bar{R}$ to be

$$\frac{d\bar{R}}{dt} = \lim_{\Delta t \to 0} \frac{\bar{R}_{\omega \Delta t}\bar{R} - \bar{R}}{\Delta t} = \begin{pmatrix} 0 & -\omega_z & \omega_y \\ \omega_z & 0 & -\omega_x \\ -\omega_y & \omega_x & 0 \end{pmatrix} \bar{R}, \tag{2.18}$$

and expressing the components of $\bar{R}$ in terms of ϕ, θ, and ψ, the derivatives of ϕ, θ, and ψ can be solved for in terms of current angular velocity $\vec{\omega} = \omega_x\hat{x} + \omega_y\hat{y} + \omega_z\hat{z}$ to give

$$\begin{pmatrix} \dot{\psi} \\ \dot{\theta} \\ \dot{\phi} \end{pmatrix} = \bar{T} \begin{pmatrix} \omega_x \\ \omega_y \\ \omega_z \end{pmatrix} = \begin{pmatrix} 1 & \frac{\phi}{2} & -\frac{\theta}{2} \\ -\frac{\phi}{2} & 1 & \frac{\psi}{2} \\ \frac{\theta}{2} & -\frac{\psi}{2} & 1 \end{pmatrix} \begin{pmatrix} \omega_x \\ \omega_y \\ \omega_z \end{pmatrix} + \tag{2.19}$$

$$\frac{(1 - \frac{\Phi}{2}\cot(\frac{\Phi}{2}))}{\Phi^2} \begin{pmatrix} -(\theta^2 + \phi^2) & \psi\theta & \psi\phi \\ \theta\psi & -(\psi^2 + \phi^2) & \theta\phi \\ \phi\psi & \phi\theta & -(\psi^2 + \theta^2) \end{pmatrix} \begin{pmatrix} \omega_x \\ \omega_y \\ \omega_z \end{pmatrix}.$$

Although this expression looks complicated, the position dependencies cancel to give the identity matrix if the current angular velocity is about the same axis as the current orientation. For angular velocities about other axes, there is partial cancellation.

Thus, for both orientation representations, the 3D extension of the 1D model can be achieved with a model of the form shown in Figure 2.1, the only difference being the nature of the position dependencies in the $\bar{T}$ matrix. In primary orientation, the

$\bar{T}$ matrix reduces to the identity matrix in both cases (discounting signs, which merely indicate the chosen definitions for positive rotations about a given axis). This reflects the collapse of $\dot{\psi}$, $\dot{\theta}$, and $\dot{\phi}$ to torsional, vertical, and horizontal angular velocities respectively.

2.2.3 Effect of Orientation Representation

To illustrate the relevance of orientation representation, consider a non-ideal integrator, with vertical and horizontal variable time constants of 30s, but a torsional variable time constant of 2s. The 30s time constant is used for illustrative purposes because it falls within the range of experimentally determined gaze-holding values, but the effects of representation would also be observed for other values. Figure 2.3 shows the results for the cases where the first and second representations are used to implement the model. The second representation results have been re-expressed in terms of the first representation for comparison. The plots labeled 'Ideal' in Figure 2.3 and in subsequent illustrations show the output of a perfect (infinite time constant) integrator. The vertical line in the three position plots indicates when the external input goes to zero.

The differences result from the fact that in the first representation, the torsional variable is $\arcsin\left(k_y k_z(1-\cos\Phi)+k_x\sin\Phi\right)$ rather than $k_x\Phi$ for the second representation. This makes no difference for the case where all three variables decay at the same rate, but does affect the results when the time constants vary. To determine the expected effects, consider the decay of ϕ, θ, and ψ in the two representations. For

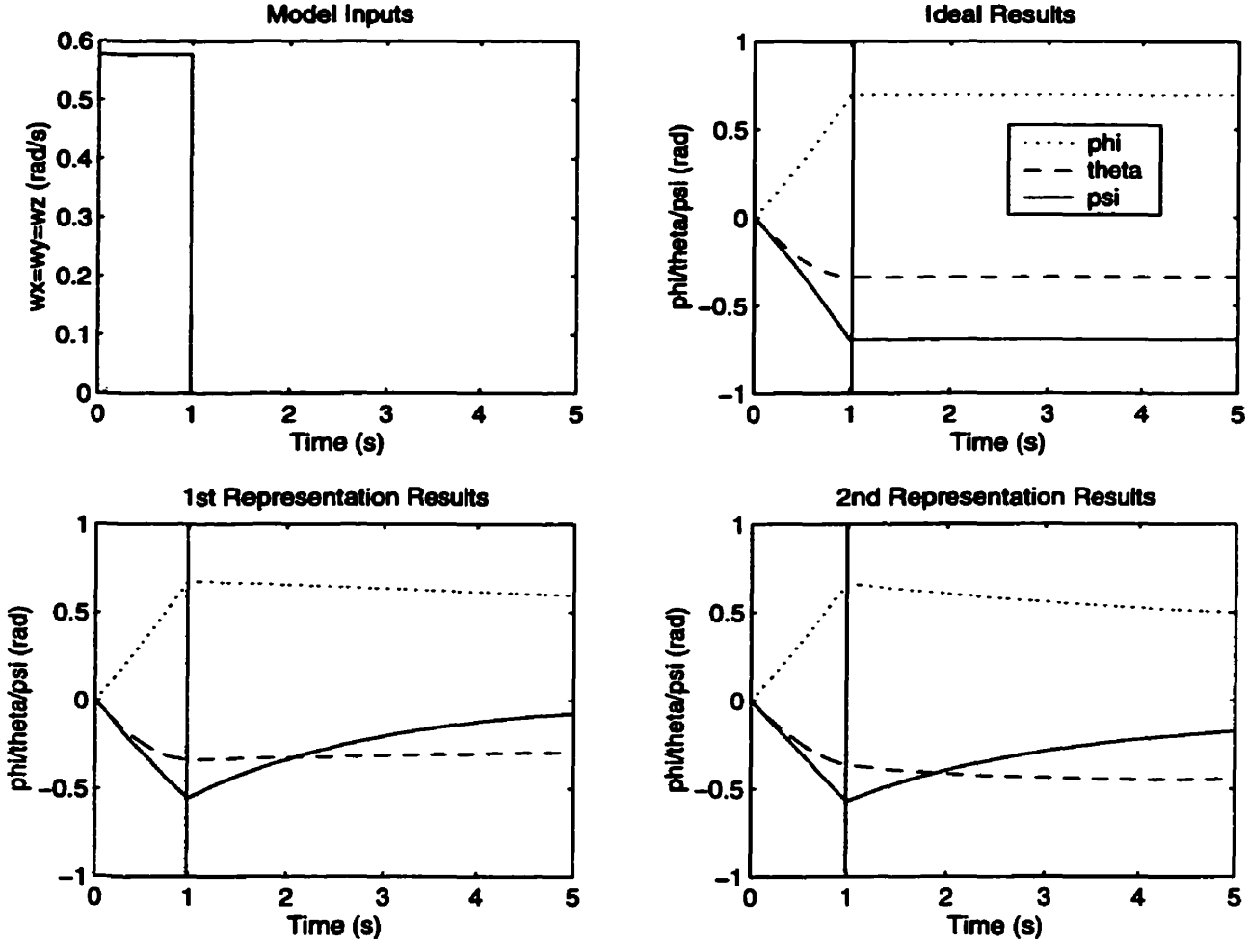

Figure 2.3: Demonstration of the effects of different orientation representations for the case where the vertical and horizontal time constants are 30s, but the torsional constant is 2s. All results are expressed in terms of the first representation.

zero input, the cross-talk between pathways disappears, and the position variables decay independently:

$$\phi_{new} = \phi_0 \exp(-t/\tau_\phi) \tag{2.20}$$

$$\theta_{new} = \theta_0 \exp(-t/\tau_\theta) \tag{2.21}$$

$$\psi_{new} = \psi_0 \exp(-t/\tau_\psi)\ . \tag{2.22}$$

In the first representation,

$$\phi = \arcsin(k_x k_y(1-\cos\Phi) + k_z \sin\Phi) \tag{2.23}$$

$$\theta = \arcsin(k_x k_z(1-\cos\Phi) - k_y \sin\Phi) \tag{2.24}$$

$$\psi = -\arcsin(k_y k_z(1-\cos\Phi) + k_x \sin\Phi)\ . \tag{2.25}$$

Now consider re-representing the second representation variables in terms of the first representation. The general axis-angle description for the new position is:

$$\hat{k}_{new} = \frac{(\exp(-t/\tau_\psi)k_x\hat{x} + \exp(-t/\tau_\theta)k_y\hat{y} + \exp(-t/\tau_\phi)k_z\hat{z})}{\sqrt{\exp(-2t/\tau_\psi)k_x^2 + \exp(-2t/\tau_\theta)k_y^2 + \exp(-2t/\tau_\phi)k_z^2}} \tag{2.26}$$

$$\Phi_{new} = \Phi_0\sqrt{\exp(-2t/\tau_\psi)k_x^2 + \exp(-2t/\tau_\theta)k_y^2 + \exp(-2t/\tau_\phi)k_z^2} \tag{2.27}$$

If these values are substituted back into the first representation, the $k_x k_y(1-\cos\Phi)$ component of ϕ and the $k_x k_z(1-\cos\Phi)$ component of θ will decay faster than they would in the original representation. As the $k_x k_y(1-\cos\Phi)$ component has the same sign as the $k_x \sin\Phi$ component in the illustrated case, ϕ appears to decay faster than it should. In the case of θ, the two contributions are of opposite signs, and θ actually

becomes more negative as the opposing positive contribution decays faster than the $-k_y \sin\Phi$ contribution. ψ appears to decay at a similar rate in both cases, but to an offset in the second representation. The apparent offset is actually the contribution of the $k_y k_z(1-\cos\Phi)$ term, which is decaying, but with a much slower time constant.

2.3 Alternate Forms of the Model

The above model can be implemented in other ways without altering its input or output. Although it is not linear, the nonlinearities are dealt with entirely by the position dependent gains of the $\bar{T}$ matrix. If the model is frozen at any instant, the structure appears linear and, with caution, can be thought of in terms of transfer functions. Now consider the structure shown in Figure 2.4.

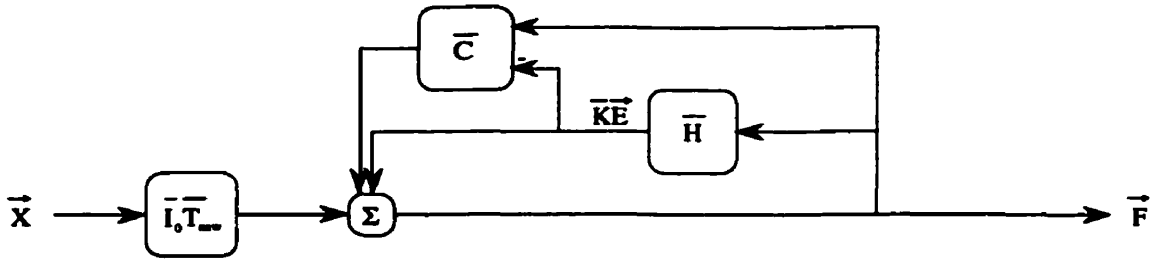

Figure 2.4: 3D monocular model, second form.

If $\bar{C} = \bar{I} - \bar{I}_0\bar{T}_{new}(\bar{I}_0\bar{T})^{-1}$ for any given position, where $\bar{I}$ denotes the identity matrix, this gives the instantaneous equation:

$$\vec{F} = \bar{I}_0\bar{T}_{new}\vec{X} + (\bar{I} - \bar{I}_0\bar{T}_{new}(\bar{I}_0\bar{T})^{-1})(F - \bar{H}\vec{F}) + \bar{H}\vec{F} \tag{2.28}$$

where $\bar{H} = \frac{K}{(0.15s+1)}$, which simplifies to

$$\bar{I}_0\bar{T}_{new}(\bar{I}_0\bar{T})^{-1}\vec{F} = \bar{I}_0\bar{T}_{new}\vec{X} + \bar{I}_0\bar{T}_{new}(\bar{I}_0\bar{T})^{-1}\bar{H}\vec{F} \tag{2.29}$$

Multiplying through both sides by $\bar{I}_0\bar{T}(\bar{I}_0\bar{T}_{new})^{-1}$ gives the same equation (and transfer function for $\vec{F}$) as the original model. This form is interesting in that it allows some or all of the position dependencies to be removed from feedforward and placed in feedback, with appropriate choice of T_{new}. This form would require a velocity component in the feedback loop for some non-primary orientations. It also assumes there are no delays in the system- slight errors would be introduced for uncompensated delays in an actual implementation. It should be noted that having identical instantaneous frequency-domain equations is not sufficient for ensuring correct results; the nonlinearities must encounter the same dynamic elements for both forms (for the above case this holds).

For this thesis, $\bar{T}_{new}$ was chosen to be the primary orientation value of $\bar{T}$, ie. from Figure 2.4, $\bar{T}_{new} = \bar{T}_{\phi,\theta,\psi=0}$. Figure 2.5 shows the net feedback input to the summing junction for the horizontal pathway for various values of vertical eye position and angular eye velocities plotted versus horizontal eye position, assuming the first orientation representation. Thus, this alternate model form predicts position-dependent velocity sensitivity changes in output firing rate as before, but additionally imbeds these changes in a feedback pathway rather than on the direct feedforward projection. This leads to position-dependent velocity sensitivities in the feedback pathway as well as at the output level. It is interesting to note that the feedback contribution to the diagonal component depends only on the magnitude of θ, not on its direction. Some neurons in the VN and INC, known as type III neurons, display the rectified behaviour that might be expected in this case ([71], [28]).

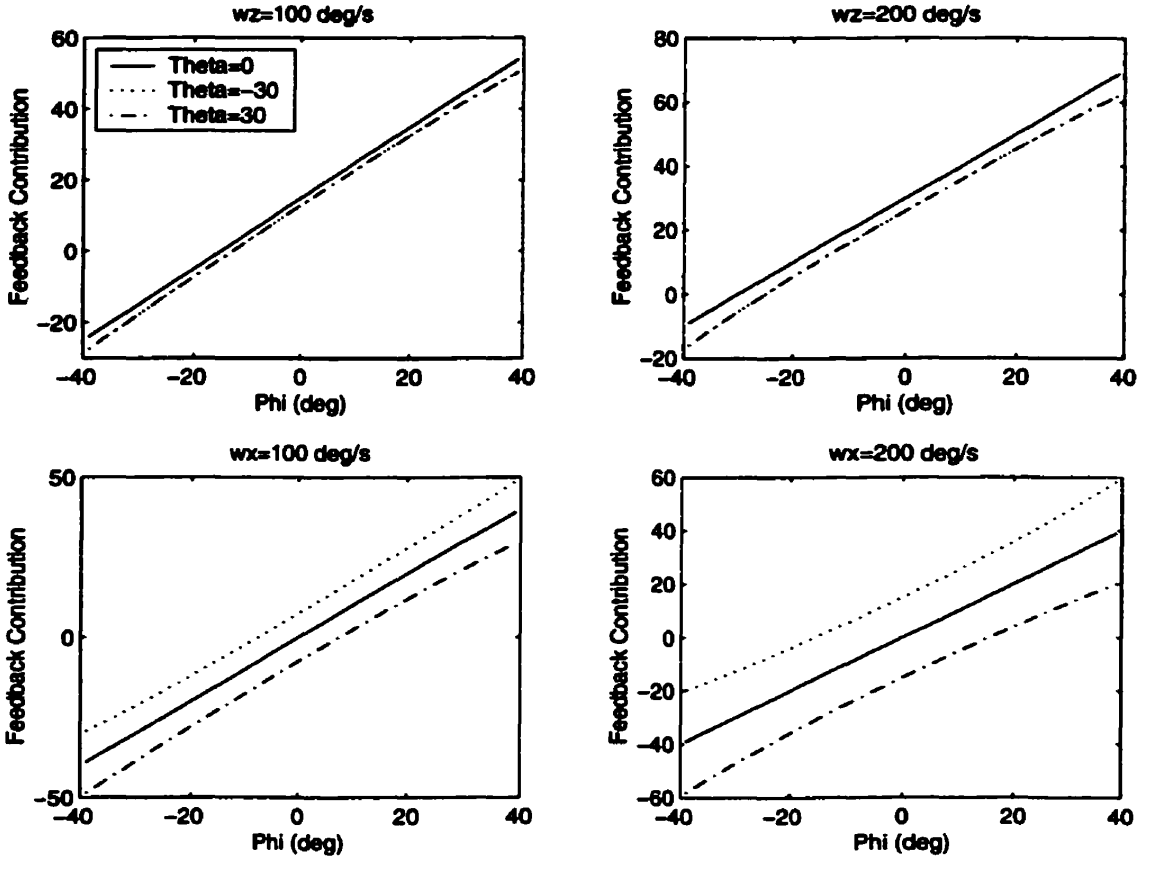

Figure 2.5: Feedback contribution to horizontal pathway for various positions and angular velocities, 1st representation, 2nd model form.

2.4 A Commutative Variation

The models developed here assume that the brainstem will account for the non-commutativity of rotations. The feedback filter integrator model is not limited to this approach, however. Consider the first structure with $\bar{T} = \bar{M}\bar{D}$ and $\bar{H} = \bar{C}_p\bar{G}_p(\bar{D}s + (\bar{C}_p\bar{G}_p - \bar{H}_p\bar{D}))^{-1}$, where $\bar{C}_p$, $\bar{G}_p$, $\bar{D}$, $\bar{H}_p$ and $\bar{M}$ are the matrices of the Schnabolk/Raphan model (Figure 1.7). This form of Figure 2.1 should give results identical to those of the Schnabolk/Raphan model when interpreted using the second representation, but uses a different internal structure. Schnabolk and Raphan focused on 3D saccadic eye movements, where the input is assumed to come from burst neurons, known to encode the derivative of eye orientation. However, because the canal afferents encode angular velocity rather than the derivative of eye orientation, this form would not be a viable option for the VOR and was not investigated further (see section 1.5.5 of chapter 1).

Chapter 3

Bilateral Extension of the Model

Chapter two presented a monocular (conjugate) form for central VOR processing that uses a feedback filter instead of the standard feedforward integrator used in other three-dimensional models of VOR integration. This chapter will consider bilateral extensions of this monocular model. The first sections describe how the two model forms were extended to the bilateral case, and the third section investigates the model output for various parameter values and for some artificial lesions. Simulations were conducted using the first orientation representation, although the analysis is general and applies to both representations. The details of the position dependencies will vary with representation. This thesis considers mainly conjugate eye movement.

3.1 Extension of the First Form

The first suggested form for the three-dimensional integrator is much like three parallel one-dimensional integrators, the only difference being the position dependence of the

primary afferent contribution. This suggests that a logical bilateral extension of this model form would be as shown in Figure 3.1.

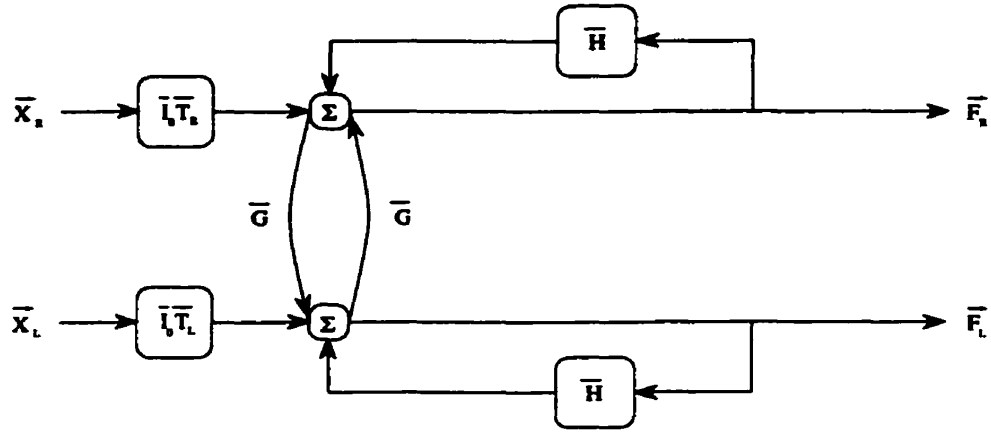

Figure 3.1: Bilateral 3D model, first form (afferent projection nonlinearity).

$\bar{H}$ is the same as in the monocular 3D case and $\bar{G}$ is a diagonal scalar matrix since there is no cross-talk after the initial position dependent gains. Here, $\bar{T}_L$ and $\bar{T}_R$ are the $\bar{T}$ matrix of the monocular form, calculated with ϕ_L, θ_L, ψ_L and ϕ_R, θ_R, ψ_R respectively. $\vec{X}_R$ and $\vec{X}_L$ are the right and left canal inputs. This model now follows the equations

$$\vec{F}_R = \bar{I}_0\bar{T}_R\vec{X}_R + \bar{H}\vec{F}_R + \bar{G}\vec{F}_L \tag{3.1}$$

$$\vec{F}_L = \bar{I}_0\bar{T}_L\vec{X}_L + \bar{H}\vec{F}_L + \bar{G}\vec{F}_R \tag{3.2}$$

For normal canal inputs in the VOR, $\vec{X}_R = (\omega_x, \omega_y, \omega_z)^T$ and $\vec{X}_L = (-\omega_x, \omega_y, -\omega_z)^T$ for a head angular velocity of $-(\omega_x\hat{x}, \omega_y\hat{y}, \omega_z\hat{z})^T$. Note that the two sides of the model inhibit each other for ϕ and ψ, but excite each other for θ. The necessary extraocular muscle commands for conjugate movement are equal and opposite for movement about the x and z axes, but equal for movement about the y axis because of the

mirror symmetry of the muscles across the midline (the x-z plane). In the actual VOR, this excitation is more likely accomplished by mutual inhibition of CW-up and CCW-down and CCW-up and CW-down integrators of opposing sides, but this was represented in this model by mutually exciting vertical and mutually inhibiting torsional integrators for simplicity.

For notational simplicity in some of the following calculations, $\bar{K}$ and $\bar{G}$ will sometimes be broken down as follows:

$$\bar{K} = \begin{pmatrix} k_\psi & 0 & 0 \\ 0 & k_\theta & 0 \\ 0 & 0 & k_\phi \end{pmatrix} \tag{3.3}$$

$$\bar{G} = \begin{pmatrix} -1 & 0 & 0 \\ 0 & 1 & 0 \\ 0 & 0 & -1 \end{pmatrix} \begin{pmatrix} g_\psi & 0 & 0 \\ 0 & g_\theta & 0 \\ 0 & 0 & g_\phi \end{pmatrix} = \begin{pmatrix} -1 & 0 & 0 \\ 0 & 1 & 0 \\ 0 & 0 & -1 \end{pmatrix} \bar{g} \tag{3.4}$$

Referring to the calculations in 1.4.2,

$$\bar{K} = (1 - \frac{0.15}{T_D}) \begin{pmatrix} 1 - g_\psi & 0 & 0 \\ 0 & 1 - g_\theta & 0 \\ 0 & 0 & 1 - g_\phi \end{pmatrix} \tag{3.5}$$

should give a conjugate movement time constant of T_D in each pathway. The $\bar{I}_0$ matrices must be changed to allow different g's for the three pathways:

$$I_0 = \begin{pmatrix} \frac{0.15(1-g_\psi)K_D}{(1-\frac{0.15}{T_{D\psi}})} & 0 & 0 \\ 0 & \frac{0.15(1-g_\theta)K_D}{(1-\frac{0.15}{T_{D\theta}})} & 0 \\ 0 & 0 & \frac{0.15(1-g_\phi)K_D}{(1-\frac{0.15}{T_{D\phi}})} \end{pmatrix} \tag{3.6}$$

where K_D is the desired difference-mode (conjugate movement) gain.

It should be noted that it is actually *necessary* that one set of pathways be effectively mutually exciting. This is because of the result that the sequence of rotations ϕ_1 about $-\hat{k}_1$ and ϕ_2 about $-\hat{k}_2$ does not in general give a net rotation that is the negative of that given by the sequence ϕ_1 about $\hat{k}_1$ and ϕ_2 about $\hat{k}_2$. Thus, a bilateral model where one side is tracking position for rotations $\Phi_i\hat{k}_i$ and the other tracking for $-\Phi_i\hat{k}_i$ will fail. However, a sequence of rotations Φ_i about $(-k_{xi}, k_{yi}, -k_{zi})^T$ will yield a result Φ_{net} about $(-k_{xnet}, k_{ynet}, -k_{znet})^T$, where Φ_{net} about $(k_{xnet}, k_{ynet}, k_{znet})^T$ is generated by the sequence of rotations Φ_i about $(k_{xi}, k_{yi}, k_{zi})^T$, $i = 1...N$. Thus, a bilateral model which tracks $\Phi(-k_x, k_y, -k_z)$ on one side and $\Phi(k_x, k_y, k_z)$ on the other with mutually inhibiting x and z pathways and mutually exciting y pathways should work. Tracking with $\Phi(k_x, -k_y, -k_z)$ or $\Phi(-k_x, -k_y, k_z)$ could also work, but these would not be appropriate in this case, as the extraocular muscle symmetry is about the xz plane. Although the first representation tracks

$$\phi = \arcsin\left(k_x k_y(1-\cos\Phi) + k_z \sin\Phi\right) \tag{3.7}$$

$$\theta = \arcsin\left(k_x k_z(1-\cos\Phi) - k_y \sin\Phi\right) \tag{3.8}$$

$$\psi = -\arcsin\left(k_y k_z(1-\cos\Phi) + k_x \sin\Phi\right) \tag{3.9}$$

the overall tracking is the same because

$$\arcsin\left(k_x k_y v_\Phi + k_z \sin\Phi\right) = -\arcsin\left((-k_x)k_y v_\Phi + (-k_z)\sin\Phi\right) \tag{3.10}$$

$$\arcsin\left(k_x k_z v_\Phi - k_y \sin\Phi\right) = \arcsin\left((-k_x)(-k_z)v_\Phi - k_y \sin\Phi\right) \tag{3.11}$$

$$\arcsin\left(k_y k_z v_\Phi + k_x \sin\Phi\right) \;=\; -\arcsin\left(k_y(-k_z)v_\Phi + (-k_x)\sin\Phi\right) \tag{3.12}$$

where v_Φ denotes $(1-\cos\Phi)$. This property has implications for vergence (disconjugate) movements as well. Torsional and horizontal vergence movements would result from having both sides track $\Phi(k_x, k_y, k_z)^T$. However, vertical vergence movements in addition to horizontal and torsional (ie. one side tracking $\Phi(k_x, -k_y, k_z)^T$) would again bring up the problem of the net rotations not maintaining the same form as the individual ones relative to the side tracking $\Phi(k_x, k_y, k_z)^T$. This will not be considered further here, but would be relevent in extending this model to include other types of eye movement.

To examine the bilateral model output, define two new difference and common modes $\vec{X}_D$ and $\vec{X}_C$:

$$\vec{X}_D = \frac{\bar{T}_R\vec{X}_R - \begin{pmatrix} 1 & 0 & 0 \\ 0 & -1 & 0 \\ 0 & 0 & 1 \end{pmatrix}\bar{T}_L\vec{X}_L}{2} \tag{3.13}$$

$$\vec{X}_C = \frac{\bar{T}_R\vec{X}_R + \begin{pmatrix} 1 & 0 & 0 \\ 0 & -1 & 0 \\ 0 & 0 & 1 \end{pmatrix}\bar{T}_L\vec{X}_L}{2} \tag{3.14}$$

This gives an output:

$$\vec{F}_R = \frac{0.15(1-\bar{g})K_D\vec{X}_C}{(1-\frac{0.15}{T_D})(1+\bar{g})} + \frac{0.15(1-\bar{g})^2K_D\vec{X}_C}{(1+\bar{g})(0.15(1+\bar{g})s+(1+\bar{g}-\bar{K}))} + \frac{0.15K_D\vec{X}_D}{(1-\frac{0.15}{T_D})} + \frac{0.15(1-\bar{g})K_D\vec{X}_D}{(0.15(1-\bar{g})s+(1-\bar{g}-\bar{K}))} \tag{3.15}$$

and

$$\vec{F}_L = \begin{pmatrix} 1 & 0 & 0 \\ 0 & -1 & 0 \\ 0 & 0 & 1 \end{pmatrix} \left[\frac{0.15(1-\bar{g})K_D\vec{X}_C}{(1-\frac{0.15}{T_D})(1+\bar{g})} + \frac{0.15(1-\bar{g})^2K_D\vec{X}_C}{(1+\bar{g})(0.15(1+\bar{g})s+(1+\bar{g}-\bar{K}))} - \frac{0.15K_D\vec{X}_D}{(1-\frac{0.15}{T_D})} - \frac{0.15(1-\bar{g})K_D\vec{X}_D}{(0.15(1-\bar{g})s+(1-\bar{g}-\bar{K}))} \right] \tag{3.16}$$

which, for $T_D \gg 1$ and $K_D = 1$, gives:

$$\vec{F}_R = \frac{0.15(1-\bar{g})}{(1+\bar{g})}\vec{X}_C + \frac{0.15(1-\bar{g})^2\vec{X}_C}{(1+\bar{g})(0.15(1+\bar{g})s+(1+\bar{g}-\bar{K}))} + 0.15\vec{X}_D + \frac{X_D}{s} \tag{3.17}$$

$$\vec{F}_L = \begin{pmatrix} 1 & 0 & 0 \\ 0 & -1 & 0 \\ 0 & 0 & 1 \end{pmatrix} \left[\frac{0.15(1-\bar{g})}{(1+\bar{g})} \vec{X}_C \right. \tag{3.18}$$
$$+ \frac{0.15(1-\bar{g})^2 \vec{X}_C}{(1+\bar{g})(0.15(1+\bar{g})s + (1+\bar{g}-\bar{K}))}$$
$$\left. -0.15\vec{X}_D - \frac{\vec{X}_D}{s} \right] .$$

For strictly conjugate movement when the eyes have identical starting positions, T_R and T_L change together such that only the X_D mode is activated and the bilateral model output is the same as that of the monocular case. If there are mixed modes in the input or if the eyes have different starting positions, T_R and T_L will not change in a complementary fashion, and deviations from the monocular model occur. The relative weights of g and K can be different for each dimensional pathway without affecting X_D mode output, provided g and K are chosen such that the overall X_D mode time constants $T_{D\phi} = \frac{0.15(1-g_\phi)}{(1-g_\phi-k_\phi)}$, $T_{D\theta} = \frac{0.15(1-g_\theta)}{(1-g_\theta-k_\theta)}$, and $T_{D\psi} = \frac{0.15(1-g_\psi)}{(1-g_\psi-k_\psi)}$ of each pathway are identical.

3.2 Extension of the Second Form

The extension of the feedback position-dependent form is a bit more complicated than the feedforward case. With the $\bar{C}_L$ and $\bar{C}_R$ matrices recalculated with the new values of $\bar{I}_0$, scalar cross-midline gains yield:

$$\vec{F}_R = \bar{I}_0 \bar{T}_R \vec{X}_R + \bar{H}\vec{F}_R + \bar{I}_0 \bar{T}_R (\bar{I}_0 \bar{T}_0)^{-1} \bar{G} \vec{F}_L \tag{3.19}$$

$$\vec{F}_L = \bar{I}_0\bar{T}_L\vec{X}_L + \bar{H}\vec{F}_L + \bar{I}_0\bar{T}_L(\bar{I}_0\bar{T}_0)^{-1}\bar{G}\vec{F}_R \tag{3.20}$$

instead of

$$\vec{F}_R = \bar{I}_0\bar{T}_R\vec{X}_R + \bar{H}\vec{F}_R + \bar{G}\vec{F}_L \tag{3.21}$$

$$\vec{F}_L = \bar{I}_0\bar{T}_L\vec{X}_L + \bar{H}\vec{F}_L + \bar{G}\vec{F}_R \tag{3.22}$$

for the first form. However, if $\bar{G}_{LtoR} = \bar{I}_0\bar{T}_0(\bar{I}_0\bar{T}_R)^{-1}\bar{G}$ and $\bar{G}_{RtoL} = \bar{I}_0\bar{T}_0(\bar{I}_0\bar{T}_L)^{-1}\bar{G}$ the equations reduce to those of the first model form. With this modification, the output of the second form of the model is now the same as the output of the first. Figure 3.2 shows the second bilateral model form.

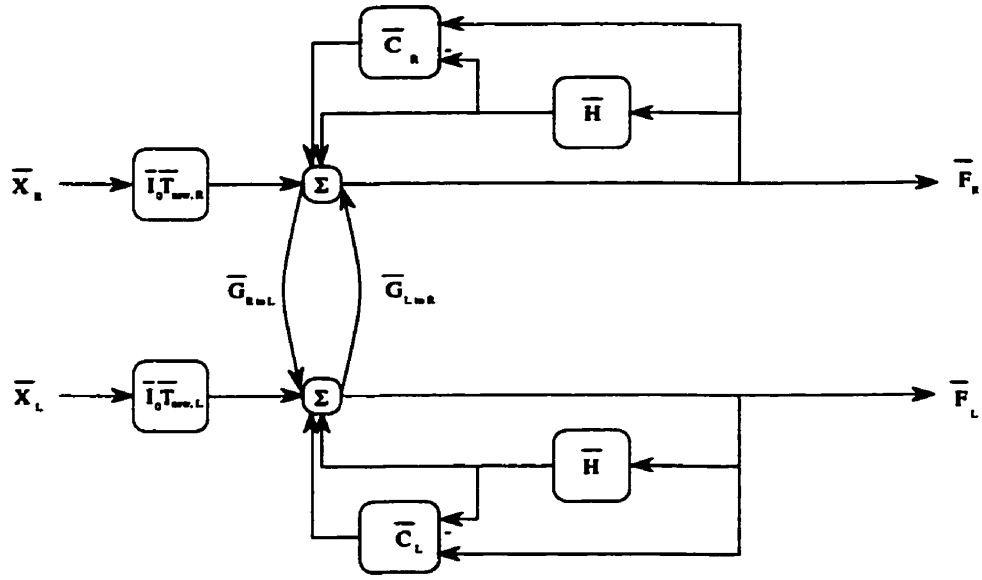

Figure 3.2: Bilateral 3D model, second form (central feedback nonlinearity).

The output of the second (central feedback nonlinearity) model form under normal conditions should be the same as that of the first (primary afferent nonlinearity) form for identical parameter values. This can now be used as an exploration base to

examine predictions regarding the effect of localized lesions.

3.3 Effects of Parameter Variation and Lesion

3.3.1 Effects of Commissural Gains on Time Constants

For parameter variation, the first and second forms of the model give the same results, as they were designed to have the same transfer function in non-lesion conditions. The difference mode time constant is a function of g and k:

$$T_D = \frac{0.15(1-g)}{(1-g-k)} \tag{3.23}$$

The integrator's response to common-mode input can be varied without affecting the conjugate response via the relative weightings of g and k, provided the input is scaled properly. For a given g,

$$T_C = \frac{0.15(1+g)}{(1+g-k)} \tag{3.24}$$

or, in terms of the difference mode time constant T_D,

$$T_C = \frac{0.15(1+g)T_D}{2T_D g + 0.15(1-g)} \tag{3.25}$$

Figure 3.3 shows how T_C decreases as a function of g for constant $T_D = 30s$. The common mode gain also decreases with increasing g, its velocity component gain varying as $\frac{(1-g)}{(1+g)}$ and its position component gain with $\frac{(1-g)^2}{(1+g)^2}$ (see Equations 3.17 and 3.18).

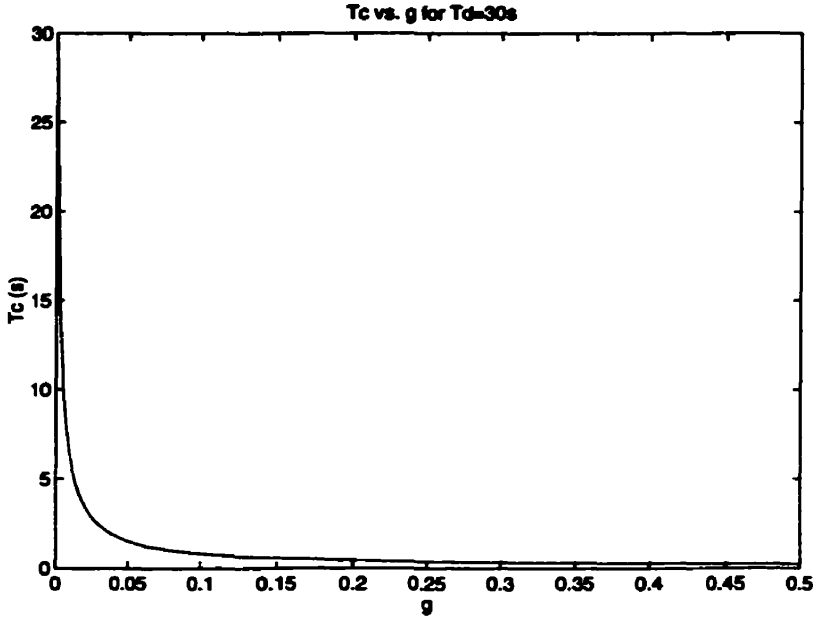

Figure 3.3: Common mode time constant as a function of g for a difference mode time constant of 30s (both model forms).

3.3.2 Sensory Projection Pattern Anomalies

Although this thesis is largely concerned with conjugate movement, the following analysis and figures are included to give an idea of what might be expected in the case of malfunctioning sensors. Figure 3.4 displays the output of the model for the case where the horizontal and torsional inputs increase together. This is an artificial condition that wouldn't occur for normal sensor function, but was chosen to demonstrate the lower time constant of $\vec{X_C}$ mode inputs. Such a situation might arise in abnormal conditions if input pathways were crossed. The results were plotted along with the kinematically correct tracking of the right side inputs for comparison. The parameter values are K=0.74625 and g=0.25 for all 3 coordinates.

The ϕ and ψ components of the output show reduced gain and faster decay, but the decay of the vertical response (dashed line, Figure 3.4) is unaffected. The gain

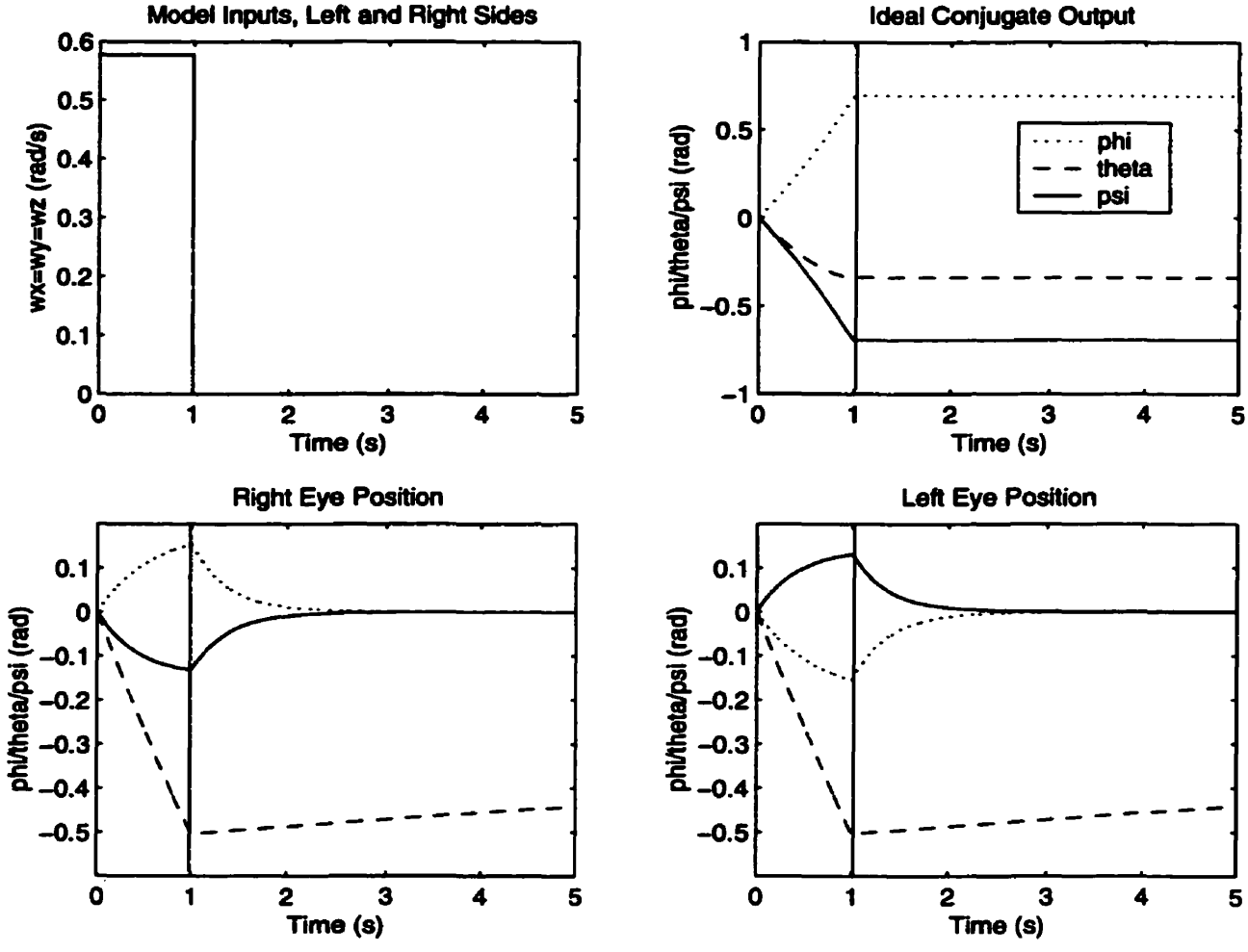

Figure 3.4: Model output when horizontal and torsional pathways are operating in vergence mode.

of the vertical response appears to be higher, reflecting the fact that the position-dependent desired vertical gain has changed because ϕ and ψ no longer have their original values. The ϕ and ψ components of the left and right eyes now have opposite directions.

3.3.3 Unilateral Labyrinthectomy

Figure 3.5 displays the output of the model for the case where the right inputs take their original values but the left inputs are zero. This is equivalent to the case where one set of canals is destroyed.

In this case, $\vec{X}_D = \vec{X}_C = \frac{\vec{T}_R \vec{X}_R}{2}$. The two sides should have a long time constant component from $\vec{X}_D$ with a magnitude of half that of the normal conjugate case. In addition, there should be a short time-constant contribution with components of opposing signs for the two sides. It is the latter contribution that leads to the initial slight rise in ϕ and ψ magnitude for the left eye just after the external input goes to zero in Figure 3.5. The common mode component decays quickly, such that the decrease in this opposing contribution temporarily outweighs the decay of the difference mode contribution to give a net increase in magnitude. The right eye shows complementary dips in output magnitude. The dips are small relative to the overall response, a reflection of the reduced gain and time constant of the common mode.

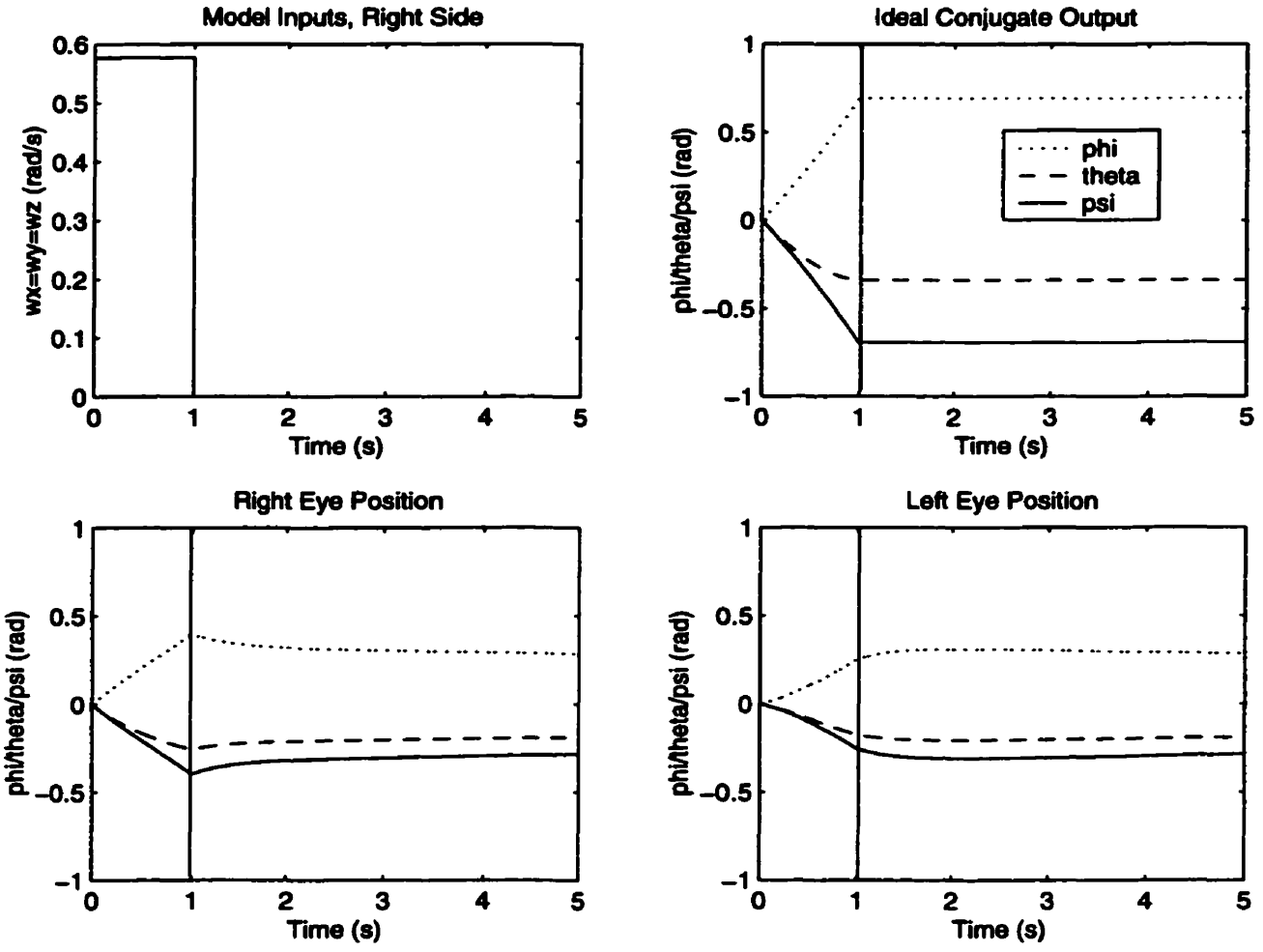

Figure 3.5: Model output for the case where there are only unilateral inputs.

3.3.4 Commissural Implications

If the commissural connections of the model are cut, the integrator reduces to the monocular case with a smaller position gain and time constant $\frac{0.15}{(1-K_{ii})}$ for pathways i=1..3 of both model forms. This can be seen by setting the cross-term contributions to zero. In the feedforward case,

$$\vec{F}_R = \bar{I}_0\bar{T}_R\vec{X}_R + \bar{H}\vec{F}_R \qquad \text{or} \qquad \vec{F}_R = \frac{\bar{I}_0\bar{T}_R\vec{X}_R(0.15s+1)}{0.15s+(1-\bar{K})} \tag{3.26}$$

$$\vec{F}_L = \bar{I}_0\bar{T}_L\vec{X}_L + \bar{H}\vec{F}_L \qquad \text{or} \qquad \vec{F}_L = \frac{\bar{I}_0\bar{T}_L\vec{X}_L(0.15s+1)}{0.15s+(1-\bar{K})} \tag{3.27}$$

This gives a gain reduced by a factor of $(1-g_{ii})$ and a time constant $\frac{0.15}{(1-K_{ii})} = \frac{0.15T_D}{0.15(1-g_{ii})+g_{ii}T_D}$ for each pathway because g_{ii} is now zero, but the remaining circuit is still scaled to be appropriate for the original value of g_{ii}.

In the feedback case,

$$\vec{F}_R = \bar{I}_0\bar{T}_0\vec{X}_R + (\bar{I} - (\bar{I}_0\bar{T}_0)(\bar{I}_0\bar{T}_R)^{-1})(\vec{F}_R - \bar{H}\vec{F}_R) + \bar{H}\vec{F}_R \tag{3.28}$$

$$\vec{F}_L = \bar{I}_0\bar{T}_0\vec{X}_L + (\bar{I} - (\bar{I}_0\bar{T}_0)(\bar{I}_0\bar{T}_L)^{-1})(\vec{F}_L - \bar{H}\vec{F}_L) + \bar{H}\vec{F}_L \tag{3.29}$$

Recombining,

$$0 = \bar{I}_0\bar{T}_0\vec{X}_R - (\bar{I}_0\bar{T}_0)(\bar{I}_0\bar{T}_R)^{-1}(\vec{F}_R - \bar{H}\vec{F}_R) \tag{3.30}$$

$$0 = \bar{I}_0\bar{T}_0\vec{X}_L - (\bar{I}_0\bar{T}_0)(\bar{I}_0\bar{T}_L)^{-1}(\vec{F}_L - \bar{H}\vec{F}_L) \tag{3.31}$$

Multiplying through by $(\bar{I}_0\bar{T}_R)(\bar{I}_0\bar{T}_0)^{-1}$ for the $\vec{F}_R$ equation and $(\bar{I}_0\bar{T}_L)(\bar{I}_0\bar{T}_0)^{-1}$ for the $\vec{F}_L$ equation and rearranging, the results are the same as for the feedforward case.

This may seem counterintuitive given the position dependency of the cross-midline gains in the feedback case. In actuality, these serve only to undo the unwanted position dependencies that will be introduced to this contribution by the additional feedback loop of the second model form. The effective contribution of the cross-midline components is the same for the primary afferent nonlinearity and central feedback nonlinearity model forms once this is considered.

In normal VOR operation, the relative weights of g and K affect the strength of the feedback contributions in both model forms. The addition, the commissural pathways, supplies a third component to the VN summing junction that reduces the required position and velocity contributions of the ipsilateral input and feedback components. In the first model form, this means that the feedforward input is scaled differently and the feedback neural filter coefficients are reduced. In the second model form, the input scaling and feedback neural filter coefficients are reduced as in the first form, and the $\bar{C}$ matrices change to accomodate the new values of $\bar{I}_0$ (unchanged if the K's and g's of all pathways are the same, as then $\bar{I}_0$ takes the form $I_0\bar{I}$ and $\bar{I}_0^{-1} = \frac{1}{I_0}\bar{I}$, so $\bar{C} = \bar{I} - \bar{I}_0\bar{T}_0\bar{T}^{-1}\bar{I}_0^{-1}$ reduces to $\bar{C} = \bar{I} - \bar{T}_0\bar{T}^{-1}$). Consider the case where the K's and g's of all three pathways are the same, so the C matrices are unchanged and the velocity components are the same as in the monocular case. For a difference mode gain of 1 and large time constant, the changed feedback filter coefficients lead to a net ipsilateral feedback component $\bar{H}\vec{F} + (\bar{I} - \bar{T}_0\bar{T}^{-1})(\vec{F} - \bar{H}\vec{F})$. When all is functioning properly, $\bar{H}\vec{F} = (1-g)(1-\frac{0.15}{T_D})(\psi,\theta,\phi)^T \approx (1-g)(\psi,\theta,\phi)^T$ (for large T_D) and $\vec{F} = 0.15\bar{T}\vec{\omega} + (\psi,\theta,\phi)^T$, so the feedback component becomes $(I - \bar{T}_0\bar{T}^{-1}g)(\psi,\theta,\phi)^T + (\bar{T} - \bar{T}_0)0.15\vec{\omega}$. This introduces a position dependence to

the position sensitivities, and position component cross-talk between pathways. For the monocular case, only the velocity components were position dependent, and there was no position component cross-talk between pathways.

3.3.5 Corrective Feedback Effects (Second Model Form)

In the second model form, the required position-dependent corrections are implemented with a second feedback loop, C, rather than in the forward path (first model form). The effects of removing this additional feedback loop from the second form can be investigated by setting $\bar{C}_R = 0$ (Figure 3.6). Letting $\bar{H} = \frac{\bar{K}}{(0.15s+1)}$, $\bar{I}$ be the identity matrix, and absorbing the scalar factor $\bar{I}_0$ into $\bar{T}_0$, $\bar{T}_L$ and $\bar{T}_R$ for notational simplicity, this gives the equations

$$\vec{F}_R = \bar{T}_0\vec{X}_R + \bar{H}\vec{F}_R + \bar{T}_0\bar{T}_R^{-1}\bar{G}\vec{F}_L \tag{3.32}$$

$$\vec{F}_L = \bar{T}_L\vec{X}_L + \bar{H}\vec{F}_L + \bar{G}\vec{F}_R \tag{3.33}$$

or

$$\vec{F}_R = \frac{(\bar{I}-\bar{H})^{-1}[(\bar{T}_0\vec{X}_R) + \bar{T}_0\bar{T}_R^{-1}\bar{G}(\bar{I}-\bar{H})^{-1}(\bar{T}_L\vec{X}_L)]}{\bar{I} - (\bar{I}-\bar{H})^{-1}\bar{T}_0\bar{T}_R^{-1}\bar{G}(\bar{I}-\bar{H})^{-1}\bar{G}} \tag{3.34}$$

$$\vec{F}_L = \frac{(\bar{I}-\bar{H})^{-1}[(\bar{T}_L\vec{X}_L) + \bar{G}(\bar{I}-\bar{H})^{-1}(\bar{T}_0\vec{X}_R)]}{\bar{I} - (\bar{I}-\bar{H})^{-1}\bar{G}(\bar{I}-\bar{H})^{-1}\bar{T}_0\bar{T}_R^{-1}\bar{G}} \tag{3.35}$$

If the g's and K's are different for each dimension, this is very difficult to break down further, as the $(\bar{I}-\bar{H})^{-1}$ matrices don't commute with $\bar{T}_0\bar{T}_R^{-1}$. However, if the g's

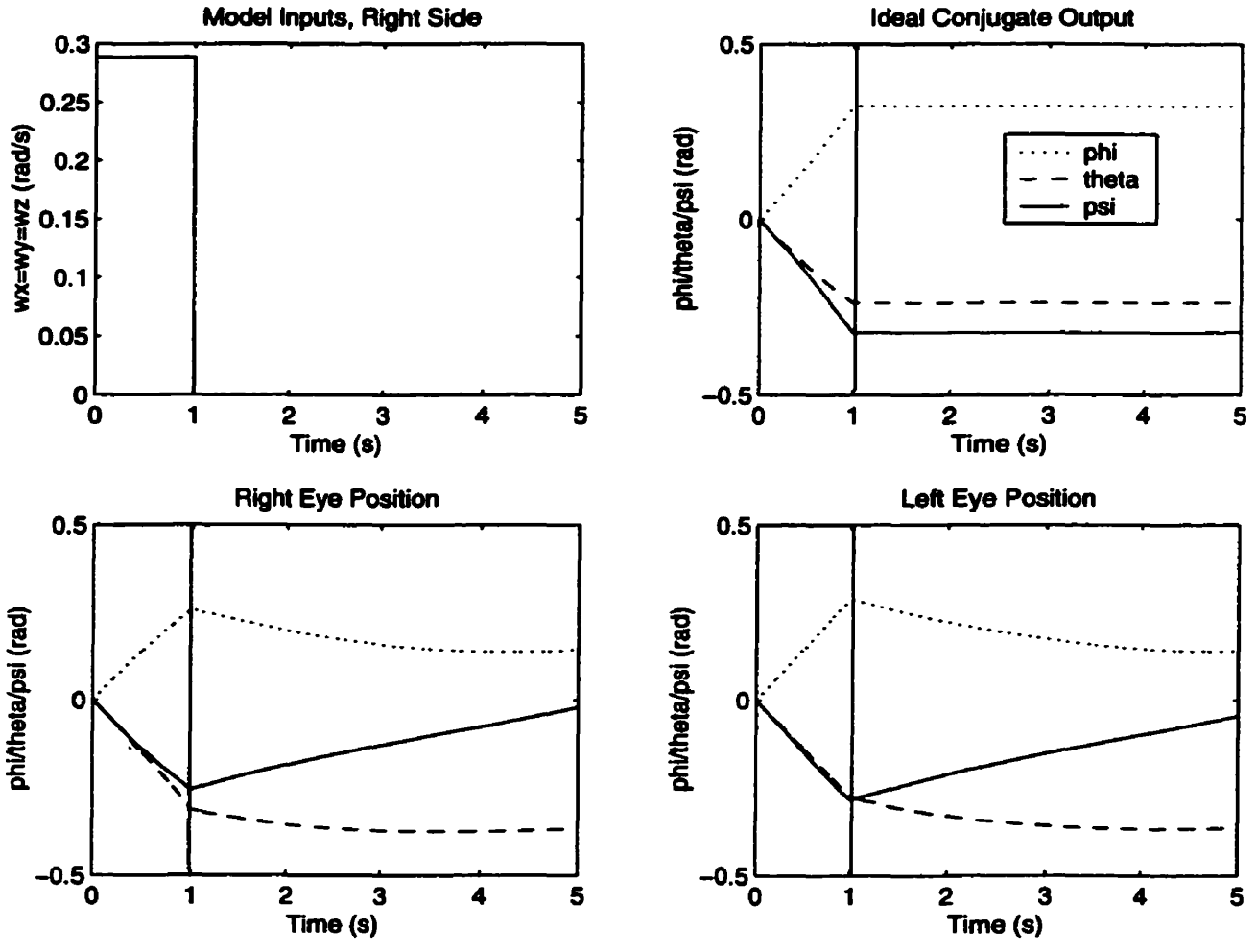

Figure 3.6: Effects of removing the right C matrix pathway in second model form.

and K's are the same for each pathway,

$$\bar{G} = \begin{pmatrix} -1 & 0 & 0 \\ 0 & 1 & 0 \\ 0 & 0 & -1 \end{pmatrix} g \tag{3.36}$$

$$(\bar{I} - \bar{H})^{-1} = \frac{\bar{I}}{(1 - H)} \tag{3.37}$$

and the above equations can be rewritten (where division implies left hand side multiplication by the inverse):

$$\vec{F}_R = \frac{(\bar{I} - \bar{H})\bar{T}_0\vec{X}_R - g\bar{T}_0\bar{T}_R^{-1}\bar{I}_g\bar{T}_L\vec{X}_L}{(\bar{I} - \bar{H})^2 - \bar{T}_0\bar{T}_R^{-1}g^2} \tag{3.38}$$

$$\vec{F}_L = \frac{(\bar{I} - \bar{H})\bar{T}_L\vec{X}_L - g\bar{I}_g\bar{T}_0\vec{X}_R}{(\bar{I} - \bar{H})^2 - \bar{I}_g\bar{T}_0\bar{T}_R{}^{-1}\bar{I}_g g^2} \tag{3.39}$$

where

$$\bar{I}_g = \begin{pmatrix} 1 & 0 & 0 \\ 0 & -1 & 0 \\ 0 & 0 & 1 \end{pmatrix} . \tag{3.40}$$

If two matrices $\bar{b}_L$ and $\bar{b}_R$ are defined such that $\bar{b}_L^2 = \bar{T}_0\bar{T}_R^{-1}g^2$ and $\bar{b}_R^2 = \bar{I}_g\bar{T}_0\bar{T}_R^{-1}\bar{I}_g g^2$, $\vec{F}_R$ can be divided into two modes with position dependent transfer function denominators $(\bar{I} - \bar{H} \pm \bar{b}_R)$ and likewise for $\vec{F}_L$. $\bar{b}_L$ and $\bar{b}_R$ collapse to $g\bar{I}$ when the right eye is in primary orientation. These results imply that the dynamics of responses from both eyes will depend on the position of the right eye.

It is possible to get a more qualitative feel for what is occuring by looking at the simulation plot for the case of a unilateral C lesion (Figure 3.6). The decay rates of

both sides are clearly affected- the magnitude of θ continues to increase even in the absence of input, while the other two components decay more quickly. Considering the previously developed equations, $\vec{F}_R = \bar{H}\vec{F}_R + \bar{G}\vec{F}_L$ for zero external input in the absence of lesion. With the lesion ($\bar{C} = 0$), the equation for $\vec{F}_R$ reduces to $\vec{F}_R = \bar{H}\vec{F}_R + \bar{T}_0\bar{T}_R^{-1}\bar{G}\vec{F}_L$, so the change in contribution of $\vec{F}_L$ to $\vec{F}_R$ is $(\bar{T}_0\bar{T}_R^{-1} - \bar{I})\bar{G}\vec{F}_L$. For the right side, the horizontal path firing rate is positive and the other two firing rates are negative. Accounting for the mirror symmetry of the required muscle commands, the horizontal and vertical path firing rates are negative and the torsional firing rate is positive on the left side. From this information, the signs of the terms of $\bar{T}_0\bar{T}_R^{-1}$ can be computed to show that there is now a negative contribution from the left torsional pathway to the right horizontal and vertical pathways, leading to an increase in the magnitude of θ and a decrease in ϕ on the right side. These changes are then partially carried over to the left side via the cross-midline contribution of $\vec{F}_R$ to $\vec{F}_L$. The other cross-terms and changes in diagonal terms also contribute to the dynamics. Thus, a unilateral $\bar{C}$ lesion introduces position-dependent dynamics on both sides, even in the absence of external input (provided the eyes are not initially in primary orientation).

If $\bar{C}$ is removed on both sides,

$$\vec{F}_R = \bar{T}_0\vec{X}_R + \bar{H}\vec{F}_R + \bar{T}_0\bar{T}_R^{-1}\bar{G}\vec{F}_L \tag{3.41}$$

$$\vec{F}_L = \bar{T}_0\vec{X}_L + \bar{H}\vec{F}_L + \bar{T}_0\bar{T}_L^{-1}\bar{G}\vec{F}_R \tag{3.42}$$

which is again position dependent. In this case, the instantaneous transfer function seen by the modes of each eye will depend on the positions of both eyes. It is

interesting to consider decay in this case:

$$\vec{F}_R = \bar{H}\vec{F}_R + \bar{T}_0\bar{T}_R^{-1}\bar{G}\vec{F}_L \tag{3.43}$$

$$\vec{F}_L = \bar{H}\vec{F}_L + \bar{T}_0\bar{T}_L^{-1}\bar{G}\vec{F}_R \tag{3.44}$$

If all the input has been of the form $\vec{X}_L = -\bar{I}_g\vec{X}_R$, then by symmetry

$$\vec{F}_L = \begin{pmatrix} -1 & 0 & 0 \\ 0 & 1 & 0 \\ 0 & 0 & -1 \end{pmatrix} F_R \tag{3.45}$$

$$\bar{G}\vec{F}_L = g\begin{pmatrix} -1 & 0 & 0 \\ 0 & 1 & 0 \\ 0 & 0 & -1 \end{pmatrix}\begin{pmatrix} -1 & 0 & 0 \\ 0 & 1 & 0 \\ 0 & 0 & -1 \end{pmatrix}\vec{F}_R = g\vec{F}_R \tag{3.46}$$

Substituting this into the equation above for $\vec{F}_R$, with $\bar{H} = \frac{\bar{K}}{0.15s+1}$, rearranging and converting from Laplace to time domain,

$$\dot{\vec{F}}_R = -\frac{(\bar{I} - \bar{T}_0\bar{T}_R^{-1}g - \bar{K})}{0.15(\bar{I} - \bar{T}_0\bar{T}_R^{-1}g)}\vec{F}_R \tag{3.47}$$

If there were no cross-talk, this would reduce to an exponential decay with position dependent time constants provided the terms $(\bar{I} - \bar{T}_0\bar{T}_R^{-1}g - \bar{K})$ and $(\bar{I} - \bar{T}_0\bar{T}_R^{-1}g)$ remained positive. With cross-talk, oscillatory components could be introduced, as the solutions to equations of the form

$$\begin{pmatrix} \dot{X}_1 \\ \dot{X}_2 \end{pmatrix} = \begin{pmatrix} a_{21} & 0 \\ 0 & -a_{12} \end{pmatrix}\begin{pmatrix} X_1 \\ X_2 \end{pmatrix}$$

are oscillatory. The results of Equation 3.47 will be more complicated, as there will be both oscillatory and exponential decay components, and all the coefficients vary with position.

Figure 3.7 shows a simulation where both $\bar{C}$ matrices have been removed. The movements are conjugate, as expected, and θ and ψ appear to display damped oscillatory components.

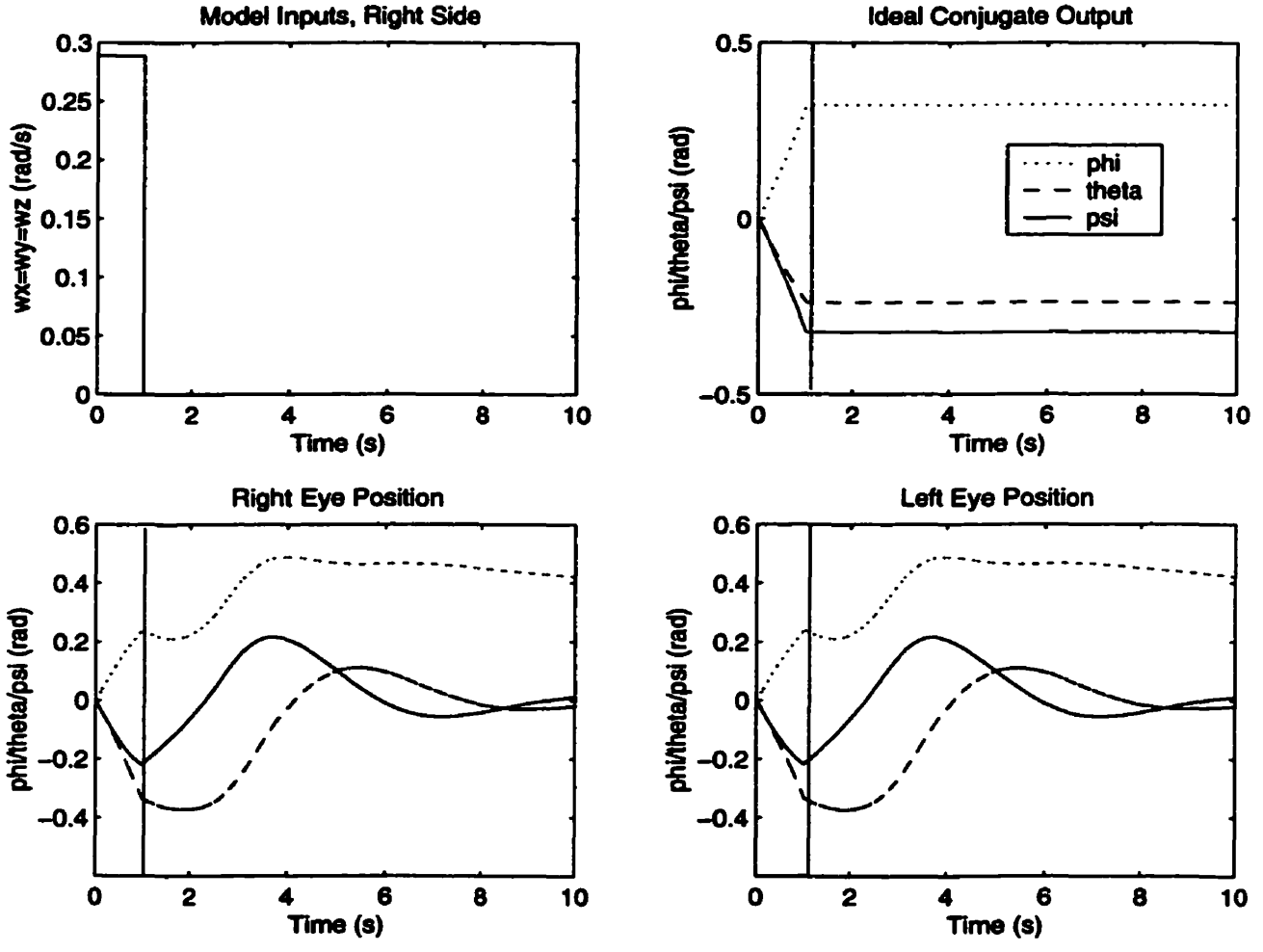

Figure 3.7: Effects of removing both C matrix pathways in 2nd model form.

As the matrix coefficients depend on position, orientation representation would be an important consideration if more specific predictions of eye trajectory were

required. For the orientation representation used here, there are no cross-terms from the horizontal pathway to the vertical and torsional pathways cross-midline, but all other cross-terms are non-zero.

3.3.6 Lesions of the Neural Filters (Both Model Forms)

Lesions of the neural filter can be simulated by setting the numerator of $\frac{1}{(0.15s+1)}$ in $\bar{H}$ to a value less than one for one or more of the 3D coordinates. Experimentally, this would correspond to lesioning of the nucleus prepositus hypoglossi (NPH) or interstitial nucleus of cajal (INC). This has two effects on the model. First, the position component coefficient and time constant of the affected pathway will be reduced. Even the non-lesioned side will be affected strongly, as it sees a reduced cross-midline contribution for the pathway(s) corresponding to the contralateral lesion, leading to effects similar to those of a cut in commissural pathways. Second, the calculation of the $\bar{T}$ (first form) or $\bar{C}$, $\bar{G}_{LtoR}$ and $\bar{G}_{RtoL}$ (second form) matrices on the lesioned side will be thrown off by the miscaculation of the position component corresponding to the affected pathway. This has the same effect on both model forms, as the equations reduce to $\vec{F}_R = \bar{T}'_R\vec{X}_R + \bar{H}_R\vec{F}_R + \bar{G}\vec{F}_L$ and $\vec{F}_L = \bar{T}'_L\vec{X}_L + \bar{H}_L\vec{F}_L + \bar{G}\vec{F}_R$ in both cases, where $\bar{T}'_R$ and $\bar{T}'_L$ denote the modified first model form $\bar{T}$ matrices. The $\bar{C}$ and $\bar{G}$ matrices of the second form are based on the same miscalculated position components as in the first form case, so the overall effect is the same.

The second effect will be more noticeable when the velocity component dominates the motor command (i.e. during saccades). The first effect will tend to bring the

affected position component to zero in the absence of velocity input, reducing the magnitude of matrix miscalculations.

Figures 3.8 and 3.9 show the effects of unilateral and bilateral reduction of the horizontal neural filter numerator by half.

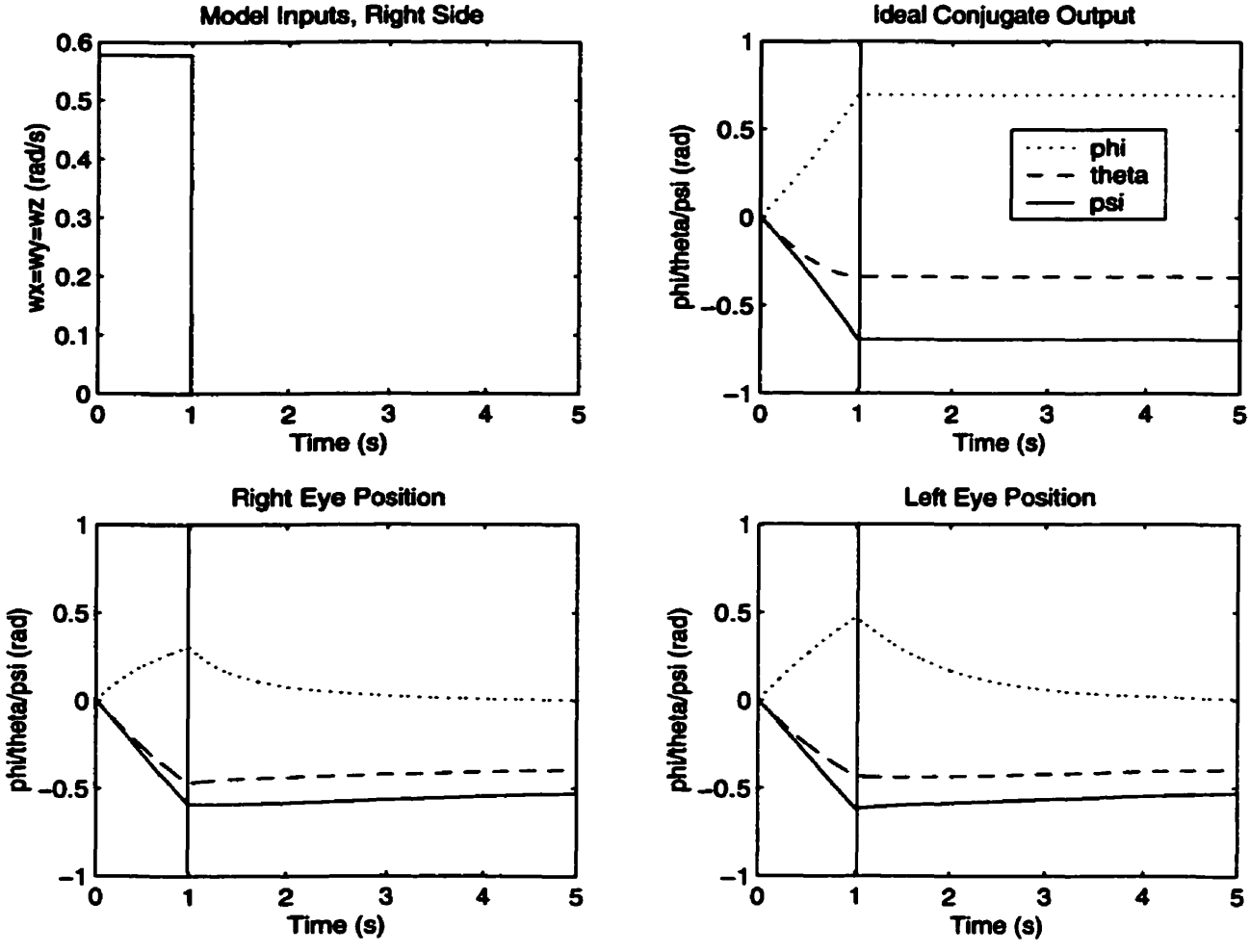

Figure 3.8: Effects of unilateral (right) horizontal neural filter reduction.

Unilateral filter reduction reduces the gain and time constant of ϕ on both sides, affecting the lesioned side more. The time constants of the other two coordinates are not affected (the slight decay seen in ψ and θ relative to the ideal result is due to the non-infinite 30s time constant observed in normal VOR operation). The ψ

component gain in this case is also slightly reduced. On the left side, the decay in the value of ϕ affects the desired changes in ψ (the matrix gains are still calculated correctly). On the right side, this effect is compounded by the fact that the desired changes in ψ are calculated based on a reduced estimate of ϕ. The θ component is also affected, for the same reasons.

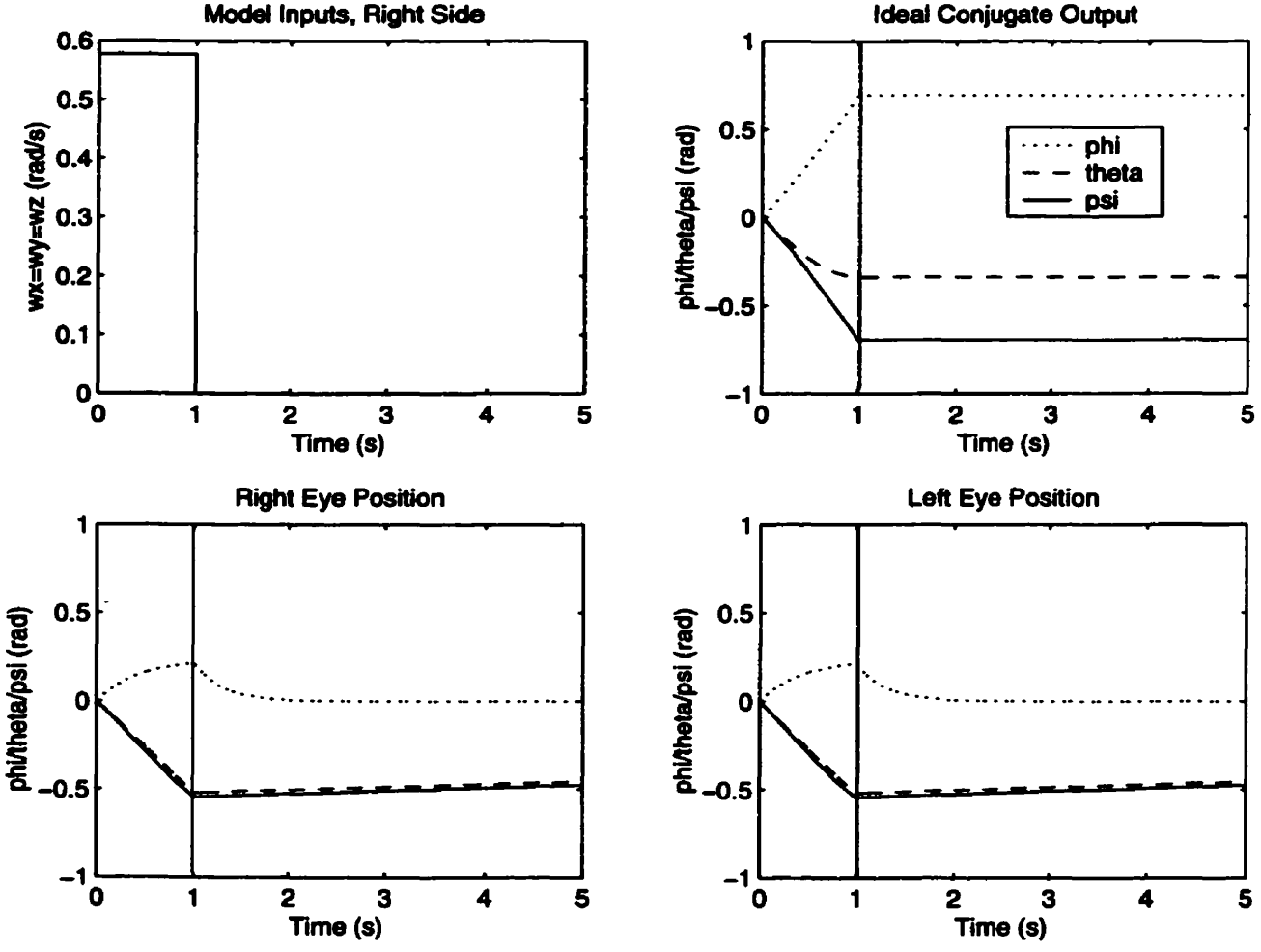

Figure 3.9: Effects of bilateral horizontal neural filter reduction.

In the bilateral neural filter reduction case, the yaw response is further reduced and not maintained. The change in ψ and θ values is more noticeable than in the unilateral lesion case. There is a further change in required gains due to the additional decrease

in horizontal component, and this is now compounded by the internal underestimation of ϕ in calculating position-dependent matrices on both sides rather than just one. As the structure is again symmetric, the movements are still conjugate, though incorrect, for normal inputs.

The following chapter will explore possible anatomical substrates for the computational elements in the postulated model forms.

Chapter 4

Linking Anatomy to 3D Formulation

This chapter will deal with how the brain actually implements the mathematics proposed in the preceding chapters. It is divided into two parts, the first concerned with the brain structures and interconnections involved in slow-phase VOR processing, and the second discussing neural network implementations of the oculomotor integrator. A summary of the abbreviations used here is provided in Appendix B.

4.1 Anatomical Pathways of the VOR

The objective of this section is to develop an anatomically relevant substrate for the 3-D slow-phase of the VOR. These pathways are based on the cat except where otherwise stated; some differences are observed in rabbits and monkeys. Structures such as the paramedian pontine reticular formation (PPRF) and Forel's Field H that are

considered more important for saccades and other types of eye movement have been left out. The first two subsections will review previously proposed anatomical interconnections for the horizontal and vertical pathways, and will consider them in the context of other literature and more recent studies. The third subsection proposes connections that may be relevant for crosstalk. It should be noted that literature dealing with cross-talk and 3-D eye movements is incomplete, so this study focused on interconnections between known important components of the horizontal and vertical integrators. It is possible that later studies may reveal other structures important for cross-talk. The final subsection summarizes these sections with a suggested anatomical mapping of the bilateral model given in chapter 3.

4.1.1 The Horizontal VOR

A bilateral feedback model of the horizontal integrator circuit was proposed by Galiana and Outerbridge in 1984 [48] and revised by Green and Galiana [55]. The relevant connections were the following:

- Excitatory horizontal canal (HC) neurons in the vestibular nucleus (VN) projecting to the contralateral nucleus prepositus hypoglossi (NPH) and abducens nucleus, and to inhibitory HC neurons in the contralateral VN ([74], [37]).

- Inhibitory HC VN neurons projecting to ipsilateral excitatory HC VN neurons and to ipsilateral NPH and abducens nucleus.

- Excitatory projection of canal afferents to both excitatory and inhibitory ipsilateral HC VN neurons.

• Excitatory projection of NPH to contralateral VN excitatory HC neurons, and inhibitory projection of NPH to ipsilateral inhibitory HC neurons.

Referring to the 1-D bilateral model of Figure 1.4, the NPH is proposed to perform the neural filtering function and VN neurons are taken to be the output neurons. Motorneurons in the abducens nucleus are assumed to take the form of a weighted sum of NPH and VN outputs. The inhibitory cross-midline contributions with gain g are accomplished via the connections mentioned in the first two points above.

There are numerous studies that support the role of the NPH as the horizontal neural integrator ([22], [16], [77]). The NPH contains a continuum of horizontal movement-related neurons ranging from largely velocity-sensitive to purely position sensitive in their firing rates ([29], [69]). Bilateral lesions to the NPH drastically reduce the time constant of horizontal gaze-holding- in one study, such lesions reduced the constant to 200ms [16]. In this case, the VOR response was reduced to a step in eye position instead of a ramp for constant head velocity input. In another study, unilateral injections of muscimol into the NPH lead to bilateral gaze holding failure and inappropriate, asymmetric VOR responses [77]. A review of studies concerning the role of the NPH in horizontal oculomotor integration is provided in [44].

The argument for a feedback neural filter model of the NPH rather than a model of the NPH as a feedforward integrator stems from the position sensitivity of VN neurons [37]. Many VN neuron firing rates vary with eye position as well as eye velocity [103]. This would not be required in a purely feedforward model of the integrator pathways, but is predicted by a feedback neural filter model. This idea is further supported by the anatomical projection of the NPH back to the ipsilateral

and contralateral VN [44].

The bilateral model also has commissural connections, shown by the pathways of gain g. Removal of these pathways should result in gaze-holding failure as the position component time constant is reduced to that generated with the unilateral neural filter alone. A study conducted by Godaux and Cheron [50] investigated the effects of severing the vestibular commissural pathways in the cat, and found the results to be consistent with those predicted by the Galiana/Outerbridge bilateral model of 1-D horizontal VOR pathways.

Fukushima et al. [43] also proposed an anatomical basis for the horizontal integrator, though they did not attempt to map individual structures to separate mathematical functions. This circuit showed connections between bilateral NPH as important, as well as an inhibitory connection from the medial flocculus to ipsilateral HC related neurons in the VN. They indicated an excitatory, contralaterally-projecting floccular target neuron (FTN), although literature indicates that HC FTN's are ipsilaterally-projecting and probably inhibitory [98]. The flocculus is not thought to play a large role in the normal horizontal VOR, but has been included here because it is significant for the vertical VOR, so may be relevant for cross-talk.

Further literature review revealed projections of MVN and NPH HC-related neurons to the contralateral medial flocculus ([21],[36]). The NPH also sends ipsilateral excitatory and contralateral inhibitory afferents to the abducens nucleus [38]. A summary of the main horizontal VOR-related pathways is shown in Figure 4.1. In the diagram, the MVN-contralateral flocculus projections are assumed to be excitatory. The abducens nucleus projections were left out to avoid clutter.

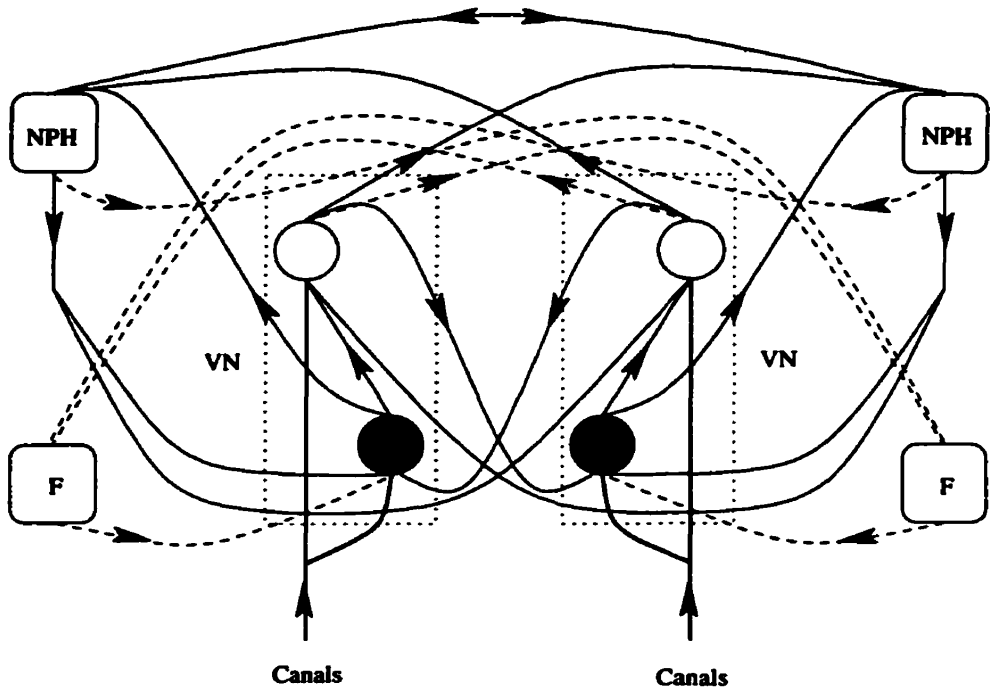

Figure 4.1: Horizontal integrator pathways. Clear circles denote excitatory cells, filled nodes are inhibitory; NPH- nucleus prepositus hypoglossi, F- flocculus, VN- vestibular nucleus. Owing to the large number of connections, some pathways are drawn with dashed lines to avoid confusion.

4.1.2 The Vertical/Torsional VOR

The vertical/torsional VOR pathways start with the anterior and posterior canal afferents, which synapse on secondary neurons in the medial and superior vestibular nuclei. As with the horizontal case, the secondary VN neurons of the vertical pathways display both position and velocity sensitivity [61], consistent with a feedback neural filter model for position signal creation. In the case of the vertical and torsional VOR, it is the interstitial nucleus of Cajal (INC) that is thought to perform the feedback neural filtering. Neurons in the INC display strong vertical eye position sensitivity [41], and unilateral and bilateral lesions of the INC impair gaze holding and vertical VOR [39]. A comprehensive description of the role of the INC in eye movement is

provided in [39], and arguments for its importance in vertical/torsional position signal generation are given in [44].

Fukushima et al. [43] provided a summary of important connections for the vertical integrator circuit. These are:

• From excitatory anterior canal (AC) and posterior canal (PC) VN neurons to contralateral INC, contralateral oculomotor and trochlear nuclei, and contralateral inhibitory interneurons. For further details on these connections, the reader is referred to ([54], [53], [116], [20], [58], [61], [62]).

• Excitatory connections from INC to ipsilateral AC and PC inhibitory type II interneurons, and from these interneurons to ipsilateral excitatory PC and AC type I neurons, respectively (see also [47]).

• From INC to contralateral INC ([28], [67], [81]- these references refer to primate studies).

• From excitatory PC neurons to contralateral middle and caudal flocculus [40].

• Inhibition from rostral flocculus to ipsilateral excitatory and inhibitory type I AC neurons ([98], [59]) and from caudal flocculus to neurons in the ipsilateral dorsal cell Y group ([100], [97]).

• Excitatory connections from cells in Y group to the contralateral oculomotor and trochlear nuclei and contralateral INC. Note that the oculomotor and INC projections are done by separate dorsal and ventral groups within the Y group [97]. It has been suggested that these connections may help compensate for a relative lack of posterior-anterior commissural connections in the VN.

These connections were simplified; not all neurons in a given group necessarily

project or receive all efferent/afferent projections. In particular, AC and PC canal related neurons in the SVN differ from those of the MVN subdivision. Inhibitory vertical canal-related neurons in the MVN don't project to the oculomotor nuclei; those in the SVN do [115]. Most of the AC cells that are inhibited by the flocculus are in the SVN [59]; PC cells aren't inhibited by the flocculus in the cat. Furthermore, the inhibitory PC neurons in the SVN receive contralateral inhibition [115] although the inhibitory AC neurons in the SVN don't. These inhibitory type I PC neurons, not included in the Fukushima circuit, project ipsilaterally to the IO and SR motorneuron pools. The Y group also projects back to the SVN bilaterally [20]. The SVN does not receive many INC inputs [20]. A summary of the major connections for the vertical-torsional system is shown in Figure 4.2. For illustrative simplicity, type I inhibitory and type II inhibitory VN neurons are represented together, and projections to the oculomotor nuclei are left out.

4.1.3 Possible Sites of Cross-Talk

Most models of the 3D VOR have treated the horizontal and vertical/torsional reflex pathways separately. Although Tweed and Vilis ([114], [110]) do propose interconnection between the two systems, no attempt is made to map these transformations onto known anatomical connections. Tensor and matrix approaches have been used to analyze what transformations must take place, but do not indicate precisely where they occur. This section will examine known projections and neuron firing properties and propose tentative sites for cross-talk for the movement planes.

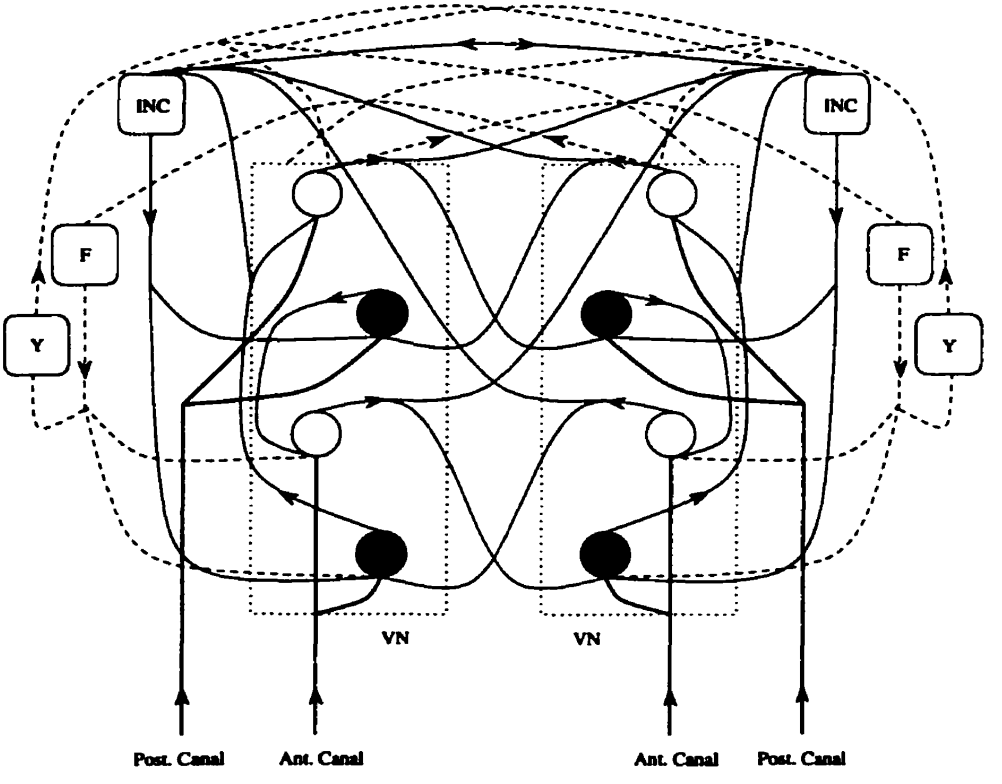

Figure 4.2: Vertical integrator pathways. INC- interstitial nucleus of Cajal, F- flocculus, Y- cell y group, VN- vestibular nucleus.

Two probable sites for interaction are the NPH and the INC. A study examining 116 cells in the NPH of the alert cat found their on-directions to be 59 percent horizontal, 17 percent vertical, and 24 percent oblique [69]. Other studies have also shown mixed vertical and horizontal sensitivities in the cat NPH ([9], [29]). In one of the studies, several NPH neurons carrying signals related to vertical and oblique eye position and/or velocity were found to project to the ipsilateral INC and to be antidromically activated from it [29]. In another study, 3/10 cat BT cells in the INC were found to respond to horizontal rotation with a gain 14-17 percent of their maximal vertical gain [42]. It therefore seems likely that the connection between ipsilateral INC and NPH may play a role in cross-talk. Connections between contralateral INC and NPH may also exist, or they may occur indirectly as a result of cross-midline INC-INC or NPH-NPH interaction combined with the known ipsilateral projection; however, the ipsilateral influence is stronger [44].

Another possible site for interaction is from the VN to the NPH. In one study examining the anatomical and physiological characteristics of the VOR in the squirrel monkey, some of the vertical movement related MVN neurons projected to the contralateral NPH [75]. Three of the four neurons shown displayed some horizontal sensitivity as well. In a study on rabbits and cats, excitatory posterior canal neurons were shown to send collaterals to the contralateral NPH in both species [54]. A later study on cat anterior-canal related neurons did not display an NPH collateral, though many did branch to the contralateral VN [53]. In the cat, weak bilateral projections from the SVN to prepositus were also observed [73].

The possibility of convergence of more than one primary canal afferent onto a

single VN neuron has been examined directly by Kasahara and Uchino [64]. Kasahara and Uchino stimulated the six ampullary nerves of both labyrinths separately in anaesthetized cats and recorded VN responses. Most responded with monosynaptic excitation to stimulation of one ipsilateral nerve and with disynaptic inhibition to stimulation of the contralateral same-plane nerve. The authors found some neurons that responded to stimulation of more than one ipsilateral canal nerve, but upon closer examination found that this could have been due to stimulus spread. They concluded that there was no definite evidence for primary afferent convergence upon individual canal neurons. A later paper by Baker et al. [8] found widespread canal convergence at the VN level, but suggested that this could be attributed to monosynaptic input from one canal coupled with polysynaptic input from others.

While the former studies failed to show signs of primary afferent convergence, they did demonstrate another possible means of convergence. In the Kasahara/Uchino study, 6/28 neurons responding with a monosynaptic excitatory post-synaptic potential (EPSP) to ipsilateral nerve stimulation and disynaptic or trisynaptic inhibition (IPSP) to contralateral nerve stimulation were not plane-specific in this pairing. Two lateral and four posterior ipsilaterally-responding neurons displayed non plane-specific convergence, the horizontal neurons receiving contralateral anterior canal inhibition, and the posterior canal neurons receiving contralateral horizontal (3) or posterior (1) canal inhibition. Although they didn't say explicitly what inhibition was displayed, they did say that of the 28 neurons exhibiting ipsilateral EPSPs and contralateral IPSPs, 13 showed anterior canal inhibition, 10 showed horizontal canal inhibition, and 5 showed posterior canal inhibition. They further stated that, of those display-

ing plane-specific inhibition, 11 showed AC inhibition- PC excitation, 7 showed HC inhibition- HC excitation, and 4 showed PC inhibition- AC excitation. This leaves 2 AC, 3 HC, and 1 PC inhibition unaccounted for. As AC inhibition- PC excitation would be plane- specific, the 2 AC inhibitions must have been imposed upon the HC neurons displaying non-plane specific inhibiton, and the 4 PC neurons must have shown contralateral HC (3) and PC (1) inhibition. Some other non-plane specific combinations were also observed, including some contralateral EPSPs.

Possible Role for Non Plane-Specific Canal Convergence

To illustrate what sort of effects contralateral non plane-specific canal convergence could have, consider the two types of non-specific convergence observed more than once in Kasahara/Uchino study; that is, AC inhibition of contralateral HC neurons, and HC inhibition of contralateral PC neurons. Figures 4.3 and 4.4 show possible complete circuits for these two types of non-plane specific inhibition. As the neurons in these cases did not exhibit mixed contralateral effects, the circuits allow only one type of contralateral inhibition on each cell.

Considering first Figure 4.3, application of Mason's rule (see Appendix C) to the pathways gives the following equations for the neurons M_R and M_L (assuming the VN units act as linear summing junctions):

$$M_L = H_L - \frac{gA_R}{(1-g^2)} + \frac{g^2P_L}{(1-g^2)} \tag{4.1}$$

$$M_R = H_R - \frac{gA_L}{(1-g^2)} + \frac{g^2P_R}{(1-g^2)} \tag{4.2}$$

Thus the two sides will be modulated with both pitch and torsion; they will

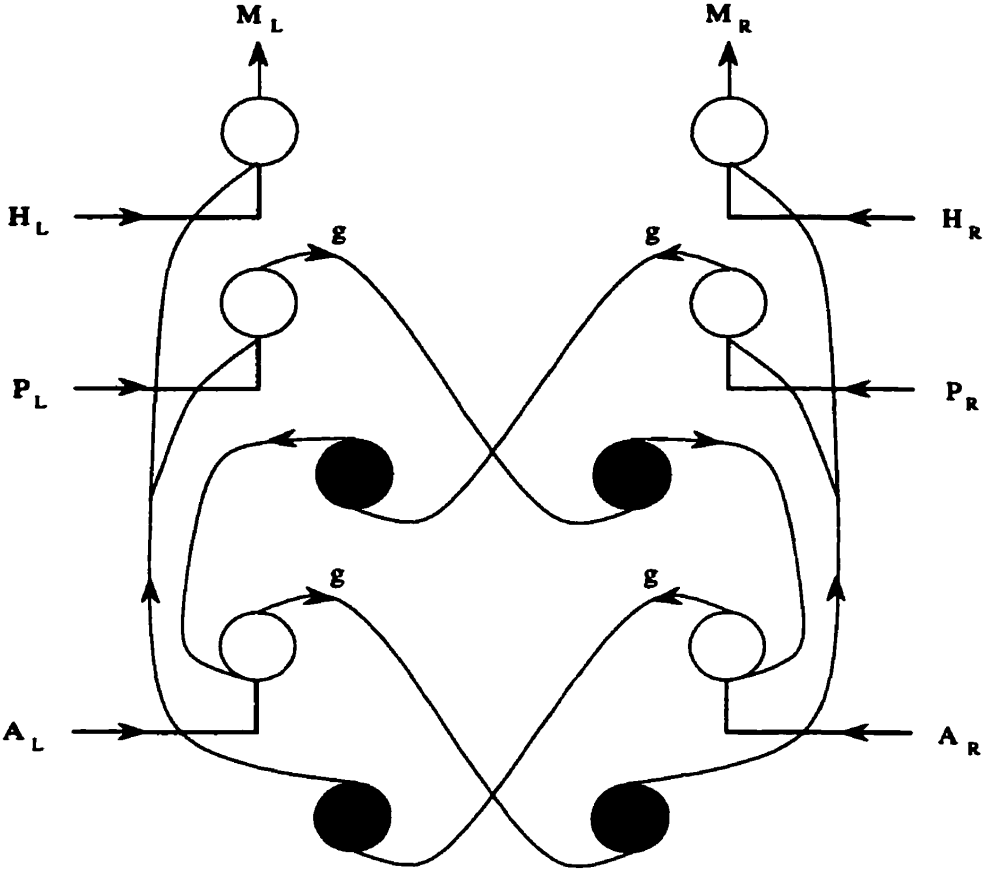

Figure 4.3: VN crosstalk pathway, vertical-horizontal.

modulate symmetrically with pitch and asymmetrically for torsion. The torsional component will appear to be that of the ipsilateral vertical canals, since the ipsilateral contribution is excitatory and the inhibition increases as the opposing contralateral torsional component increases.

Now consider the H-P circuit.

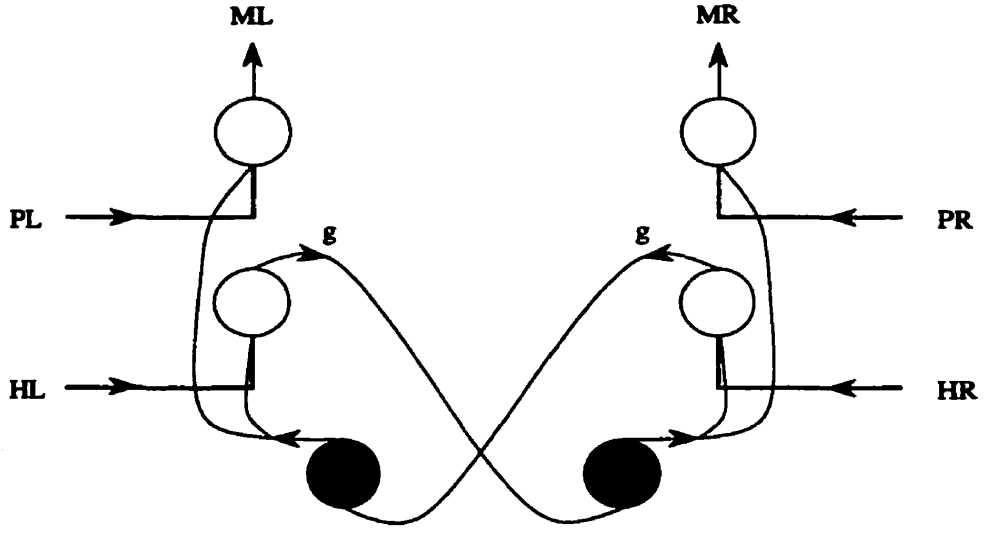

Figure 4.4: VN crosstalk pathway, horizontal-vertical.

A similar analysis yields

$$M_L = P_L - \frac{gH_R}{(1-g^2)} + \frac{g^2H_L}{(1-g^2)} \tag{4.3}$$

$$M_R = P_R - \frac{gH_L}{(1-g^2)} + \frac{g^2H_R}{(1-g^2)} \tag{4.4}$$

Again, this gives symmetric pitch and asymmetric torsion and horizontal results for the two sides. The horizontal component modulation is ipsilateral to the torsional component.

These calculations are meant only to illustrate the potential of such convergence in contributing to cross-talk; obviously it would be premature to draw conclusions based

on five neurons. However, it is interesting to note that in both cases, the horizontal component appears ipsilateral to the torsional component. In an article concerning sensorimotor transformations of the cat VOR [52], Graf et al. noted that 18/22 PC neurons receiving HC input had ipsilateral convergent input. They also noted that all the AC neurons receiving HC input (9 contralaterally projecting and 2 ipsilaterally projecting) received it from the ipsilateral side. In another study regarding vertical eye movement related secondary VN neurons, Iwamoto et al [61] noted that in the 12 units whose activity was found to be correlated with horizontal movement, the units always increased their firing rate for contralateral horizontal eye positions.

It is also interesting to note that the convergence maintained the antisymmetric (across the midline) torsional and horizontal, and symmetric vertical, responses generated by the canals. In frontal-eyed animals, the extraocular muscles are oriented such that the commands should be antisymmetric for rotation about the z and x (horizontal and torsional) axes, but symmetric about y (vertical) for conjugate movement. A more thorough examination of secondary vestibulo-ocular neurons by direct stimulation (similar to the Kasahara-Uchino study) might shed more light on the role of commissural cross-talk in VOR transformations.

'Integrator'-VN Cross-Talk

The INC-MVN connection also provides a possible site for cross-talk. Studies have shown that stimulation of the ipsilateral INC excites horizontal type II neurons in the MVN at monosynaptic or polysynaptic latencies ([47], [71], [70]). Lesions of the ipsilateral INC have been found to reduce the gain of HC VN type II neurons and to increase the gain of HC VN type I neurons [45]. Thus, ipsilateral INC excitation of

horizontal type II neurons should be investigated as a possible cross-talk site.

Similarly, there may be cross-talk from the NPH to the SVN. Labelling studies revealed weak projections from the NPH to the SVN in the cat [73]. Other studies showed modest projections from the caudal NPH to the SVN and Y group in the cat [20],[10].

The possibility of horizontal-responding neurons projecting to the INC was raised by Markham et al [71], who found 10 instances of antidromic activation of type I HC neurons from the contralateral INC and 5 from the ipsilateral. However, a later study by Fukushima et al. [46] indicated that these probably project preferentially to interstitiospinal and reticulo-spinal neurons in the INC region. They found that vestibular-projecting INC neurons did not respond to HC nerve stimulation, though they did respond frequently to vertical canal stimulation. Thus the probability of an MVN HC-INC connection playing a direct role in cross-talk seems slim.

Flocculus-VN Interconnections

The flocculus provides another site where cross-talk may occur. The flocculus is known to inhibit VOR relay neurons, its middle zone affecting some horizontal inhibitory interneurons, its rostral zone inhibiting excitatory and inhibitory anterior canal-related neurons, and its caudal zone influencing the dorsal cell group y ([98], [59], [96], [99], [100], [97]). These last two relations are important for the vertical VOR in cats. Anatomical studies have indicated bilateral projections from the MVN to the flocculus in the rabbit and cat ([35], [109], [101]). In studies conducted on middle floccular-projecting MVN and PH neurons in the cat ([21], [36]), Cheron et al. and Escudero et al. found largely contralateral MVN-HC neuron projections, but

some ipsilateral ones. They suggested that MVN axons with ipsilateral projections terminate mainly in the rostral and caudal zones of the flocculus, and as some of the ipsilaterally-projecting neurons were HC responding, cross-talk could occur here. A study by Zhang et al. on floccular-projecting neurons (FPNs) in the SVN of monkeys found that some displayed both horizontal and vertical eye position sensitivities [118]. The flocculus is known to be essential for VOR adaptation [34], and is required for generation of downward eye position signals in the vertical system [40]. The flocculus projects ipsilaterally as well as contralaterally to the NPH and MVN ([72], [73]), and excitatory PC neurons project contralaterally to the medial flocculus as well as the caudal [40]. These connections may play a role in vertical-horizontal cross-talk.

For simplicity, this investigation has considered only connections between the sites that are thought to be most important for VOR integration; namely, the VN, the NPH, the INC, and the flocculus. However, there are numerous other places where cross-talk could occur as well- the superior colliculus, the PPRF, and many other structures receive projections from, and project back to, neurons of both pathways. These connections could be particularly important once other eye movements such as saccades are considered. Cross-talk can also occur at the level of the motoneurons, for example between contralateral abducens and oculomotor nuclei [23], but Figure 4.5 summarizes only the premotor pathways.

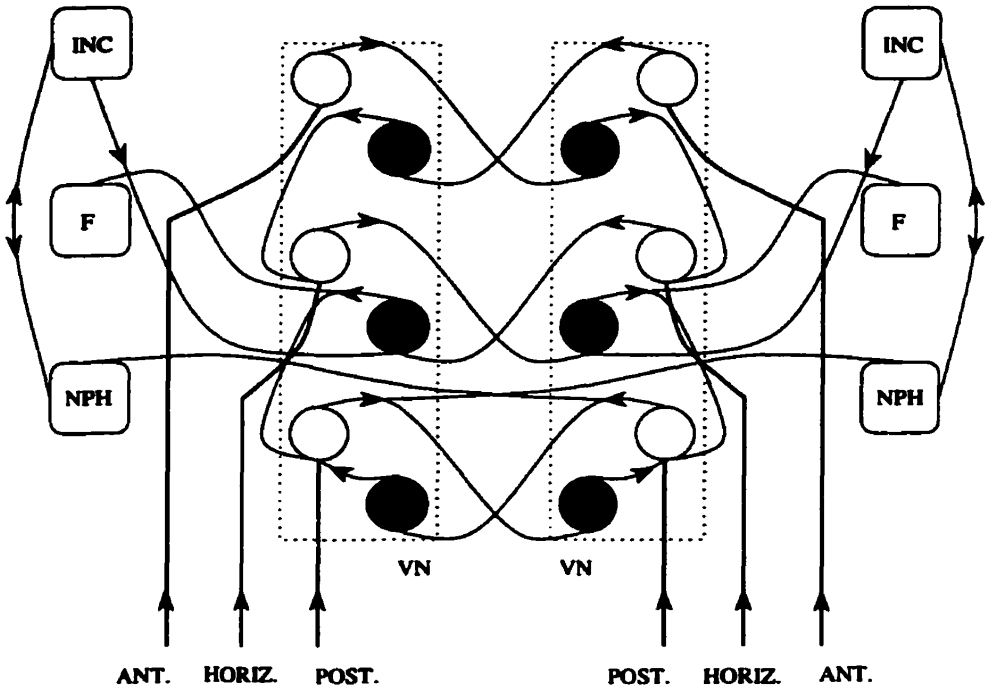

Figure 4.5: Summary of potential cross-talk pathways. INC- interstitial nucleus of Cajal, F- flocculus, NPH- nucleus prepositus hypoglossi, VN- vestibular nucleus.

4.1.4 Model Mapped to Anatomy

Based on the literature, a possible mapping of the 3D model onto anatomy might be as shown in Figure 4.6, where the flocculus (F) implements the $\bar{C}$ matrix, the $\bar{T}_{new}$ matrix is implemented in the VN, and the NPH and INC represent the neural filter $\bar{H}$.

This would be consistent with the interpretation of the INC and NPH as leaky integrators [44]. The cross-midline pathways correspond to the VN-VN and possibly INC-INC and NPH-NPH interactions. The flocculus was proposed to implement the $\bar{C}$ matrix for two reasons:

- There are connections from the VN and NPH to the flocculus and back for both horizontal and vertical canal-related neurons.

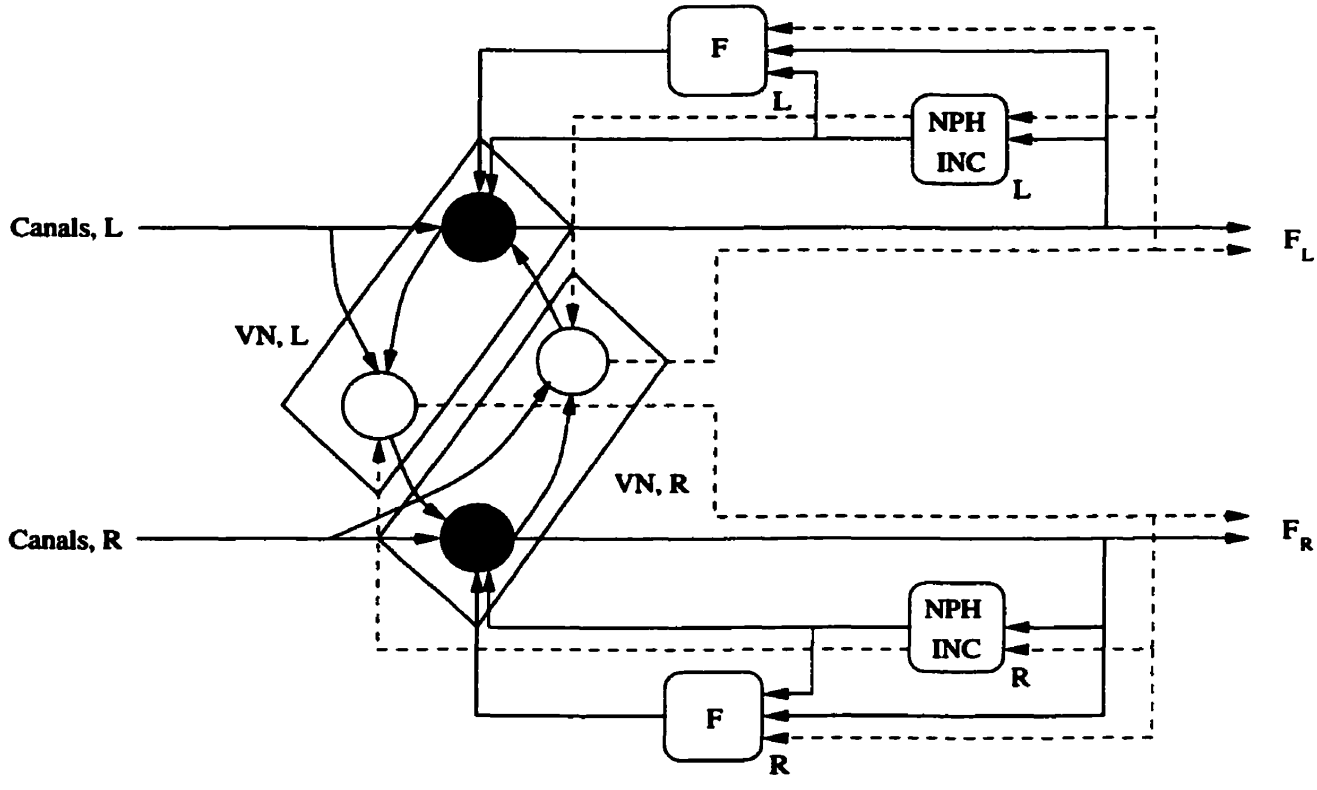

Figure 4.6: Suggested mapping of bilateral model to anatomical pathways. NPH- nucleus prepositus hypoglossi, INC- interstitial nucleus of Cajal, VN- vestibular nucleus, F- flocculus. Contralateral projections from VN to NPH and F and back have been drawn with dashed lines for illustrative simplicity.

• Experimental results concerning the effect of floccular lesion on the VOR vary, with the effects generally being more noticeable in vertical/torsional VOR than in normal horizontal VOR. In [66], two theories of the floccular effect on the VOR are cited; one that would lead to the flocculus increasing VOR gain and the other decreasing it. Examining the second model form (Figure 3.2), the diagonal terms of the $\bar{C}$ matrix would lead to decreasing gain, but the off-diagonal terms would have mixed effects. Furthermore, the magnitude of floccular lesion effects would depend on the relative distribution of the position dependencies between the $\bar{T}_{new}$ matrix (proposed to be VN implemented) and the $\bar{C}$ matrix. Decreased gain for pure horizontal, torsional, or vertical VOR might also occur if some of the primary orientation gain was transferred to the feedback loop. For example, if $\bar{T}_{new} = 0.9\bar{I}$, $\bar{C} = \bar{I} - \bar{T}_{new}\bar{T}^{-1}$ would be $0.1\bar{I}$ in primary orientation.

A number of problems still remain to be worked out. For instance, in a 1987 study by Cannon and Robinson [16], bilateral lesions of the NPH were found to reduce the time constant of the horizontal integrator to 200ms, but also the time constant of the vertical integrator to 2.5s. Bilateral INC lesions, by contrast, have little effect on horizontal integration [44] . Some of the INC's actions may be routed through the NPH or other structures. Cross-midline INC-INC and NPH-NPH connections may be important for this function. A more detailed mapping of the proposed anatomical structure to the model will have to be formed to explain the distribution of neural filtering between the INC and NPH. This thesis considered only a very simple bilateral model in the context of slow-phase conjugate movement. The model will have to be re-examined in the context of vergence movements and saccades, along with further

literature review.

The diagrams in subsections 1-3 above give known connections based on the literature, but further study will be required before the diagram of Figure 4.6 can be mapped more precisely onto these connections.

4.2 Neural Network Models of the Oculomotor Integrator

This thesis has so far proposed a model of the three dimensional integrator in the VOR, expressed in the form of a block diagram. An important consideration from a biological perspective, however, is whether or not such a model can be implemented using neurons, and how the distributed nature of their processing might affect model predictions in the case of lesion or disease [26]. A number of articles have been written on this subject ([4], [95], [26]). Neural networks have been constructed to simulate velocity storage ([1], [2]), the integrator itself ([63], [18], [17], [5], [6], [7], [33], [32], [2]), and the VOR arc as a whole ([87], [88]). The following subsections will outline the major considerations involved, and the evolution of the models around them. A small neural network model to implement one aspect of the proposed 3D model is also presented.

4.2.1 Issues to Consider

The issues involved in creating a neural network implementation of the oculomotor integrator include:

- Avoiding integration of the resting firing rates of the neurons, even in the case where the background rate varies from neuron to neuron.
- Increasing the time constant of the network without putting unreasonably tight restrictions on the underlying physiology. For instance, if the network were trying to achieve integration through positive feedback, the synaptic weights between individual neurons should not all be required to stay within a small percentage of their total magnitude.
- The network should be robust to loss or change of a small percentage of its connections.
- Allowed connections should follow known anatomical pathways. Learning should only affect those that are known to adapt.
- The network must be consistent with experimentally observed phenomena such as Dale's law (neurons are either inhibitory or excitatory, not both).
- The network should have a physiological learning algorithm. Arnold and Robinson [7] suggested that such an algorithm should only use information readily available to the pre and post-synaptic neuron, shouldn't require complex computation and memory tasks, and should converge in a length of time independent of the number of neurons in the network.

The final network should give results and neuron characteristics in agreement with

experimentally observed values. Lesions to the network could be simulated by setting some weights to zero, and used as a test of the model to see if the modified network outputs resemble experimental lesion and disease results.

4.2.2 Existing Models

The models that follow generate the integrating properties of the oculomotor integrator via the interconnections of the neurons involved. This section will not describe proposals such as that of Shen [104] in which the integration is achieved through special properties of the membrane in certain types of neurons, (in the Shen case short-term potentiation), rather than through neuron interconnections.

One of the earliest neural network models of the oculomotor integrator was proposed by Kamath and Keller [63]. In this model each neuron has a firing rate of the form $y(x,t) = y(x)(1 - e^{-t/\tau})$ in response to a step input, or $y(x,s) = \frac{y(x)}{s(1+\tau s)}$ in the Laplace domain, where x is the effective input and τ (5 ms) is the membrane time constant of an individual neuron. y(x) is zero until some cell threshold x_T, beyond which it increases asymptotically with x to some saturation firing rate. The cell thresholds and saturation firing rates are drawn from Gaussian distributions. The model consists of two populations of neurons. The summed output of the first population of neurons, denoted by Y, forms the output of the oculomotor integrator. These neurons have feedback connections of strength k to every neuron in the population, including themselves. This population on its own can act as an integrator, but is too sensitive to changes in k to be physiological and would tend to be leaky. The introduction

of a second population of neurons, this time composed of uninterconnected neurons, was designed to increase the time constant further. The resultant model is shown in Figure 4.7.

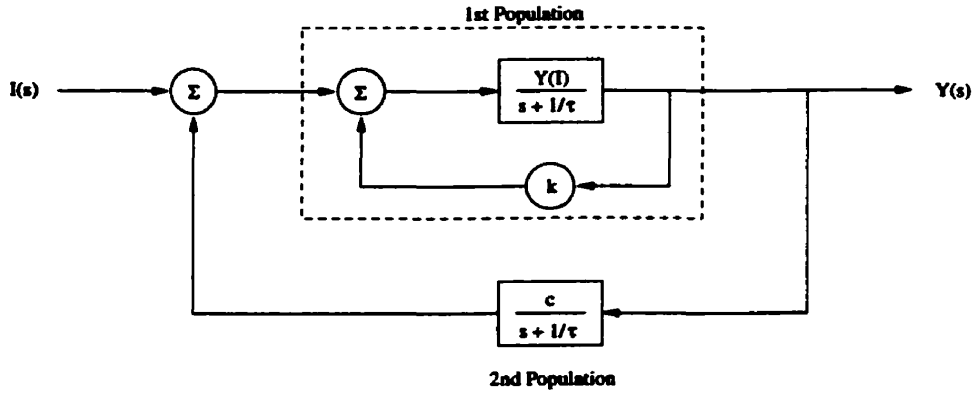

Figure 4.7: Kamath/Keller model, redrawn from [63]

This gives an increased integrator time constant that is relatively insensitive to changes in c. The model is still sensitive to changes in k, but the second population could compensate for fluctuations in k if allowed to adapt. Both forms would have to be modified to avoid integration of the neurons' resting rates, and require constant-magnitude input to function properly.

Cannon et al [18] proposed a lateral inhibitory model of the oculomotor integrator that avoids integration of the background rates and the extreme parameter sensitivity of the Kamath/Keller model.

This model was comprised of a pool of 32 homogeneous neurons whose firing rates obeyed the equation $\tau\dot{x}(t) + x(t) = i(t)$, where x(t) was the firing rate, i(t) was the net effective presynaptic input, and τ was the time constant of the first order cell dynamics. The neurons were assumed to be operating in a linear range about their

background rates. The net presynaptic input to neuron i was given by

$$i(t) = \sum_{j=1..M} v_{ij} u_j(t) - \sum_{j=1..N} w_{ij} x_j(t) \tag{4.5}$$

where u_j, j=1...M were the inputs to the network, and the weights w_{ij} represented the lateral inhibition of other neurons. The distribution of the weights was chosen to optimize the time constant of the network, achieving net positive feedback through the mutual inhibition of nearby neurons. The network was taken to have a ring-like structure to avoid the edge effects that would be introduced by end neurons having fewer laterally- inhibiting neurons. In the case where half the neurons receive a net external input $+\Delta$ and the other half $-\Delta$ at regular spacings, this results in a push-pull integrating network that is robust to noise on the connection weights and to the loss of one neuron.

Cannon and Robinson [17] later modified this network in two respects:

- They allowed a Gaussian distribution of afferent background rates.
- Neurons were permitted to carry both eye velocity and eye position signals, as is observed experimentally.

This was accomplished using a double-layer network of inhibitory and excitatory cells. The velocity inputs were only presented to local areas of the network, resulting in cells that carry different eye- velocity signals for different types of eye movements, as well as the integrated signal. The neurons of both layers received input afferents and projections from other neurons within their layer and from the other layer. The weights were consistent with Dale's law. Both layers served as outputs. This model still has shortcomings in that it would lead to firing rates less than zero for saccades

because nonlinearities have not been accounted for yet, and it does not give an idea of how the network would learn the appropriate connection weights to start with.

Quinn et al. ([87], [88]) formed an 8-neuron model of the bilateral integrator as a part of their model of the entire 3-neuron VOR arc. The model is shown in Figure 4.8. They used a method of global optimization described by Bremermann [14] to set the weights. This method gave low error solutions and allowed unbiased exploration of computational solutions.

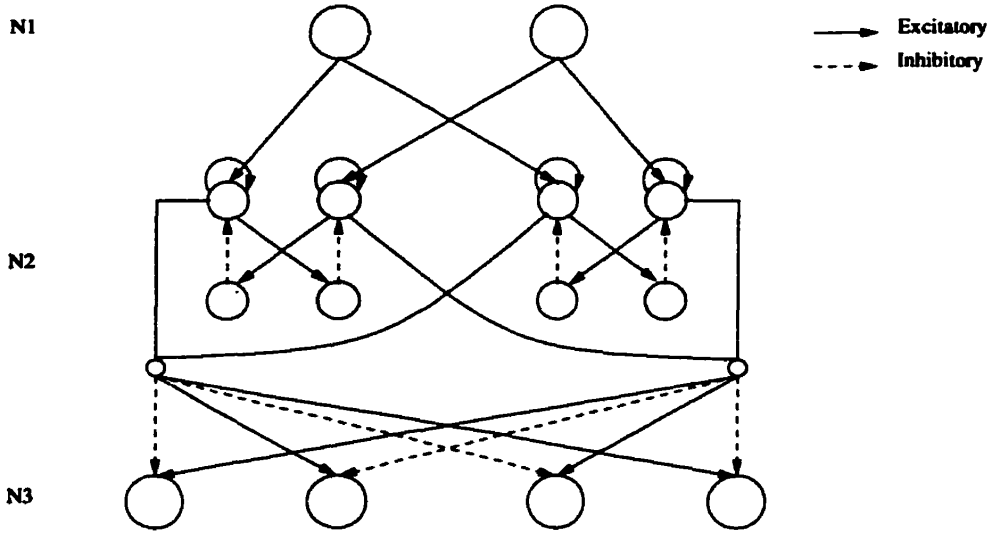

Figure 4.8: Quinn model, redrawn from [88].

Arnold and Robinson [6] proposed a self-organizing neural network that learned to integrate vestibular velocity commands using retinal image slip as an error signal. The method employed did not require backpropagation of information. The basic network consisted of push-pull input from 2 canals, a variable number of interneurons, and two motoneurons. Each input projected to each interneuron, each interneuron projected to all other interneurons, to itself, and to both motoneurons. The network learned

by considering the rms value of gaze velocity error over a set time period:

$$E = \sqrt{\int_{t=t_0}^{t=t_1} (g(t))^2 dt} \tag{4.6}$$

The weight changes were calculated using

$$\omega'_{ij} = \omega_{ij} - k(E)\frac{\frac{\partial E}{\partial \omega_{ij}}}{|\frac{\partial E}{\partial \omega_{ij}}|_{max}} \tag{4.7}$$

where $|\frac{\partial E}{\partial w_{ij}}|_{max}$ is the maximum value of $\frac{\partial E}{\partial w_{ij}}$ for that iteration over all network connection weights w_{ij}. The values of $\frac{\partial E}{\partial w_{ij}}$ were estimated using a brute-force method: by changing one weight at a time by an amount Δw_{ij}, and calculating the new error $E(w_{ij} + \Delta w_{ij})$ over the trajectory.

$$\frac{\partial E}{\partial \omega_{ij}} \approx \frac{E(\omega_{ij} + \Delta\omega_{ij}) - E}{\Delta\omega_{ij}} \tag{4.8}$$

k(E) was an adaptive learning rate to prevent rapid, unstable changes.

Two versions of the model were constructed: one to generate only a position command, the other to generate the velocity component as well. The networks were constructed with constraints on the weights to satisfy observed effects of neurons on each other within and between groups, and the necessary changes for this were described.

Arnold and Robinson [7] described an updated version of this model that learns using a more physiologically plausible Hebbian-like learning algorithm. This model attempted to make the network connections reflect known anatomy more closely, using four groups of neurons representing vestibular (V), NPH-MVN (P1,P2), and motoneurons (M) as shown in Figure 4.9.

This model was also trained first as an integrator, then to compensate for eye orbital mechanics as well. The learning rule was $\Delta w_{ij} = \pm k_{ij} \times RS \times \Delta f_{yj}$, where

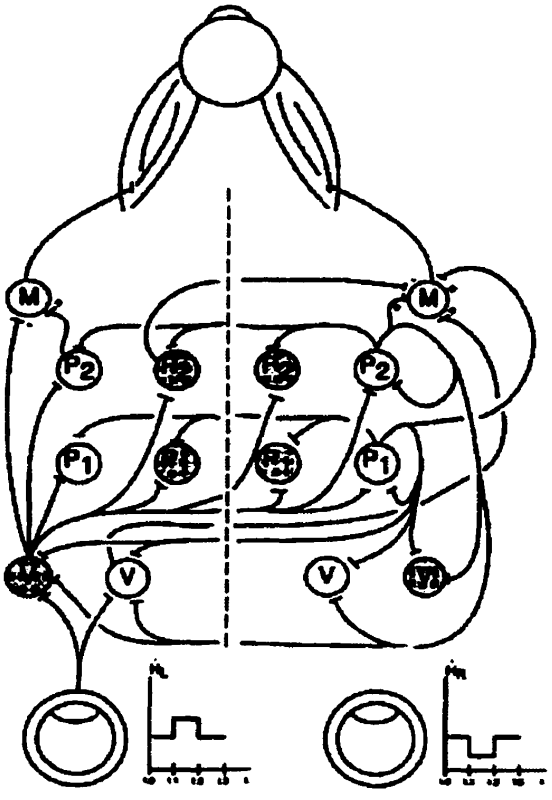

Figure 4.9: Arnold/Robinson model, reprinted from [7] with the permission of Springer-Verlag New York, Inc. Some types of connections are shown only once to avoid clutter.

Δf_{vj} is the change in firing rate from resting rate, RS is the retinal slip, k_{ij} is a scale factor controlling learning rate. This rule goes to zero as the retinal slip does. Some frequency dependent modifications were used for the plant-compensating network, but the basic idea was the same.

Draye et al. ([33], [32]) used the 1991 model of Arnold and Robinson as a basis for their model, but sought to improve it by requiring the neurons to follow Dale's law (Dale's law states that a neuron's actions on other neurons must be either excitatory or inhibitory, not both), and by introducing a notion of distance in the form of synaptic delays between units to avoid an over-distributed model. The learning algorithm of this model involved adaptation of both the classical weights between units and the time constant associated with each neuron. They found that the constraint that the weights obey Dale's law led to the spontaneous emergence of clusters of particularly strong interconnections between some neighbourhoods of interneurons. This was an interesting development, as such clusters have been observed in Goldfish NI and in the NPH of the cat [33]. Draye et al. used a biologically plausible learning process involving the Levenberg-Marquardt minimization technique [49] for their recurrent network.

A number of neural network models have been constructed to deal with other aspects of VOR such as velocity storage ([1], [2]), the coordinate transformation between canal and muscle frames [4], and the combination of oculomotor signals of different origins [3].

4.2.3 Further Considerations

It should be noted that the models constructed so far have used retinal slip as an error source, but it may be possible that extraocular muscle afferent feedback plays a role in generating a teaching signal as well, as several articles have indicated evidence of EOM afferents influencing neurons in the vestibulo-oculomotor system [15], [31], [65]. The nature of the retinal slip error for 3D movement should be considered thoroughly before deciding on representations and learning algorithms. Some researchers have started to investigate 3D retinal slip [51], and demonstrated a spatial preference for its coordinate system, similar to vestibular sensors. Other important considerations will include the degree of interconnectivity (distributivity) of the network, and the number of groups of neurons representing the INC, NPH and flocculus, each of which have more than one functional group ([72], [28]).

4.2.4 A Possible Use for Neural Thresholds in 3D

Although a full neural network model for the 3D integrator is beyond the scope of this project, one interesting aspect was investigated: that is, the use of thresholds and saturation in generating the required nonlinearities for the 3D model. The nonlinearities of the models described in the second and third chapters could be accomplished by neurons in a number of ways, but one feature stands out as interesting: that is, the wide range of neuronal thresholds, and their dependence upon the cell's position sensitivity. This has previously been attributed to the need to accomodate eye plant nonlinearities, but could potentially also play a role in accounting for rotational non-

commutativity. The model described in this thesis requires matrix gains that depend on position. However, if some neurons only turned on for position/velocity combinations above a certain value, the overall input seen at the VN level could vary with position even if the individual neurons behaved linearly once activated. As many VN neurons do appear to have almost linear rate-position responses ([103], [76]), it was felt that this would be an interesting point to examine.

To test this idea, a simple feedforward neural network consisting of 3 input units, 20 hidden units and one output unit was constructed and trained using a backpropagation algorithm. The inputs were w_x, θ, and ϕ, referring respectively to input torsional angular velocity, vertical position, and horizontal position in the model of Figure 2.1. The hidden unit outputs were taken to be T_i for weighted summed inputs below their threshold T_i, and equal to the weighted summed input above the threshold until a saturation point at a fixed level above the on-threshold, beyond which the neuron's output was taken to be the saturation value. The output unit had a threshold of zero and no saturation value, as it had to supply the full output for the whole range of inputs. All input units were connected to all hidden units, and all hidden ones to the output, with initially random weightings. The network was trained using a backpropagation algorithm (see Appendix D for code).

It should be noted that the idea of this exercise was solely to investigate whether thresholds and saturation alone could aid in linearizing the required 3D neuron functions. No attempt was made to use a plausible learning algorithm or to examine the effects of other nonlinearities, as these would require much more detailed knowledge

of the system. The network was trained to produce the output $w_x \frac{\sin\theta}{\cos\phi}$, the desired contribution of roll input to ϕ as a function of position for the first representation in Chapter 2. This was chosen for illustration because the desired response is zero for any value of w_x when θ is zero, but a position-dependent constant times w_x for non-zero θ. Thus, any non-position dependent approximation will perform terribly. After 4000 iterations, the network output was as shown in Figure 4.10, with the desired output shown beside it.

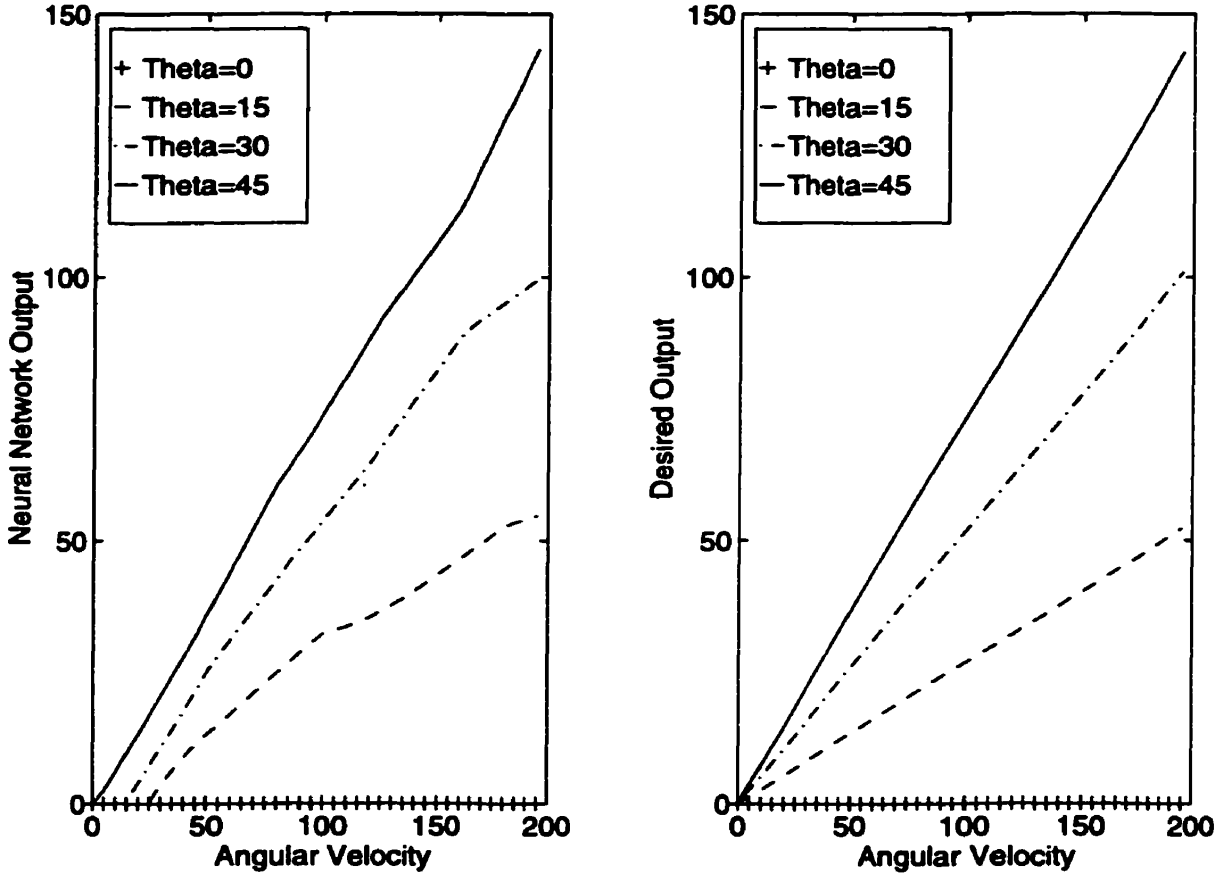

Figure 4.10: Torsional angular velocity contribution to horizontal neuron firing rate as a function of θ for ϕ equal to 15 degrees. Plots show neural network and desired output versus ω_x (deg/s).

Although this response is far from perfect, it does nonetheless display a posi-

tion dependent response that is better than a constant gain would be. Thus, with an ad-hoc network of only 20 hidden units behaving linearly except for a threshold and saturation, already there is significant capacity for position-dependent behaviour. Although neurons have other means of adjusting gains, the threshold/saturation solution might be appealing over the long term because it wouldn't involve control of synaptic gains on the fly: by accepting a feedback efference copy of eye position, these nonlinearities alone could account for some of the position dependence.

This result may seem trivial, given that it has been proven theoretically that feedforward neural networks employing somewhat similar activation functions can approximate any static function to arbitrary accuracy given an appropriate number of input, hidden and output units and proper interconnecting weights [27]. However, it does serve as a reminder that complex 3D math computations could be achieved in a straightforward manner, without requiring special separate computational stages.

Chapter 5

Discussion/Conclusions

A 3D model of VOR central processing to provide for the non-commutativity of eye rotations was presented. It is based on feedback through a neural filter in place of a feedforward integrator. The necessary adjustments to account for rotational non-commutativity could be achieved with a position- dependent matrix in either the forward or a feedback path, or distributed between the two. A bilateral implementation of the model that gives different common mode and difference mode time constants was also considered.

A possible anatomical substrate for the model was also presented based on literature regarding horizontal and vertical integrator pathways and their interaction. This solution is compatible with known anatomy linking VN brainstem sites to INC, NPH, and cerebellar flocculus. A small neural network model to illustrate how the position dependent gains might be accomplished was presented. The issue of orientation representation and how it could affect the interpretation of experimental results was also discussed.

5.1 Predicted Responses and Effects of Lesions

The conclusions drawn based on bilateral model simulations were as follows:

• The gain between the canals and extraocular muscles must be position-dependent for rotations that are not about the current orientation axis.

• Cutting commissural fibres will still have the same result in 3D responses as in one dimension: reduction of the overall time constant, but no new position dependencies.

• Eliminating feedback corrections ($\bar{C}$ matrix) on one or both sides of the model in the feedback implementation will result in eye position dependent dynamics (assuming the commissural connections are left unaffected and are still position-dependent).

• Lesions to the feedback filter will have potentially two effects: 1) The time constant of the affected pathway will be reduced, and 2) The estimated position for that component will be too small, which could affect other pathways via miscalculation of their appropriate matrix gains. The first effect would tend to make the affected component go to zero, so the second effect may not be noticeable except when the velocity component is large enough to dominate and keep the affected component nonzero.

5.2 Anatomical Support of 3D Bilateral Model

For the second part of the thesis, an anatomical mapping of the second bilateral model form was proposed as follows based on literature review:

• VN implementation of the feedforward matrix $\bar{T}_{new}$ and the cross-midline gain

matrices $\bar{G}_{LtoR}$ and $\bar{G}_{RtoL}$. Bilateral VN-VN connections would be involved here. INC-INC and NPH-NPH connections may augment the cross-midline contributions.

• INC implementation of the vertical and torsional neural filters, and NPH implementation of the horizontal neural filters.

• Floccular implementation of the ipsilateral feedback position-dependent corrections ($\bar{C}$ matrices).

A substrate for cross-talk between the horizontal and vertical pathways was also proposed, the main connections being the following:

• Bidirectional connections between ipsilateral INC and NPH.

• Excitatory connections from type I posterior canal VN neurons to contralateral NPH (rabbit, cat and monkey), and from excitatory anterior canal VN neurons to contralateral NPH in monkeys.

• Inhibitory connections from type II anterior canal VN neurons to type I horizontal VN neurons, and from inhibitory type II horizontal and posterior canal VN neurons to type I posterior canal VN neurons. Other VN-VN connections may also exist.

• Excitatory connections from ipsilateral INC to type II horizontal canal VN neurons.

• Connections from the VN to the ipsilateral flocculus.

Although this thesis restricted the search to interconnections between structures known to be important for normal horizontal and vertical slow- phase VOR, it is possible that other structures may be important specifically for cross-talk. These sites should be considered if models involving the above connections prove to be

insufficient, or if other types of eye movements are also being considered.

5.3 Neural Network Approaches

A review of neural network models of the VOR and oculomotor integrator was conducted, and a small neural network was constructed to demonstrate how thresholding and saturation of units that behave linearly between these values might contribute to the desired position-dependent behaviour. Based on the review, the following considerations were thought to be relevant for a future neural network implementation of the current model.

- Allowable neural network connections should be anatomically based; the connections given in sections one through three of chapter four might be a good starting point. The properties of individual neurons and the relative number of neighbours they project to should also be a consideration. The INC, NPH and flocculus may each require several groups of neurons for adequate representation.

- The learning algorithm should be physiologically plausible. The nature of retinal slip error and extraocular muscle proprioception and their representation in the system should be investigated thoroughly before deciding upon an appropriate algorithm.

- The resulting network should be consistent with experimentally observed phenomena such as Dale's law.

5.4 Recommendations for Future Work

There are a number of areas that remain to be explored. The interaction of the slow-phase VOR with its fast phases and with other types of eye movement such as vergence and saccades has not been considered yet. Modifications may be required for an appropriate 3D vergence response, as the model was designed and studied in the context of conjugate movement. The geometrical misalignment of the canals and extraocular muscles was not examined, as it was felt that further knowledge of VOR interaction with vision during learning and adaptation would have been required to choose an appropriate representation for these transformations. The effects of time delays in neuronal implementation were also not considered.

In conclusion, two considerations are of immediate importance if the proposed model is to be eventually made clinically relevant. First, the interaction of VOR fast and slow phases must be extended to 3D. Second, an appropriate representation of orientation for the oculomotor system should be chosen, based on a consideration of how the VOR is learned and adapted. Direct comparison of simulation results and experimentally observed 3D VOR movements will be required for both goals, as well as for validating and revising the anatomical substrate proposed in this thesis. The studies described in ([24], [25], [113], [111], [79]) would be a good starting point for examining the issue of orientation representation.

Appendix A

Rotational Math Appendix

A.1 3D Representations of Orientation

There are a number of ways to describe the 3D orientation of an object ([108], [13], [57]). Rotation matrices can be used to describe orientation in terms of consecutive rotations about three space-fixed or object-fixed axes, or in terms of a single rotation about a general axis in the space-fixed coordinate frame. Quaternions provide an alternative means of describing orientation in terms of a single rotation about a general axis in the space-fixed frame. This appendix provides a review of these methods.

A.1.1 Sequential Rotation Representations

Consider a general vector $\vec{r_0} = (x_0, y_0, z_0)^T$ in a coordinate frame defined by axes $\hat{x}$, $\hat{y}$, and $\hat{z}$, where $\hat{x}$, $\hat{y}$, and $\hat{z}$ are orthogonal. For a rotation about any of the three axes, the component of $\vec{r_0}$ along that axis will not change. The components of $\vec{r_0}$ initially along the other two axes will project onto each other with increasing rotation angle.

Thus, rotations of ψ, θ, and ϕ about the x, y and z axes respectively can be described by the rotation matrices

$$R_x = \begin{pmatrix} 1 & 0 & 0 \\ 0 & \cos\psi & -\sin\psi \\ 0 & \sin\psi & \cos\psi \end{pmatrix} \tag{A.1}$$

$$R_y = \begin{pmatrix} \cos\theta & 0 & \sin\theta \\ 0 & 1 & 0 \\ -\sin\theta & 0 & \cos\theta \end{pmatrix} \tag{A.2}$$

$$R_z = \begin{pmatrix} \cos\phi & -\sin\phi & 0 \\ \sin\phi & \cos\phi & 0 \\ 0 & 0 & 1 \end{pmatrix} \tag{A.3}$$

These rotation matrices allow only orientations that are achieved through rotation about one of the principal axes. As there are three degrees of freedom, a general orientation can be described by a composite of rotations about each of these axes. For instance, if $\vec{r_0}$ underwent a rotation ψ about $\hat{x}$, then θ about $\hat{y}$, then ϕ about $\hat{z}$, the new position $\vec{r}$ would be described by $\vec{r} = R_z R_y R_x \vec{r_0}$. This describes the new position in terms of sequential rotations about three space-fixed axes; however, there is another interpretation. Consider a coordinate system that rotates with the object. A rotation of ϕ about the z axis will rotate the x and y axes into new positions in the original x-y plane. If the eye is then rotated by θ about the new y axis, this is equivalent to a rotation $R_z R_y R_z^{-1}$ in the head-fixed frame (this rotates $\vec{r_0}$ and $\hat{y}$ back

to the original frame, rotates $\vec{r}$ about $\hat{y}$, then rotates back to the eye-fixed frame). If a third rotation about the object- fixed x axis is then considered, the equivalent head fixed rotation is $R_z R_y R_x R_y^{-1} R_z^{-1}$. Combining these rotations gives a net rotation $R = (R_z R_y R_x R_y^{-1} R_z^{-1})(R_z R_y R_z^{-1}) R_z = R_z R_y R_x$.

Thus the rotation $R = R_z R_y R_x$ can be thought of either as the sequence of rotations ψ, θ, and ϕ about the x, y and z axes in the space-fixed reference frame, or as the sequence ϕ, θ, ψ about the z, y and x axes in the object-fixed coordinate system. This latter interpretation is known as the Fick-gimbal representation. Another gimbal representation, the Helmholtz gimbal system, is identical to the Fick system except that the orientation is broken down into rotations about the y, z and x axes respectively, giving $R = R_y R_z R_x$ instead of $R = R_z R_y R_x$. For further details, the reader is referred to [108], [57].

A.1.2 Rotation about a Single, Arbitrary Axis

The above descriptions break down the overall rotation matrix into three sequential simple rotations. However, any general orientation can also be achieved by a single rotation if the axis of rotation is permitted to be general rather than only one of the three main axis. For a rotation of angle Θ about an axis (k_x, k_y, k_z), Spong and Vidyasagar [108] give the corresponding rotation matrix:

$$\bar{R}_{k,\Theta} = \begin{pmatrix} k_x^2 v_\Theta + c_\Theta & k_x k_y v_\Theta - k_z s_\Theta & k_x k_z v_\Theta + k_y s_\Theta \\ k_x k_y v_\Theta + k_z s_\Theta & k_y^2 v_\Theta + c_\Theta & k_y k_z v_\Theta - k_x s_\Theta \\ k_x k_z v_\Theta - k_y s_\Theta & k_y k_z v_\Theta + k_x s_\Theta & k_z^2 v_\Theta + c_\Theta \end{pmatrix} \tag{A.4}$$

where $c_\Theta = \cos\Theta$, $s_\Theta = \sin\Theta$, and $v_\Theta = 1 - \cos\Theta$. The angle and axis can be retrieved from a general rotation matrix R using:

$$\Theta = \arccos\left(\frac{r_{11} + r_{22} + r_{33} - 1}{2}\right) \tag{A.5}$$

$$\vec{k} = \frac{1}{2\sin\Theta}\begin{pmatrix} r_{32} - r_{23} \\ r_{13} - r_{31} \\ r_{21} - r_{12} \end{pmatrix} \tag{A.6}$$

where r_{ij} corresponds to an element in the $\bar{R}_{k,\Theta}$ matrix in the i^{th} row and j^{th} column.

A.1.3 Quaternions

Invented by Sir William Rowan Hamilton in 1843, quaternions are four-component rotational operators that provide an elegant alternative to the matrix approach for describing rotations. A general quaternion has the form $q = q_0 + q_1 i + q_2 j + q_3 k$ where q_0, q_1, q_2 and q_3 are real, $i^2 = j^2 = k^2 = -1$, $ij = -ji = k$, $jk = -kj = i$, and $ki = -ik = j$ [13]. With these definitions of directions i, j, and k, the quaternion can be regarded as the sum of a scalar and a vector. Quaternion addition, subtraction, multiplication, and division can be defined for two general quaternions p and q as follows:

$$p \pm q = (p_0 \pm q_0) + (\vec{p} \pm \vec{q}) \tag{A.7}$$

$$pq = p_0 q_0 - \vec{p}\cdot\vec{q} + p_0\vec{q} + q_0\vec{p} + \vec{p}\times\vec{q} \tag{A.8}$$

$$pq^{-1} = p_0 q_0^{-1} - \vec{p}\cdot\vec{q^{-1}} + p_0\vec{q^{-1}} + q_0^{-1}\vec{p} + \vec{p}\times\vec{q^{-1}} \tag{A.9}$$

where $q^{-1} = \frac{q_0 - \vec{q}}{\sqrt{q_0^2 + |\vec{q}|^2}}$, $\pm$ denote vector addition and subtraction, $\cdot$ denotes the vector dot product, and $\times$ denotes the vector cross product. A quaternion can also be rewritten as

$$q = \mid q \mid (\cos\Theta + \hat{e}\sin\Theta) = \mid q \mid (\cos\frac{\theta}{2} + \hat{e}\sin\frac{\theta}{2}) \tag{A.10}$$

$$\hat{e} = \frac{q_1 i + q_2 j + q_3 k}{\sqrt{q_1^2 + q_2^2 + q_3^2}} \tag{A.11}$$

where Θ is called the angle of q. It can be shown that for a general quaternion q and vector $\vec{r}$, the quaternion product $\vec{r}' = q\vec{r}q^{-1}$ will be the vector $\vec{r}$ rotated conically about $\hat{e}$ through θ (twice the angle Θ). As the scalar component of the unit quaternion contains no new information, a rotation vector $\vec{r} = \frac{\vec{q}}{q_0} = tan(\frac{\theta}{2}) \times \frac{\vec{q}}{|q|} = tan(\frac{\theta}{2}) \times \hat{n}$ can be used to represent the same information more concisely [57]. The rotation vector of a general rotation matrix R is given by

$$\vec{r} = \frac{1}{1 + r_{11} + r_{22} + r_{33}} \times \begin{pmatrix} r_{32} - r_{23} \\ r_{13} - r_{31} \\ r_{21} - r_{12} \end{pmatrix} . \tag{A.12}$$

A.2 Covariant vs. Contravariant Representations

Given an orthogonal external reference frame described by axes $\hat{i}$, $\hat{j}$ and $\hat{k}$, and a non-orthogonal intrinsic reference frame described by axes $\hat{x}$, $\hat{y}$, and $\hat{z}$, there are two different ways that a general vector $\vec{R} = r_i\hat{i} + r_j\hat{j} + r_k\hat{k}$ could be represented in the reference frame defined by $\hat{x}$, $\hat{y}$ and $\hat{z}$. These are illustrated in Figure A.1.

In the covariant representation, the x, y, and z components are the orthogonal

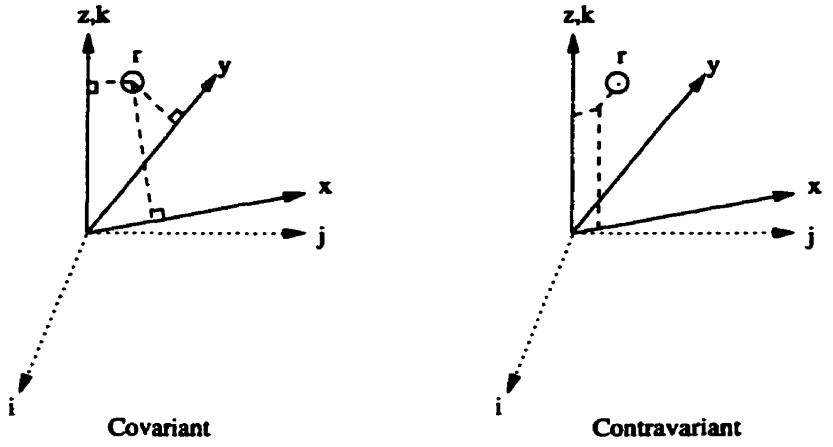

Figure A.1: Covariant and contravariant representations of a vector in a non-orthogonal reference frame.

projections of $\vec{R}$ onto the $\hat{x}$, $\hat{y}$, and $\hat{z}$ axes respectively. These components will not generally sum to give the original $\hat{R}$ if re-expressed in the original ijk coordinates. In the contravariant representation, the x, y and z components expressed in the ijk frame sum to give $\vec{R}$ in the ijk frame. The x component in this representation would be obtained as follows: 1) project $\vec{R}$ onto the xz plane such that $\vec{R}$ and the xz intersection point form a line parallel to the $\hat{y}$ axis. 2) project the xz plane intersection point onto the x-axis such that the line segment between them is parallel to the z axis. 3) the x component is the line segment from the origin to the x-axis intersection point formed in 2). The y and z coordinates are obtained in an analogous fashion. The covariant and contravariant representations are identical only for orthogonal reference frames.

Appendix B

Abbreviations

(P)PRF- (Paramedian) Pontine Reticular Formation

HC- Horizontal Canal

PC- Posterior Canal

AC- Anterior Canal

VN- Vestibular Nucleus (M- medial, S- superior)

NPH- Nucleus Prepositus Hypoglossi

F- Flocculus

Y- Cell Y Group

FTN- Floccular Target Neuron

FPN- Floccular Projecting Neuron

INC- Interstitial Nucleus of Cajal

Appendix C

Mason's Rule

Mason's Rule is used to determine the relationship between input and output nodes on a signal flow graph. The formula is as follows:

$$\frac{O}{I} = \frac{\Sigma_k M_k \Delta_k}{\Delta} \ , \tag{C.1}$$

where Δ is called the graph determinant

$$\Delta = 1 - \Sigma_m P_{m1} + \Sigma_m P_{m2} - \Sigma_m P_{m3} + \ldots \ ; \tag{C.2}$$

M_k is the forward gain of the k^{th} direct forward path between input (I) and output (0), and Δ_k is the graph determinant for the system after removing the k^{th} forward path [68]. In equation C.2, P_{mr} is the gain product of the m^{th} possible combination of r non-touching loops. $\Sigma_m P_{m1}$ is a special case adding the loop gains of all distinct loops in the graph.

To demonstrate how this is used, consider one output, M_L, in the circuit of Figure C.1. Assuming the clear nodes to be summing junctions and the filled nodes to be summing junctions followed by gain -1, there are two non-touching loops of gain

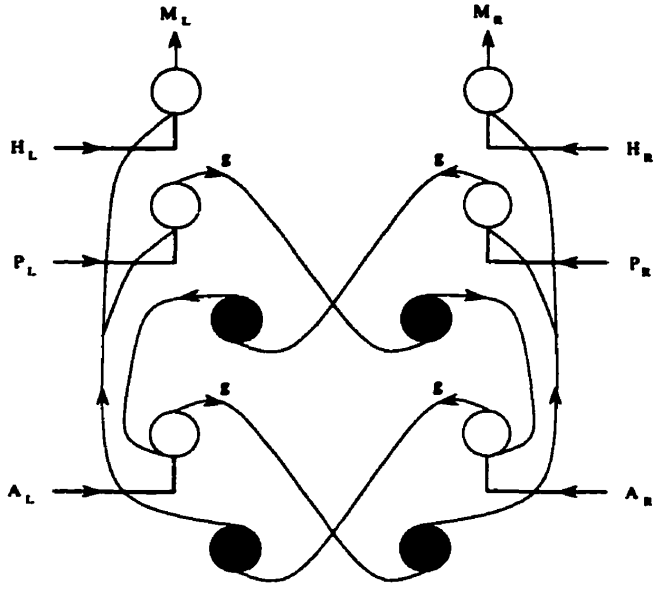

Figure C.1: AC neuron inhibition of HC neurons.

$(-g)(-g) = g^2$ in the circuit. Therefore, $\Delta = 1-(g^2+g^2)+g^4 = (1-g^2)^2$. Considering the inputs, there are pathways from H_L, P_L and A_R to M_L with feedforward gains of 1, g^2, and $-g$, respectively. There are no pathways from H_R, P_R, or A_L to M_L. The Δ_k values for each of the feedforward pathways must then be computed. For the H_L pathway, elimination of the feedforward pathway nodes gives a graph as shown in Figure C.2.

This has the same Δ as before, as neither loop is affected. For P_L, the graph reduces to the one shown in Figure C.3.

This has one intact loop, giving $\Delta_{P_L} = (1 - g^2)$. For A_R, the graph is as shown in Figure C.4, and $\Delta_{A_R} = (1 - g^2)$.

Combining these results,

$$M_L = \frac{\Delta_{H_L}(1)H_L + \Delta_{A_R}(-g)A_R + \Delta_{P_L}(g^2)P_L}{\Delta} \tag{C.3}$$

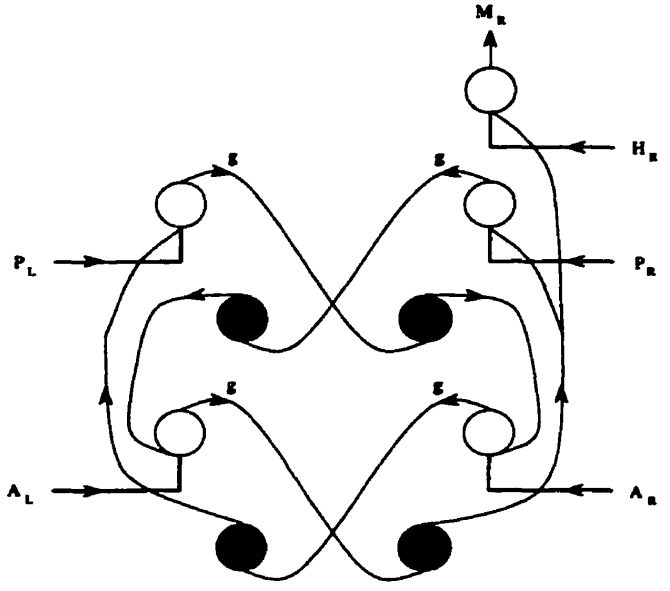

Figure C.2: Circuit with nodes joining H_L to M_L removed.

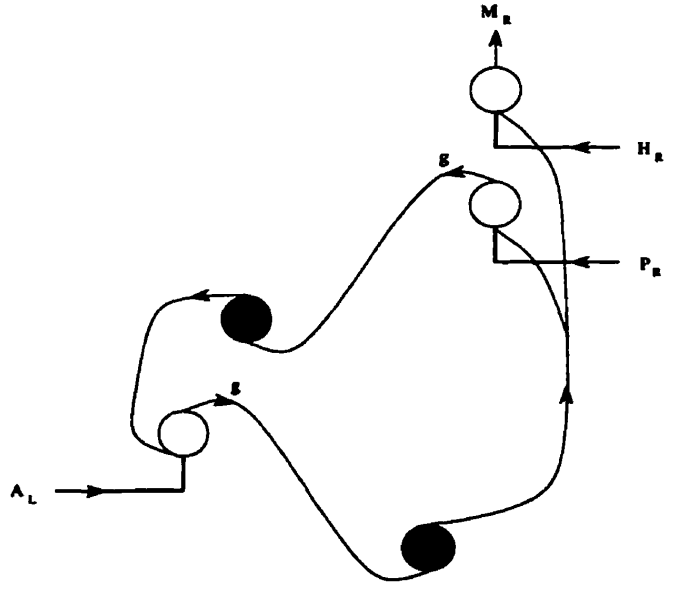

Figure C.3: Circuit with nodes joining P_L to M_L removed.

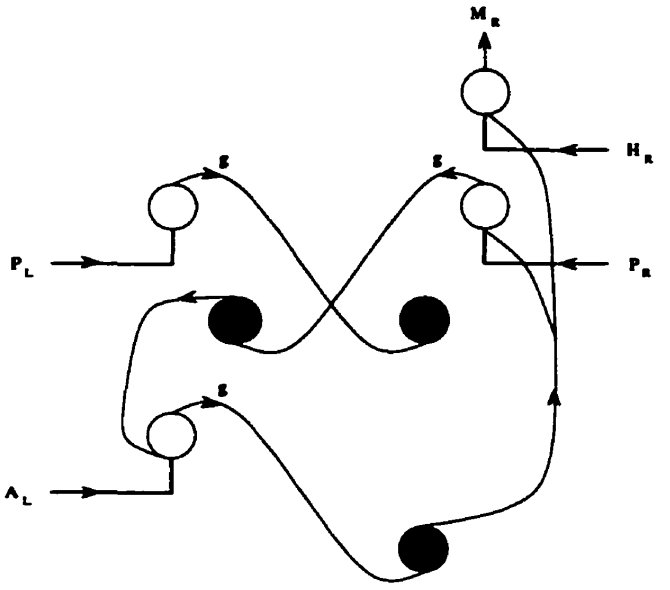

Figure C.4: Circuit with nodes joining A_R to M_L removed.

or,

$$M_L = H_L - \frac{gA_R}{(1-g^2)} + \frac{g^2 P_L}{(1-g^2)} \,. \tag{C.4}$$

Appendix D

Neural Network Code

The following Matlab code was used to create and test the feedforward network in section 2.4 of chapter 4.

```
% Neural network training code to try to generate required nonlinearities
% using units with thresholds and saturation (linear response between these
% values).

% Training input values
w=[0 50 100 150 200; 10 60 110 160 210; 20 70 120 170 220;
   30 80 130 180 230; 40 90 140 190 240];
a=[0 10 20 30 40 50; 2 12 22 32 42 52; 4 14 24 34 44 54;
   6 16 26 36 46 56; 8 18 28 38 48 58];
po=zeros(900,4);          % columns: w, theta*200/45, phi*200/45, desired o/p

% Generate input patterns and corresponding desired outputs
for N=0:4
for i=1:5
for j=1:6
for k=1:6
ind=(i-1)*36+(j-1)*6+k+180*N;
po(ind,1)=w(N+1,i);
po(ind,2)=a(N+1,j)*200/45;      % want phi, theta to
po(ind,3)=a(N+1,k)*200/45;      % determine active structure- scale so all
po(ind,4)=w(N+1,i)*sin(a(N+1,j)*pi/180)/cos(a(N+1,k)*pi/180);  % inputs have
```

```
end;                                                    % similar ranges
end;
end;
end;

% Batch mode training.
% Use 5 different sets of patterns so the network trains with
% a higher resolution of w, phi, theta without taking too long at
% each iteration (choose the set randomly at each iteration).

NJ=20;                    % Number of hidden units
Tn_arr=randn(NJ,1)*50;  % Hidden unit thresholds
S_arr=randn(NJ,1)*50+250+Tn_arr; % Hidden unit saturation
wij=randn(3,NJ)*0.3+ones(3,NJ)*0.2 ;   % Input-Hidden unit weights
wjk=randn(1,NJ)*0.15;   % Hidden unit-Output weights
wij0=wij;                % Store initial weights for comparison
wjk0=wjk;
J_arr=zeros(NJ,180);       % Activity of hidden units
Oa=zeros(180,1);           % Actual output
E=zeros(180,1);            % Error for each pattern in the set
tempEjk=zeros(NJ,180);     % Partial derivatives dE/dwjk
tempEijw=zeros(NJ,180);    % dE/dwij
tempEijt=zeros(NJ,180);
tempEijp=zeros(NJ,180);
itnum=2000;                % number of iterations
kij=0.03;                  % coefficients controlling learning rate
kjk=0.015;
dEijmax=[0 0 0];           % maximum partial derivative observed so
dEjkmax=0;                 % far (used to adapt learning rate)
Earr=zeros(itnum,1);       % save maximum error of all patterns at each
                           % iteration as a measure of the network's
                           % learning evolution.
for it=1:itnum
  nonzero=zeros(NJ,1);   % # of units that are between thres. and sat.
  pnum=fix(rand*4.9999);  % pattern set to use.
  for ind=1:180
    p=pnum*180+ind;
    uthres=zeros(NJ);          % unit is either under threshold
    for unit=1:NJ              % or at saturation if uthres==1 (0 otherwise)
      J_arr(unit,ind)=po(p,1:3)*wij(1:3,unit); % effective input to hidden u.
      if (J_arr(unit,ind)<Tn_arr(unit))     % unit below thres.
         J_arr(unit,ind)=Tn_arr(unit);
         uthres(unit)=1;
      elseif(J_arr(unit,ind)>S_arr(unit))   % unit saturated
         J_arr(unit,ind)=S_arr(unit);
```

```
          uthres(unit)=1;
        end;
      end;
      Oa(ind)=max(wjk*J_arr(1:NJ,ind),0);      % Network Output
      E(ind)=po(p,4)-Oa(ind,1);                % E'=0.5*E^2
      tempEjk(:,ind)=-1*J_arr(:,ind)*E(ind);   % dE'/dwjk=dE'/dOa*dOa/dwjk
  % Note: technically dE/dwjk is 0 if the output unit is below threshold, but
  % tempEjk provides a measure of what the derivative would be if the unit wasn't
  % below threshold.  If 0 were used, the network wouldn't adapt to
  % accomodate patterns that require non-zero output but whose inputs aren't
  % sufficient to put the unit above threshold for the current weightset
  % (this would not be a problem if many output units were used, as then at
  % least some would be above threshold and could adapt).
      for unit=1:NJ                            % hidden u. derivs.
        if (uthres(unit)>0.5)
            tempEijw(unit,ind)=0;              % if unit at sat. or below thres.
            tempEijt(unit,ind)=0;              % its deriv. wrt. ip. weight is 0.
            tempEijp(unit,ind)=0;
          else
            tempEijw(unit,ind)=-po(p,1)*wjk(unit)*E(ind);
            tempEijt(unit,ind)=-po(p,2)*wjk(unit)*E(ind);
            tempEijp(unit,ind)=-po(p,3)*wjk(unit)*E(ind);
            nonzero(unit)=nonzero(unit)+1;
        end;
      end;
    end;
    for unit=1:NJ
      denom=max(nonzero(unit),1);   % for wij's, use the average deriv. for the
      dEij(1,unit)=sum(tempEijw(unit,:))/denom;  % units that are between
      dEij(2,unit)=sum(tempEijt(unit,:))/denom;  % thres. and saturation- if
      dEij(3,unit)=sum(tempEijp(unit,:))/denom;  % this pulls weights out of
      dEjk(1,unit)=sum(tempEjk(unit,:))/180;     % good range, errors in next
    end;                                         % iteration will bring back
    for ip=1:3                  % compare deriv. magnitudes to previous max.
      dEijmax(ip)=max(max(abs(dEij(ip,:))),dEijmax(ip));
    end;
    dEjkmax=max(max(abs(dEjk)),dEjkmax);
    for unit=1:NJ                    % update weights
      for ip=1:3
        wij(ip,unit)=wij(ip,unit)-kij*dEij(ip,unit)/dEijmax(ip);
      end;
      wjk(1,unit)=wjk(1,unit)-kjk*dEjk(1,unit)/dEjkmax;
    end;
    Earr(it)=max(abs(E));
  end;
```

```
% Testcode:  look at results for values between training patterns

% make nnplot.ps
load nn0806a.mat          % network weights, thresholds, saturation
theta=[0 15 30 45];
phi=15;
w=0:5:195;
Od=zeros(4,40);
Oa=zeros(4,40);
jarr=zeros(NJ,1);

for i=1:4                  % Desired outputs
    Od(i,:)=sin(theta(i)*pi/180)*w/cos(phi*pi/180);
end;

in3=phi*200/45;           % scale input to what network is trained with
for i=1:4
  for k=1:40
     for unit=1:NJ
       in2=theta(i)*200/45;
       jarr(unit)=wij(1,unit)*w(k)+wij(2,unit)*in2+wij(3,unit)*in3;
       jarr(unit)=max(jarr(unit),Tn_arr(unit));
       jarr(unit)=min(jarr(unit),S_arr(unit));
     end;
     Oa(i,k)=max(wjk*jarr,0);
  end;
end;
```

Bibliography

[1] T.J. Anastasio. Neural network models of velocity storage in the horizontal vestibulo-ocular reflex. *Biol. Cybern.*, 64:187–196, 1991.

[2] T.J. Anastasio. Simulating vestibular compensation using recurrent back- propagation. *Biol. Cybern.*, 66:389–397, 1992.

[3] T.J. Anastasio and D.A. Robinson. The distributed representation of vestibulo-oculomotor signals by brain-stem neurons. *Biol. Cybern.*, 61:79–88, 1989.

[4] T.J. Anastasio and D.A. Robinson. Distributed parallel processing in the vertical vestibulo- ocular reflex: learning networks compared to tensor theory. *Biol. Cybern.*, 63:161-167, 1990.

[5] D.B. Arnold and D.A. Robinson. A neural network that learns to integrate oculomotor signals. *Proc. Int. Joint Conf. Neural Networks*, 2:693–697, 1990.

[6] D.B. Arnold and D.A. Robinson. A learning network model of the neural integrator of the oculomotor system. *Biol. Cybern.*, 64:447–454, 1991.

[7] D.B. Arnold and D.A. Robinson. The oculomotor integrator: testing of a neural network model. *Exp. Brain Res.*, 113:57–74, 1997.

[8] J. Baker, J. Goldberg, G. Hermann and B. Peterson. Optimal response planes and canal convergence in secondary neurons in vestibular nuclei of alert cats. *Brain Res.*, 294:133–137, 1984.

[9] R. Baker, M. Gresty and A. Berthoz. Neuronal activity in the prepositus hypoglossi nucleus correlated with vertical and horizontal eye movement in the cat. *Brain Res.* 101:366–371, 1975.

[10] D.B. Belknap and R.A. McCrea. Anatomical connections of the prepositus and abducens nuclei in the squirrel monkey. *J. Comp. Neurol.*, 268:13–28, 1988.

[11] C. Bell. On the motions of the eye, in the illustration of the uses of the muscles and nerves of the orbit. *Philosophical Transactions of the Royal Society of London*, 1:166–186, 1823.

[12] R.H.I. Blanks, I.S. Curthoys and C.H. Markham. Planar relationships of the semicircular canals in man. *Acta Otolaryngol*, 80:185–196, 1975.

[13] L. Brand. *Vector and Tensor Analysis.* John Wiley and Sons, Inc., third edition, 1948.

[14] H. Bremermann. A method of unrestrained global optimization. *Math Biosci.*, 9:1–15, 1970.

[15] C. Buisseret-Delmas, M. Epelbaum and P. Buisseret. The vestibular nuclei of the cat receive a primary afferent projection from receptors in extraocular muscles. *Exp. Brain Res.*, 81:654–658, 1990.

[16] S.C. Cannon and D.A. Robinson. Loss of the neural integrator of the oculomotor system from brain stem lesions in monkey. *J. Neurophysiol.*, 57:1383–1409, 1987.

[17] S.C. Cannon and D.A. Robinson. An improved neural-network model for the neural integrator of the oculomotor system: more realistic neuron behaviour. *Biol. Cybern.*, 53:93–108, 1985.

[18] S.C. Cannon, D.A. Robinson and S. Shamma. A proposed neural network for the integrator of the oculomotor system. *Biol. Cybern.*, 49:127–136, 1983.

[19] R.H.S. Carpenter. *Movements of the Eyes.* Pion Limited, London, second edition, 1988.

[20] M.B. Carpenter and R.J. Cowie. Connections and oculomotor projections of the superior vestibular nucleus and cell group 'y'. *Brain Res.*, 336:265–287, 1985.

[21] G. Cheron, M. Escudero and E. Godaux. Discharge properties of brain stem neurons projecting to the flocculus in the alert cat. I. medial vestibular nucleus. *J. Neurophysiol.*, 76(3):1759–1774, 1996.

[22] G. Cheron and E. Godaux. Disabling of the oculomotor neural integrator by kainic acid injections in the prepositus-vestibular complex of the cat. *J. Physiol.*, 394:267–290, 1987.

[23] R.A. Clendaniel and L.E. Mays. Characteristics of antidromically identified oculomotor internuclear neurons during vergence and versional eye movements. *J. Neurophysiol.*, 71(3):1111–1127, 1994.

[24] J.D. Crawford. The oculomotor neural integrator uses a behavior-related coordinate system. *The Journal of Neuroscience*, 14(11):6911–6923, 1994.

[25] J.D. Crawford and T.Vilis. Axes of eye rotation and Listing's law during rotations of the head. *J. Neurophysiol.*, 65(3):407–423, 1991.

[26] J.D. Crawford and T.Vilis. Modularity and parallel processing in the oculomotor integrator. *Exp. Brain Res.*, 96:443–456, 1993.

[27] G. Cybenko. Approximation by superpositions of a sigmoidal function. *Mathematical Control Signals Systems*, 2:303–314, 1989.

[28] Y. Dalezios, C.A. Scudder, S.M. Highstein and A.K. Moschovakis. Anatomy and physiology of the primate interstitial nucleus of Cajal. II. Discharge pattern of single efferent fibers. *J. Neurophysiol.*, 80:3100–3111, 1998.

[29] J.M. Delgado-Garcia, P.P. Vidal, C. Gomez and A. Berthoz. A neurophysiological study of prepositus hypoglossi neurons projecting to oculomotor and preoculomotor nuclei in the alert cat. *Neuroscience*, 29(2):291–307, 1989.

[30] J.L. Demer, J.M. Miller, V. Poukens, H.V. Vinters and B.J. Glasgow. Evidence for fibromuscular pulleys of the recti extraocular muscles. *Investigative Ophthalmology and Visual Science* 36(6):1125–1136, 1995.

[31] I.M.L. Donaldson and P.C. Knox. Evidence for corrective effects of afferent signals from the extraocular muscles on single units in the pigeon vestibulo-oculomotor system. *Exp. Brain Res.* 95:240–250, 1993.

[32] J.P. Draye, G.A. Cheron, G.A. Libert, E. Godaux. Emergence of clusters in the hidden layer of a dynamic recurrent neural network. *Biol. Cybern.*, 761:365–374, 1997.

[33] J.P. Draye, G.A. Cheron, G.A. Libert, E. Godaux. Improvements of the neural network simulation of the vestibular oculomotor integrator. *Annals of the New York Academy of Sciences*, 781:365–374, 1996.

[34] S. du Lac, J.L. Raymond, T.J. Sejnowski and S.G. Lisberger. Learning and memory in the vestibulo-ocular reflex. *Annu. Rev. Neurosci.*, 18:409–441, 1995.

[35] A.H. Epema, N.M. Gerrits and J. Voogd. Secondary vestibulocerebellar projections to the flocculus and uvulo-nodular lobule of the rabbit: a study using HRP and double fluorescent tracer techniques. *Exp. Brain Res.*, 80:72–82, 1990.

[36] M. Escudero, G. Cheron and E. Godaux. Discharge properties of brain stem neurons projecting to the flocculus in the Alert Cat. II. prepositus hypoglossi nucleus. *J. Neurophysiol.*, 76(3):1775-1785, 1996.

[37] M. Escudero, R.R. De La Cruz and J.M. Delgado-García. A physiological study of vestibular and prepositus hypoglossi neurons projecting to the abducens nucleus in the alert cat. *J. Physiol.*, 458:539–560, 1992.

[38] M. Escudero and J.M. Delgado-García Behaviour of reticular, vestibular and prepositus neurons terminating in the abducens nucleus of the alert cat. *Exp. Brain Res.*, 71:218–222, 1988.

[39] K. Fukushima. The interstitial nucleus of Cajal and its role in the control of movements of head and eyes. *Progress in Neurobiology*, 29:107–192, 1987.

[40] K. Fukushima, E.V. Buharin and J. Fukushima. Responses of floccular Purkinje cells to sinusoidal vertical rotation and effects of muscimol infusion into the flocculus in alert cats. *Neurosci. Res.*, 17:297–305, 1993.

[41] K. Fukushima, J. Fukushima, C. Harada, T. Ohashi and M. Kase. Neuronal activity related to vertical eye movement in the region of the interstitial nucleus of Cajal in alert cats. *Exp. Brain Res.*, 79:43–64, 1990.

[42] K. Fukushima, C. Harada, J. Fukushima and Y. Suzuki Spatial properties of vertical eye movement-related neurons in the region of the interstitial nucleus of Cajal in awake cats. *Exp. Brain Res.*, 79:25–42, 1990.

[43] K. Fukushima and C.R.S. Kaneko. Vestibular integrators in the oculomotor system. *Neurosci. Res.*, 22:249–258, 1995.

[44] K. Fukushima, C.R.S. Kaneko and Albert F. Fuchs. The neuronal substrate of integration in the oculomotor system. *Progress in Neurobiology*, 39:609–639, 1992.

[45] K. Fukushima, J. Kudo, K. Takahashi and M. Kato Effects of lesion on the interstitial nucleus of Cajal on vestibular horizontal canal neurons in the cat. *Neurosci. Res.* , 2:287–294, 1985.

[46] K. Fukushima, M. Ohno, K. Takahashi and M. Kato. Location and vestibular responses of interstitial and midbrain reticular neurons that project to the vestibular nuclei in the cat. *Exp. Brain Res.*, 45:303–312, 1982.

[47] K. Fukushima, K. Takahashi and M. Kato. Responses of vestibular neurons to stimulation of the interstitial nucleus of Cajal in the cat. *Exp. Brain Res.*, 51:1–15, 1983.

[48] H.L. Galiana and J.S. Outerbridge. A bilateral model for central neural pathways in vestibuloocular reflex. *J. Neurophysiol.*, 51(2):210–241, 1984.

[49] P.E. Gill, W. Murray, M.H. Wright. *Practical Optimization.* Academic Press, London, 1981.

[50] E. Godaux and G. Cheron. Effects of severance of the vestibular commissural pathway on the neural integrator of the oculomotor system in the cat. In *Oculomotor Control and Cognitive Processes*, pages 39–62. Elsevier Scince Publishers BV, 1991.

[51] W. Graf. Motion detection in physical space and its peripheral and central representation. *Annals of the New York Academy of Sciences*, 585:154–169, 1988.

[52] W. Graf, J. Baker and B.W. Peterson. Sensorimotor transformation in the cat's vestibuloocular reflex system. I. neuronal signals coding spatial coordination of compensatory eye movements. *J. Neurophysiol.*, 70(6):2425–2441, 1993.

[53] W. Graf and K. Ezure. Morphology of vertical canal related second order vestibular neurons in the cat. *Exp. Brain Res.*, 63:35–48, 1986.

[54] W. Graf, R.A. McCrea and R. Baker. Morphology of posterior canal related secondary vestibular neurons in rabbit and cat. *Exp. Brain Res.*, 52:125–138, 1983.

[55] A. Green and H.L. Galiana. Exploring sites for short-term VOR modulation using a bilateral model. *Annals of the New York Academy of Sciences*, 781:625–628, 1996.

[56] M. Hardy. Observations on the innervation of the macula sacculi in man. *Anatomical Record*, 59:403–418, 1934.

[57] T. Haslwanter. Mathematics of three-dimensional eye rotations. *Vision Res.*, 35(12):1727–1739, 1995.

[58] N. Hirai and Y. Uchino. Superior vestibular nucleus neurons related to the excitatory vestibulo-ocular reflex of anterior canal origin and their ascending course in the cat. *Neurosci. Res.*, 1:73–79, 1984.

[59] N. Hirai and Y. Uchino. Floccular influence on excitatory relay neurons of vestibular reflexes of anterior semicircular canal origin in the cat. *Neurosci. Res.*, 1:327–340, 1984.

[60] N. Isu and J. Yokota. Morphophysiological study on the divergent projection of axon collaterals of medial vestibular nucleus neurons in the cat. *Exp. Brain Res.*, 53:151–162, 1983.

[61] Y. Iwamoto, T. Kitama and K. Yoshida. Vertical eye movement-related secondary vestibular neurons ascending in medial longitudinal fasciculus in cat

I. Firing properties and projection pathways. *J. Neurophysiol.*, 63(4):902–917, 1990.

[62] Y. Iwamoto, T. Kitama and K. Yoshida. Vertical eye movement-related secondary vestibular neurons ascending in medial longitudinal fasciculus in cat II. Direct connections with extraocular motoneurons. *J. Neurophysiol.*, 63(4):918–935, 1990.

[63] B.Y. Kamath and E.L. Keller. A neurological integrator for the oculomotor control system. *Mathematical Biosciences*, 30:341–352, 1976.

[64] M. Kasahara and Y. Uchino. Bilateral semicircular canal inputs to neurons in cat vestibular nuclei. *Exp. Brain Res.*, 20:285–292, 1974.

[65] M. Kimura, T. Takeda and K. Maekawa Contribution of eye muscle proprioception to velocity-response characteristics of eye movements: involvement of the cerebellar flocculus. *Neurosci. Res.*, 12:160–168, 1991.

[66] W.W. Koehn, H.A. Jenkins, V. Honrubia and W.H. Fenton Effect of unilateral ablation of the vestibular cerebellum on visual-vestibular interaction. *Experimental Neurology* 73:618–631, 1981.

[67] T. Kokkoroyannis, C.A. Scudder, C.D. Balaban and S.M. Highstein. Anatomy and physiology of the primate interstitial nucleus of Cajal I. Efferent projections. *J. Neurophysiol.*, 75(2):725–739, 1996.

[68] B.C. Kuo. *Automatic Control Systems* Prentice-Hall Inc., Englewood Cliffs New Jersey, sixth edition, 1991.

[69] J. Lopez-Barneo, C. Darlot, A. Berthoz and R. Baker. Neuronal activity in prepositus nucleus correlated with eye movement in the alert cat. *J. Neurophysiol.*, 47(2):329–352, 1982.

[70] C.H. Markham. Midbrain and contralateral labyrinth influences on brain stem vestibular neurons in the cat. *Brain Res.*, 9:312–333, 1968.

[71] C.H. Markham, W. Precht and H. Shimazu. Effect of stimulation of interstitial nucleus of Cajal on vestibular unit activity in the cat. *J. Neurophysiol.*, 29:493–507, 1966.

[72] R.A. McCrea and R. Baker. Cytology and intrinsic organization of the perihypoglossal nuclei in the cat. *J. Comp. Neurology*, 237:360–376, 1985.

[73] R.A. McCrea and R. Baker. Anatomical connections of the nucleus prepositus of the cat. *J. Comp. Neurology*, 237:377–407, 1985.

[74] R.A. McCrea, R. Baker and J. Delgado-Garcia. Afferent and efferent organization of the prepositus hypoglossi nucleus. *Prog. Brain Res.*, 50:653–665, 1979.

[75] R.A. McCrea, A. Strassman, E. May and S.M. Highstein. Anatomical and physiological characteristics of vestibular neurons mediating the vertical vestibulo-ocular reflexes of the squirrel monkey. *J. Comp. Neurology*, 264:571–594, 1987.

[76] J.L. McFarland and A.F. Fuchs. Discharge patterns in nucleus prepositus hypoglossi and adjacent medial vestibular nucleus during horizontal eye movement in behaving macaques. *J. Neurophysiol.*, 68(1):319–332, 1992.

[77] P. Mettens, E. Godaux, G. Cheron and H.L. Galiana. Effect of muscimol microinjections into the prepositus hypoglossi and the medial vestibular nuclei on cat eye movements. *J. Neurophysiol.*, 72(2):785–802, 1994.

[78] J.M. Miller and D.A. Robinson. A model of the mechanics of binocular alignment. *Computers and Biomedical Research* 17:436–470, 1984.

[79] H. Misslisch, D. Tweed, M. Fetter, D. Sievering and E. Koenig. Rotational kinematics of the human vestibuloocular reflex III. Listing's law *J. Neurophysiol.*, 72(5):2490–2502, 1994.

[80] G. Ostriker, A. Pellionisz and R. Llinas. Tensorial computer model of gaze- I. Oculomotor activity is expressed in non-orthogonal natural coordinates. *Neuroscience*, 14(2):483–500, 1985.

[81] A.M. Partsalis, S.M. Highstein and A.K. Moschovakis. Lesions of the posterior commissure disable the vertical neural integrator of the primate oculomotor system. *J. Neurophysiol.*, 71(6):2582–2585, 1994.

[82] A.J. Pellionisz. Coordination: a vector-matrix description of transformations of overcomplete CNS coordinates and a tensorial solution using the Moore-Penrose generalized inverse. *J. Theor. Biol.*, 110:353–375, 1984.

[83] A.J. Pellionisz. Robotics connected to neurobiology by tensor theory of brain function. *IEEE International Conference on Systems, Man and Cybernetics*, pages 411–414, 1985.

[84] A.J. Pellionisz. Tensorial aspects of the multidimensional approach to the vestibulo-oculomotor reflex and gaze. In *Adaptive mechanisms in gaze control: facts and theories*, pages 281–296. Elsevier Science Publishers BV, 1985.

[85] A.J. Pellionisz and W. Graf. Tensor network model of the three-neuron vestibulo-ocular reflex-arc in cat. *J. Theoret. Neurobiol.*, 5:127–151, 1987.

[86] C. Quaia and L.M. Optican. Commutative saccadic generator is sufficient to control a 3-D ocular plant with pulleys. *J. Neurophysiol.*, 79:3197–3215, 1998.

[87] K.J. Quinn, N. Schmajuk, J.F. Baker and B.W. Peterson. Modeling the three neuron vestibulo-ocular reflex arc: contribution to eye movement computation. *Proc. Int. Joint Conf. Neural Networks*, 2:699–704, 1990.

[88] K.J. Quinn, N. Schmajuk, A. Jain, J.F. Baker and B.W. Peterson. Vestibuloocular reflex arc analysis using an experimentally constrained neural network. *Biol. Cybern.*, 67:113–122, 1992.

[89] T. Raphan. Modeling control of eye orientation in three dimensions. I. Role of muscle pulleys in determining saccadic trajectory. *J. Neurophysiol.*, 79:2653–2667, 1998.

[90] D.A. Robinson. Models of oculomotor neural organization. In *The Control of Eye Movements*, pages 519–538, Academic Press Inc. 1971.

[91] D.A. Robinson. A quantitative analysis of extraocular muscle cooperation and squint. *Invest. Ophthal.*, 14(11):801–825, 1975.

[92] D.A. Robinson. The use of control systems analysis in the neurophysiology of eye movements. *Ann. Rev. Neurosci.*, 4:463–503, 1981.

[93] D.A. Robinson. The use of matrices in analyzing the three-dimensional behaviour of the vestibulo-ocular reflex. *Biol. Cybern.*, 46:53–66, 1982.

[94] D.A. Robinson. The coordinates of neurons in the vestibulo-ocular reflex. In *Adaptive mechanisms in gaze control: facts and theories*, pages 297–311, Elsevier Science Publishers BV, 1985.

[95] D.A. Robinson. Integrating with neurons. *Annu. Rev. Neurosci.*, 12:33–45, 1989.

[96] Y. Sato, K. Kanda and T. Kawasaki. Target neurons of floccular middle zone inhibition in medial vestibular nucleus. *Brain Res.*, 446:225–235, 1988.

[97] Y. Sato and T. Kawasaki. Target neurons of floccular caudal zone inhibition in y-group nucleus of vestibular nuclear complex. *J. Neurophysiol.*, 57(2):460–480, 1987.

[98] Y. Sato and T. Kawasaki. Operational unit responsible for plane-specific control of eye movement by cerebellar flocculus in cat. *J. Neurophysiol.*, 64(2):551–564, 1990.

[99] Y. Sato, T. Kawasaki and K. Ikarashi. Zonal organization of the floccular Purkinje cells projecting to the vestibular nucleus in cats. *Brain Res.*, 232:1–15, 1982.

[100] Y. Sato, T. Kawasaki and K. Ikarashi. Zonal organization of the floccular Purkinje cells projecting to the group y of the vestibular nuclear complex and the lateral cerebellar nucleus in cats. *Brain Res.*, 234:430–434, 1982.

[101] Y. Sato, T. Kawasaki and K. Ikarashi. Afferent projections from the brain stem to the three floccular zones in cats. II. Mossy fiber projections. *Brain Res.*, 272:37–48, 1983.

[102] C. Schnabolk and T. Raphan. Modeling three-dimensional velocity-to-position transformation in oculomotor control. *J. Neurophysiol.*, 71(2):623–638, 1994.

[103] C.A. Scudder and A.F. Fuchs. Physiological and behavioral identification of vestibular nucleus neurons mediating the horizontal vestibuloocular reflex in trained rhesus monkeys. *J. Neurophysiol.*, 68(1):244–264, 1992.

[104] L. Shen. Neural integration by short-term potentiation. *Biol. Cybern.*, 61:319–325, 1989.

[105] A.A. Skavenski and D.A. Robinson. Role of abducens nucleus in vestibuloocular reflex. *J. Neurophysiol.*, 36:724–738, 1973.

[106] H.L.H. Smith and H.L. Galiana. The role of structural symmetry in linearizing ocular reflexes. *Biol. Cybern.*, 65:11–22, 1991.

[107] M.A. Smith and J.D. Crawford. Neural control of rotational kinematics within realistic vestibuloocular coordinate systems. *J. Neurophysiol.*, 80:2295–2315, 1998.

[108] M.W. Spong and M. Vidyasagar. *Robot Dynamics and Control.* John Wiley and Sons, Inc., 1989.

[109] H. Tan and N.M. Gerrits. Laterality in the vestibulo-cerebellar mossy fiber projection to flocculus and caudal vermis in the rabbit: a retrograde fluorescent double-labeling study. *Neuroscience* 47:909–919, 1992.

[110] D. Tweed. Three-dimensional model of the human eye-head saccadic system. *J. Neurophysiol.*, 77:654–666, 1997.

[111] D. Tweed, M. Fetter, D. Sievering, H. Misslisch and E. Koenig. Rotational kinematics of the human vestibuloocular reflex II. Velocity steps. *J. Neurophysiol.*, 72(5):2480–2489, 1994.

[112] D. Tweed, H. Misslisch, and M. Fetter. Testing models of the oculomotor velocity-to-position transformation. *J. Neurophysiol.*, 72(3):1425–1429, 1994.

[113] D. Tweed, D. Sievering, H. Misslisch, M. Fetter, D. Zee and E. Koenig. Rotational kinematics of the human vestibuloocular reflex I. Gain matrices. *J. Neurophysiol.*, 72(5):2467–2479, 1994.

[114] D. Tweed and T. Vilis. Implications of rotational kinematics for the oculomotor system in three dimensions. *J. Neurophysiol.*, 58(4):832–849, 1987.

[115] Y. Uchino, T. Ichikawa, N. Isu, H. Nakashima and S. Watanabe. The commissural inhibition on secondary vestibulo-ocular neurons in the vertical semicircular canal systems in the cat. *Neurosci. Letters*, 70:210–216, 1986.

[116] Y. Uchino, M. Sasaki, N. Isu, N. Hirai, M. Imagawa, K. Endo and W. Graf. Second-order vestibular neuron morphology of the extra-MLF anterior canal pathway in the cat. *Exp. Brain Res.*, 97:387–396, 1994.

[117] T. Vilis and D. Tweed. A matrix analysis for a conjugate vestibulo-ocular reflex. *Biol. Cybern.*, 59:237–245, 1988.

[118] Y. Zhang, A.M. Partsalis and S.M. Highstein. Properties of superior vestibular nucleus neurons projecting to the cerebellar flocculus in the squirrel monkey. *J. Neurophysiol.*, 69(2):642–645, 1993.